12-2014

Nonlocal Polarization Interferometry and Entanglement Detection

Brian P. Williams
University of Tennessee - Knoxville, bwilli38@vols.utk.edu

Recommended Citation

Williams, Brian P., "Nonlocal Polarization Interferometry and Entanglement Detection. " PhD diss., University of Tennessee, 2014.
https://trace.tennessee.edu/utk_graddiss/3181

To the Graduate Council:

I am submitting herewith a dissertation written by Brian P. Williams entitled "Nonlocal Polarization Interferometry and Entanglement Detection." I have examined the final electronic copy of this dissertation for form and content and recommend that it be accepted in partial fulfillment of the requirements for the degree of Doctor of Philosophy, with a major in Physics.

Joseph Macek, Major Professor

We have read this dissertation and recommend its acceptance:

Warren Grice, Robert Compton, Norman Mannella, Ray Garrett

Accepted for the Council:

Carolyn R. Hodges

Vice Provost and Dean of the Graduate School

(Original signatures are on file with official student records.)

Nonlocal Polarization Interferometry and Entanglement Detection

A Dissertation Presented for the
Doctor of Philosophy
Degree
The University of Tennessee, Knoxville

Brian P. Williams
December 2014

I dedicate this manuscript to my wife, Lydia, who endured its creation.

Acknowledgements

I would like to thank my parents and brother for endowing me with the gumption to pursue science. They also gave me a moral compass which guides me each day. While at the University of Memphis pursuing an engineering degree, my 2nd or 3rd major change, I took a physics class from Dr. Robert R. Marchini. His inspiration and love of Physics is certainly to blame for my path into science, thanks. I thank my mentor Dr. Warren Grice for his past and future teaching, allowing me to follow my experimental nose, and bringing me down from the clouds as is often necessary. I thank my experimental mentors Jason Schaake, Dr. Phil Evans, Dr. Duncan Earl, and Dr. Raphael Pooser for giving me the abilities and skills to carry out my research. I thank Dr. Travis Humble for supporting my research even when it was untested and only slightly inline with his project goals. Travis always seems enthusiastic about my ideas, which I appreciate! Lastly, I thank my wife Lydia, who has always been patient, understanding, and loving.

Quantum phenomena do not occur in a Hilbert space. They occur in a laboratory.
-Asher Peres

Abstract

At present, quantum entanglement is a resource, distributed to enable a variety of quantum information applications such as quantum key distribution, superdense coding, and teleportation. Necessarily, the distribution and characterization of entanglement is fundamental to its application. This dissertation details three research efforts to enable nonlocal entanglement detection, distribution, and characterization. Foremost of these efforts, we present the theory and demonstration of a nonlocal polarization interferometer capable of detecting entanglement and identifying Bell states statistically. This is possible due to the interferometer's unique correlation dependence on the anti-diagonal elements of the density matrix, which have distinct bounds for separable states and unique values for the four Bell states. Second, we propose a nonlocal method of interferometrically mapping time-entangled photons to polarization entangled states, capitalizing on the strengths of both the robust temporal degree of freedom and the "easy to measure" polarization degree of freedom. Finally, we propose a method of estimating and representing correlation probabilities in nonlocal two-photon experiments using Bayes' rule. Numerical simulations confirm that a vigorous consideration of the available information offers a correlation characterization superior to the standard approach.

Table of Contents

Chapter 1

Introduction

Particle A and particle B interact at a common origin and depart in opposite directions. Some distance west of the origin, a girl, Alice, sees that particle A is blue. A similar distance east of the origin, a boy, Bob, sees that particle B is red. More A and B particles depart the origin and Alice and Bob also observe these particles. Each time Alice sees red, Bob sees blue, and each time Alice sees blue, Bob sees red. Later, Alice and Bob confer and suggest two possible explanations for the correlations. The first is that particle A and B leave the origin with different definite colors determined by their interaction, and these are the colors observed. This explanation is reasonable, since it agrees with anyone's everyday experience. Their second, imaginative, explanation is that the particles are neither red nor blue, but only become red or blue when observed, with some unknown mechanism assuring the observed colors are always different. Their first explanation certainly seems that it must be the correct one. After all, the second explanation suggests the particles do not have a color until one of them is observed. Furthermore, even if they accept this reality, there's another problem. When the particles are separated by a vast distance and particle A's color is observed, particle B must instantaneously adopt a different color. Assuming simultaneous observations and that communication is bounded by the speed of light, how would particle B *know* which color it should be? While Alice and Bob's second explanation seems to have problems, quantum mechanics allows for just such an explanation, entanglement.

The quantum state shared by Alice and Bob may be written as a state or ket in Dirac notation [1, 2]

$$|{\color{red}\bullet}{\color{blue}\bullet}\rangle = |{\color{red}\bullet}\rangle \otimes |{\color{blue}\bullet}\rangle\,. \tag{1.1}$$

This separable state describes the case in which particles A and B always leave the origin with colors red and blue, respectively. Informally, they are separable in the sense that consideration of the particles as individuals or together is equivalent. If we assume that half the time Alice observes red, and half blue, we can represent the total separable mixed state, a probabilistic combination of pure states, as the density operator

$$\rho_s = \frac{1}{2}\left(|{\color{red}\bullet}{\color{blue}\bullet}\rangle\langle{\color{red}\bullet}{\color{blue}\bullet}| + |{\color{blue}\bullet}{\color{red}\bullet}\rangle\langle{\color{blue}\bullet}{\color{red}\bullet}|\right). \tag{1.2}$$

This representation conveys that while the particles definitely have a color leaving the origin, Alice and Bob simply are unaware as to this color before they observe it. For instance, an observer, Charlie, at the origin may know the color before Alice and Bob. However, Alice and Bob's observations are unaffected by this.

Alice and Bob's second explantation is that particles A and B have no color until observed, at which time they always adopt different colors. This entangled state may be written as

$$|\begin{smallmatrix}{\color{red}\bullet} & {\color{blue}\bullet}\\ {\color{blue}\bullet} & {\color{red}\bullet}\end{smallmatrix}\rangle = \frac{1}{\sqrt{2}}\left(|{\color{red}\bullet}{\color{blue}\bullet}\rangle + |{\color{blue}\bullet}{\color{red}\bullet}\rangle\right) \tag{1.3}$$

with a denisty matrix

$$\rho_e = |\begin{smallmatrix}{\color{red}\bullet} & {\color{blue}\bullet}\\ {\color{blue}\bullet} & {\color{red}\bullet}\end{smallmatrix}\rangle\langle\begin{smallmatrix}{\color{red}\bullet} & {\color{blue}\bullet}\\ {\color{blue}\bullet} & {\color{red}\bullet}\end{smallmatrix}| = \frac{1}{2}\left(|{\color{red}\bullet}{\color{blue}\bullet}\rangle\langle{\color{red}\bullet}{\color{blue}\bullet}| + |{\color{blue}\bullet}{\color{red}\bullet}\rangle\langle{\color{blue}\bullet}{\color{red}\bullet}| + |{\color{red}\bullet}{\color{blue}\bullet}\rangle\langle{\color{blue}\bullet}{\color{red}\bullet}| + |{\color{blue}\bullet}{\color{red}\bullet}\rangle\langle{\color{red}\bullet}{\color{blue}\bullet}|\right). \tag{1.4}$$

Alice and Bob still do not know which color the particles are until observed, but now it seems the particles have no color at all before they are seen. Additionally, the density operator for the entangled state has "extra" terms compared to the mixed state operator from Eq. 1.2. These terms are coherences between the two possibilities and are largely responsible for the quantum phenomena driving much of quantum information. Now, what effect does an observer Charlie at the origin have on an entangled state? If Charlie observes either particle at the origin, he *collapses the wavefunction* [3]. If he observes that particle A is red, the state becomes that given in Eq. 1.1, all coherence amplitudes vanish. A large quantity of scientific thought and experiment has considered how Alice and Bob might distinguish Eq. 1.3 from a mixture represented by Eq. 1.2. In that tradition, Chapter 2 of this dissertaion will investigate a novel apparatus that, in part, allows Alice and Bob to make this distinction.

Don't Alice and Bob have something better to do? What value does this determination have other than scientific curiosity? The determination of particle color from the state 1.3 is random. Though the particles adopt opposing color instantaneously, the randomness of this event disallows any sort of superluminal information exchange between Alice and Bob. However, Alice and Bob do share a random binary variable, 🔴🔵 $\equiv 0$ or 🔵🔴 $\equiv 1$. If Alice and Bob can confirm that their state is the entangled state of Eq. 1.3 and not a separable mixture of which Charlie could have complete information, they share a secret random bit! This can be leveraged in one time pad cryptography [4], an unbreakable method of encryption. This idea has become known as quantum key distribtuion (QKD) [5, 6] or quantum key growing, since Alice and Bob grow or expand an intial shared secret key.

Additionally, if Alice and Bob were able to make the aforementioned distinction between a separable state and an entangled state, they would confirm that quantum mechanics [7, 8] gives the correct prediction! This confirmation would lend even more credibility to quantum mechanics as the true theory of reality, and certainly secure notable accolades for Alice and Bob. But first things, first. Let us review the history of entanglement and how it can be used.

1.1 A Historical Survey of Two Photon Entanglement

As described, quantum theory predicts entanglement. Entangled particles exhibit nonlocal correlations which seem to defy reasonable ideas of reality and locality. The implications of entanglement were first discussed in 1935 by Einstein, Rosen, and Podolsky [9] who presented the now famous EPR paradox of which Alice and Bob have given us a glimpse. Later in 1935, Schrödinger published his "Shrödinger's Cat" paper [10, 11] and famously described entanglement [12] as

> *...the characteristic trait of quantum mechanics, the one that enforces its entire departure from classical lines of thought.*

In 1964 John S. Bell [13] derived an inequality, now among a collection known as Bell inequalities, that set statistical bounds on the correlations two spatially separated particles may have. Bell assumed these particles could have any deterministic explanation, even those that allow a different result for each local reality at the time of observation. The variables that allow for a specific outcome for each local reality are known as hidden variables. These inequalities hold for all hidden variable theories, but do not hold for quantum mechanics. In 1968 Clauser, Horne, Shimony, and Holt introduced the CHSH inequality as an alternative to Bell's with the purported benefit of being realizable experimentally. In 1974, Clauser and Horne went further deriving the CH inequality [14] which lowers the detection efficiency required to overcome the detection loophole. Experiments violating the Bell inequalities have again and again confirmed entanglement as predicted by quantum mechanics [15, 16, 17, 18, 19]. The most famous of these being those performed by Alain Apsect in 1981 and 1982. A common configuration for a CHSH Bell test is shown in Fig. 1.1

Bell's original paper cited David Bohm who proposed [20] tests of quantum mechanics based on the spin of electrons. Bell's inequality was then laid out with entangled electron spins as the testbed. The shift to Bell tests using polarization

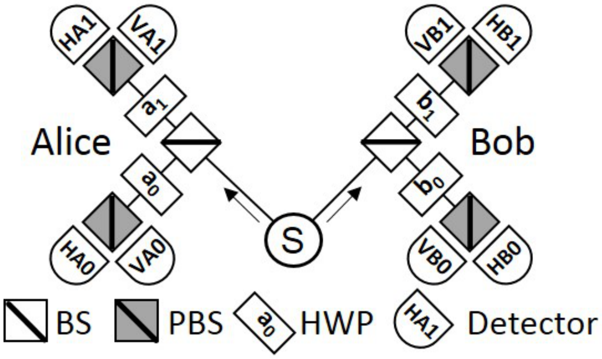

Figure 1.1: A typical Bell test. An entangled photon pair is shared between Alice and Bob whose local measurement settings or local realities a_0, a_1, b_0, and b_1 are randomly chosen by a symmetric beamsplitter (BS). HWP ≡ half-wave plate, PBS ≡ polarizing beamsplitter

entangled photons was made by Freedman and Clauser [21] who performed the first Bell test in 1972. They generated polarization entangled photons from an atomic cascade. The first Bell test using spontaneous parametric downconversion (SPDC) was performed by Rarity and Tapster [22], and at present SPDC is still the most common source of polarization entangled photons.

The simplicity of polarization entanglement makes its use ubiquitous in quantum information proofs and demonstrations. Two-photon states are relatively easy to produce from SPDC and are easy to manipulate and measure in the laboratory. The downside is that polarization entanglement is fragile, especially when distributed over optical fiber, the most convenient method of long distance photon transport. This limitation on polarization entanglement led, in part, to proposals to test Bell inequalities using two photon time entanglement and nonlocal interferometry.

Numerous experiments involving local and nonlocal two photon interferometry have been carried out. While many of these experiments precede the following, those mentioned here are both historically significant and also related to the reported research. A more comprehensive history of two-photon interferometry is given by Ou [23].

An experiment carried out by Hong, Ou, and Mandel [24] is local in nature and involves two identical photons incident on the two input ports of symmetric beamsplitter as seen in Fig. 1.2.

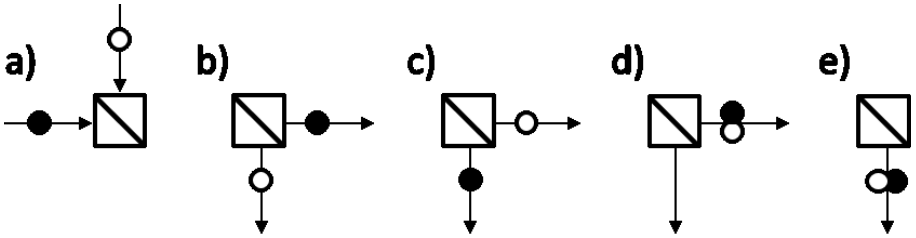

Figure 1.2: Hong Ou Mandel interference occurs when indistinguishable photons are incident on the two input ports of a symmetric beamsplitter as seen in a). The output cases b) and c) are indistinguishable and out of phase by π due to the phase properties of the symmetric beamsplitter. Thus, these cases perfectly and destructively interfere leaving only the cases d) and e). The HOM dip is observed as the different port coincident rate is extinguished.

When temporally overlapped, the two cases in which the photons exit different ports of the beamsplitter (BS) are indistinguishable. This leads to two photon interference, which in this case, due to the fixed phase relationship between the photons, is perfectly destructive for the different port cases. This leaves the photon pair always exiting the same port of the BS resulting in a HOM dip in the coincidence rate for different ports. Since the visibility of HOM interference depends on the temporal and spectral properties of the two photons, it is a versatile tool to characterize photons and sources [25]. HOM interference is integral to local deterministic Bell state identification [26], and can also be used to create two photon N00N states [27, 28].

In 1990, Rarity and Tapster [29] performed a two-photon experiment using a Mach-Zehnder interferometer such that the coincidence rate at the output ports varied as the phase in the interferometer is changed. This was true beyond a path length difference greater than the coherence length of the individual photons. Thus, they demonstrated the biphoton nature of the entangled pair which has a coherence length in excess of the individual photons.

In 1989, James Franson proposed an experiment [30] in which time-entanglement is harnessed to exhibit interference in the correlations observed from two spatially separated unbalanced Mach-Zehnder interferometers as depicted in Fig. 1.3.

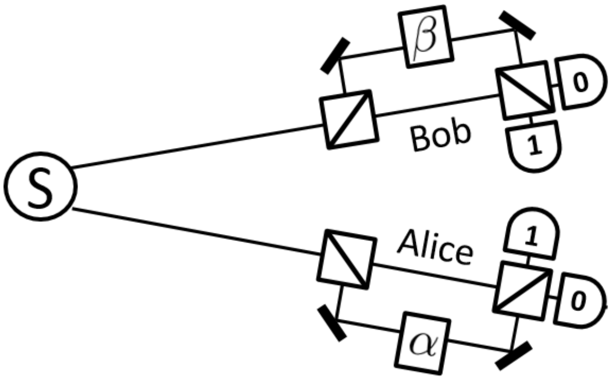

Figure 1.3: Franson's interferometer consists of two unbalanced Mach-Zehnder interferometers fed by a shared two-photon source. Correlations are seen in the detection port coincidence rates. These correlations vary as the phase from the path mismatch α or β are changed.

The interferometer imbalance is larger than the single photon coherence time, suppressing single photon interference, but smaller than the biphoton coherence time. In this configuration, the photon detection ports exhibit correlations under appropriate choices of the phases α and β. Rarity and Tapster also proposed a nonlocal experiment [31], though due to spatial considerations it is not as practical as Franson's design. Franson's interferometer was first demonstrated by Ou [32], though a clever implementation was also demonstrated by Kwiat [33]. While initially proposed to test Bell's inequality, the prevalence of Franson's design has been due to the robust nature of time entanglement, which enables long distance entanglement distribution over optical fiber. By comparison, distribution of polarization entanglement is presently greatly limited, though strides are being made [34]. Robustness aside, Franson's design is subject to its own problems. One of which is that half the photon path choices are distinguishable and must be removed using time discrimination. Strekalov, Pittman, and Kwiat demonstrated an experiment [35] avoiding this problem, but it requires distribution of polarization entanglement.

Another problem is that the interferometers must be stabilized. Historically this has been accomplished using local lasers to separately "lock" the interferometers, by using especially stable fiber configurations, or in the case of Strekalov, Pittman, and Kwiat very short interfering paths in a Pockels cell. The last case is only possible due to the unique nature of the experiment which again uses polarization distribution. Modern entanglement distribution demonstrations using Franson interferometry have achieved distances exceeding 300 km [36, 37]. These demonstrations use extremely stable planar lightwave circuits (PLC) [38, 39] whose phases are adjusted using temperature regulation. In Chapter 3, a Franson-like design is proposed which is phase-stable and also maps robust time-entangled states to easy-to-measure polarization entangled states.

The success, popularity, or boom of quantum information has resulted, in part, from a few key proposed uses of entanglement, entanglement based quantum key distribution (QKD) as proposed by Ekert [6], superdense coding [40], and teleportation [41]. While Ekert's QKD proposal uses distributed entanglement in which measurements on the photon pairs are spatially separated, both teleportation and superdense coding ultimately rely on a local Bell state measurement. However, both local measurements promise a nonlocal benefit, a teleported state or an effective increase in the information carried by a single photon. This brief survey of two photon entanglement history is an insufficient representation of the breadth of two photon quantum information. More thorough reviews include [42, 43].

1.2 Entanglement Detection

An entangled two-photon state is any that cannot be represented by the density matrix

$$\rho_{AB} = \sum_i a_i \rho_i^A \otimes \rho_i^B. \tag{1.5}$$

For instance, Alice and Bob's state given in Eq. 1.3 cannot be written in this form. Actually, there are simpler criteria for pure states, but pure states are not practically realizable. Thus, I will choose to exclude their discussion. A cornucopia of theoretical work exists [42, 44] investigating the nature of entanglement and how it may be detected, verified, or "witnessed". The typical goal of this research is to find methods of determining whether or not a quantum state may be described using Eq. 1.5. One method of ensuring a distributed state is entangled is to perform a Bell test such as that proposed by Clauser, Horne, Shimony, and Holt (CHSH) [45]. This is exactly the method Ekert proposed in his 1991 QKD proposal as a verification of security. By breaking Bell's inequality the state is confirmed to be inseparable, entangled, and secure. Bell tests require four measurement settings at which sub-maximal correlations generate the statistics necessary for entanglement verification. This is fewer measurements needed than full state tomography which is required for tests of negativity [46]. Negativity is a quantity calculated from a modified form of the density matrix. It is based on criteria for a density matrix to be separable as proposed by Peres [47]. Entanglement may also be revealed via an entanglement witness $\mathcal{W}$ [48, 49] which is an experimentally measurable quantity such that for all separable states $\langle\mathcal{W}\rangle \geq 0$ and for at least one entangled state $\langle\mathcal{W}\rangle < 0$. For example, the Bell inequality may be written as an entanglement witness. The first witness implementation [50] required three experimental settings at which statistics are generated. Though there are other quantifications and measures of entanglement [42, 44], Bell tests, negativity, and some witnesses are among a small number of tests which can presently be carried out by experimental linear optical measurements. In Chapter 2, a nonlocal interferometer is presented that enables entanglement detection and statistical Bell state identification.

1.3 Polarization Entangled Photons

This dissertation focuses on two-photon entanglement. The photons can be entangled in time, energy, polarization, space, momentum, all of these, or combinations of them. The experiments described herein involve photon pairs entangled in energy, time, and polarization. A commonly used source of entangled photon pairs is collinear spontaneous parametric downconversion (SPDC) [51] which is theoretically described in [23, 25] and Appendix A. Though this method of pair generation is assumed throughout this manuscript, the experiments and propositions will carry over to other sources of entangled pairs as they become available, for instance, from quantum dots [52, 53].

Photons entangled in polarization have an especially simple description as qubits in a linear vector space in which all states are representable by the superposition of the photons' individual and combined polarizations. In this description, the quantum mechanical treatment reduces to linear algebra. A photon with a horizontal polarization H or vertical polarization V is represented as a ket $|H\rangle$ or $|V\rangle$, but these are often interchangeable with the computational basis $|0\rangle$ and $|1\rangle$, for instance $|H\rangle \equiv |0\rangle$ and $|V\rangle \equiv |1\rangle$. As an example, the maximally entangled Bell states are abstractly

$$\left|\Phi^{\pm}\right\rangle = \frac{1}{\sqrt{2}}\left(|00\rangle \pm |11\rangle\right) \tag{1.6}$$

$$\left|\Psi^{\pm}\right\rangle = \frac{1}{\sqrt{2}}\left(|01\rangle \pm |10\rangle\right). \tag{1.7}$$

with $|00\rangle \equiv |0\rangle \otimes |0\rangle$. In terms of photon polarization the Bell states are

$$\left|\Phi^{\pm}\right\rangle = \frac{1}{\sqrt{2}}\left(|HH\rangle \pm |VV\rangle\right) \tag{1.8}$$

$$\left|\Psi^{\pm}\right\rangle = \frac{1}{\sqrt{2}}\left(|HV\rangle \pm |VH\rangle\right). \tag{1.9}$$

The gedanken state in Eq. 1.3 from the opening discussion would be a Ψ^+ state. Much of quantum information theory uses these Bell states as an entanglement resource, including this research.

Polarization entangled photon states retain their entanglement in other polarization bases. The bases commonly considered are the rectilinear Z, diagonal X, and circular Y bases. The Z basis is the "starting" basis with

$$|0\rangle_Z = |H\rangle \qquad |1\rangle_Z = |V\rangle \,. \tag{1.10}$$

In the diagonal basis, photons are represented as

$$|0\rangle_X = \frac{1}{\sqrt{2}}\left(|0\rangle_Z + |1\rangle_Z\right) \qquad |1\rangle_X = \frac{1}{\sqrt{2}}\left(|0\rangle_Z - |1\rangle_Z\right). \tag{1.11}$$

Lastly, in the circular basis,

$$|0\rangle_Y = \frac{1}{\sqrt{2}}\left(|0\rangle_Z + i\,|1\rangle_Z\right) \qquad |1\rangle_Y = \frac{1}{\sqrt{2}}\left(|0\rangle_Z - i\,|1\rangle_Z\right). \tag{1.12}$$

The conjugate relations for the diagonal basis are

$$|0\rangle_Z = \frac{1}{\sqrt{2}}\left(|0\rangle_X + |1\rangle_X\right) \qquad |1\rangle_Z = \frac{1}{\sqrt{2}}\left(|0\rangle_X - |1\rangle_X\right) \tag{1.13}$$

and in the circular basis

$$|0\rangle_Z = \frac{1}{\sqrt{2}}\left(|0\rangle_Y + |1\rangle_Y\right) \qquad |1\rangle_Z = \frac{-i}{\sqrt{2}}\left(|0\rangle_Y - |1\rangle_Y\right). \tag{1.14}$$

It is then easy to show that starting with the Bell state Φ_Z^+ in the Z basis the state is retained in the X basis $\Phi_Z^+ \rightarrow \Phi_X^+$ while a bit is flipped in the Y basis $\Phi_Z^+ \rightarrow \Psi_Y^+$.

This is of course not true of a separable state, in the rectilinear basis

$$|\psi_s\rangle_Z = |0_A\rangle_Z\,|0_B\rangle_Z \tag{1.15}$$

will always lead to Alice and Bob observing 0, but in the diagonal basis,

$$|\psi_s\rangle_X = \frac{1}{2}\left(|0_A\rangle_X + |1_A\rangle_X\right)\left(|0_B\rangle_X + |1_B\rangle_X\right), \tag{1.16}$$

Alice and Bob will have no correlation.

In Chapter 2, we present the nonlocal polarization interferometer which detects polarization entangled states and enables statistical Bell state identification. In Chapter 3, we propose distributing robust time entangled photons and mapping them to polarization entangled Bell states, allowing polarization measurements in the Z, X, and Y bases with entanglement preservation.

1.4 Time Entangled Photons

Time entangled photons are robust to decoherence in optical fiber transmission lines compared to polarization entanglement. This makes the temporal degree of freedom a convenient choice for entanglement distribution. As mentioned previously, the Franson interferometer is the most common experimental exhibition of time entanglement. The Franson interferometer overlaps two temporal components, one from earlier and one from later, of a long coherence time two-photon state. When the single-photon temporal information does not reveal which case, earlier or later, the components are indistinguishable, thereby leading to nonlocal interference. In this introduction to time entanglement, the Franson interferometer and its theoretical representation are briefly described.

Unless considerable hand waving is used, representing time entangled states is more involved than polarization entangled states. A continuous or integral representation is typically used to represent the coherence properties of the time entangled two-photon state. For example, the range over which the nonlocal Franson interferometer may be mismatched and still produce nonlocal correlations [23] or the width of the Hong-Ou-Mandel dip [25] are both calculated with this treatment. Often, the experimental design allows simplification of these calculations, which can become increasingly complex as the treatment becomes more general or detailed. Thus, where possible, reasonable approximations are made to simplify the calculation while still retaining the core predictions.

A detailed description of two-photon pair creation from spontaneous parametric downconversion (SPDC) is given in Appendix A. From this calculation, we determine that two-photon states from SPDC may be represented by the state

$$|\psi\rangle \propto \int d\omega d\omega' A(\omega+\omega')\phi(\omega,\omega')\hat{a}^{\dagger}_{H}(\omega)\hat{a}^{\dagger}_{V}(\omega')\,|0\rangle \tag{1.17}$$

where we have assumed a Type II SPDC process in which the photon pair includes one horizontal (H) and one vertical (V) polarization photon. $A(\omega+\omega')$ is the spectral amplitude of the pump photon, which is related to the pump's power spectrum. In the case of a narrowband continuous-wave pump, the phase matching function $\phi(\omega,\omega')$ is responsible for the coherence properties of the downconverted photons. The creation operator $\hat{a}^{\dagger}(\omega)$ operates on the vacuum state, creating a photon in an infinitely narrow energy band ω. Consider that from this state the H photon is sent to Alice and the V to Bob. These photons are then incident to a nonlocal Franson interferometer as seen in Fig. 1.3. In each interferometer, photons may travel the long or short paths. We assume that cases where photons take different paths are excluded using time discrimination. This is possible when the interferometer imbalance is large enough that single photons are macroscopically separated in time, on the order of nanoseconds. With these photons disregarded, we are left with photons both taking the short or both the long paths. These cases are indistinguishable due to the long coherence time of the pump. This leaves the post interferometer state

$$\begin{aligned}|\psi'\rangle \propto & \frac{1}{4}\int d\omega d\omega' A(\omega+\omega')\phi(\omega,\omega') \\ & \times \Big[\Big(\hat{a}^{\dagger}_{A0}(\omega)\hat{a}^{\dagger}_{B0}(\omega') - \hat{a}^{\dagger}_{A1}(\omega)\hat{a}^{\dagger}_{B1}(\omega')\Big)\Big(1+e^{-i(\omega T_A+\omega' T_B)}\Big) \\ & \quad + \Big(\hat{a}^{\dagger}_{A0}(\omega)\hat{a}^{\dagger}_{B1}(\omega') + \hat{a}^{\dagger}_{A1}(\omega)\hat{a}^{\dagger}_{B0}(\omega')\Big)\Big(1-e^{-i(\omega T_A+\omega' T_B)}\Big)\Big]|0\rangle \end{aligned} \tag{1.18}$$

where the irrelevant polarization notation has been replaced by interferometer labels $A \equiv$ Alice and $B \equiv$ Bob and detection port labels 0 and 1. Times T_A and T_B are the temporal delays between Alice and Bob's unbalanced interferometer arms, respectively. The probability of a coincidence at Alice port j and Bob port s is found by integrating the second order correlation function

$$\Gamma^{(2)}(t,t+\tau) = |\langle 0|\, \hat{a}_{Aj}(t)\hat{a}_{Bs}(t+\tau)\, |\psi'\rangle|^2 \tag{1.19}$$

with time dependent annihilation operator

$$\hat{a}_j\left(t\right) = \left(2\pi\right)^{-1/2}\int d\omega \hat{a}_j\left(\omega\right)e^{i\omega t} \tag{1.20}$$

over the temporal window of coincidence

$$P_{js} = \int_T d\tau \Gamma^{(2)}(t,t+\tau). \tag{1.21}$$

Through involved calculations it can be shown that this probability is approximately

$$\begin{aligned}P_{js} \propto \quad & \frac{1}{4}\left(\delta_{j0}\delta_{s0}+\delta_{j1}\delta_{s1}\right)\left\{1+\mathrm{Cos}\left[\frac{\omega_p}{2}(T_A+T_B)\right]\right\} \\ & + \frac{1}{4}\left(\delta_{j0}\delta_{s1}+\delta_{j1}\delta_{s0}\right)\left\{1-\mathrm{Cos}\left[\frac{\omega_p}{2}(T_A+T_B)\right]\right\}. \end{aligned} \tag{1.22}$$

In Chapter 2 and 3, the veil is lifted, and a more rigorous treatment of both multi-mode polarization and time entangled states in the context of the research is presented.

1.5 Research Summary

This dissertation is composed of three research components, the nonlocal polarization interferometer, time-to-polarization mapper, and correlation estimation with Bayes' rule. This summary provides a short description, research motivation, and research results.

Nonlocal Polarization Interferometer

Description

The nonlocal polarization interferometer (NPI) is a composite interferometer consisting of two spatially separated interferometers that share a source of polarization entangled photons.

Motivation

The NPI enables entanglement detection and characterization for use in quantum information experiments and applications. This research is also fundamental science.

Results and Prospects

The nonlocal polarization interferometer was successfully implemented in a novel phase-stable configuration. The NPI was confirmed to detect entanglement for the four Bell states, a type of entangled state. The NPI also allowed implementation of a novel Bell inequality test in which bound breaking was confirmed for each of the Bell states. In addition, the Bell states were concurrently identified from these statistics.

Time-to-Polarization Mapper

Description

This is a nonlocal interferometric configuration allowing spatially separated time entangled photons to be mapped to polarization entangled states. The time-to-polarization mapper (TPM) can be considered a variation on the Franson interferometer or as a two-photon source, part of which extends to the end users.

Motivation

Time entanglement is robust to decoherence over optical fiber links. Therefore, time-entangled photons retain their entanglement over longer distances than polarization entangled states. The TPM uses time distribution, but allows the end users to share a polarization entangled state.

Results and Prospects

TPM is a phase-stable alternative to current implementations of Franson interferometry, and should be competitive with losses observed in those systems. TPM can be used to implement quantum information tasks relying on polarization entanglement over long distances. For example, polarization based Quantum Key Distribution (QKD). Polarization based QKD has more stringent security proofs than time, and the TPM allows these to be used without alteration. Generating Bell states in time is not trivial. TPM simplifies Bell state generation over long distances by mapping to polarization.

Correlation Estimation with Bayes' Rule

Description

This a statistical approach using Bayes' rule, a rule for probability assignment, to estimate the probability of correlation in nonlocal two-photon experiments.

Motivation

The standard approach of correlation estimation does not take full advantage of the information available. It also leads to logical pitfalls when mapping experimental quantities into probability distributions.

Results and Prospects

Estimating the correlation probability with Bayes' rule, in which the underlying physics are more closely modeled, results in superior correlation estimations in numerically simulated experiments. Additionally, this method of correlation characterization allows a more logical and useful interpretation of the correlation probabilities.

Chapter 2

The Nonlocal Polarization Interferometer

In this chapter a nonlocal interferometer capable of detecting entanglement and identifying Bell states statistically is discussed and investigated. These capabilities are possible due to the interferometer's unique correlation dependence on the anti-diagonal elements of the density matrix, which have distinct bounds for separable states and unique values for the four Bell states. The interferometer consists of two spatially separated balanced Mach-Zehnder or Sagnac interferometers that share a polarization entangled source. Correlations between these interferometers exhibit nonlocal interference, while single photon interference is suppressed. This interferometer also allows for a unique version of the CHSH-Bell test where the local reality is the photon polarization. The relevant theory and experimental results are presented.

A brief version of this chapter was published in Physical Review A with special selection as an Editor's Suggestion [54].

2.1 Overview

Entanglement enables a variety of proposed quantum information applications [43] such as quantum key distribution [6, 55], superdense coding [40], teleportation [41], and quantum computing [56]. Necessarily, the detection, quantification, and characterization of entanglement is fundamental to its application [42, 44]. One method of ensuring a distributed state is entangled is to perform a Clauser-Horne-Shimony-Holt (CHSH) Bell test [45], with entanglement detected for Bell parameters $|S| > 2$. A second method is to measure the negativity [46] of the state, which is an entanglement measure requiring full state tomography. Entanglement may also be revealed via an entanglement witness [48, 49] which typically requires significantly fewer measurements than full state tomography. The broad class includes witness forms of CHSH-Bell tests and negativity tests. In addition to these quantifications and measures there are others [42, 44]. We report a nonlocal polarization interferometer (NPI) that enables entanglement detection and nonlocal statistical Bell state identification. This form of Bell state identification is nonlocal and statistical. Therefore, it is distinct from the local and deterministic measurements used for teleportation and super-dense coding. Instead, nonlocal Bell state identification permits characterizing entanglement between spatially remote subsystems. This is possible due to the NPI's unique correlation dependence on the anti-diagonal elements of the density matrix, which have separable state bounds and unique values for the four Bell states. Additionally, we report an NPI based CHSH-Bell test with the resulting statistics also identifying the Bell state.

The balanced Mach-Zehnder implementation of the NPI is illustrated in Fig. 2.1. Polarization entangled photon pairs are distributed amongst Alice and Bob, each of whom has a balanced Mach-Zehnder interferometer that includes a half-wave plate (HWP) in one path. The HWP is oriented so as to rotate horizontal (vertical) polarization to vertical (horizontal). Upon exiting the interferometers, the photons are directed to polarizing beam splitters (PBSs) monitored by single-photon detectors.

Single-photon interference is suppressed by polarization rotation in one path, but two-photon interference remains observable as the phases α and β are modulated. Though similar in appearance, the NPI is distinct from the well known Franson interferometer [30]. Franson's design harnesses time-bin entangled states to demonstrate nonlocal interference while the NPI requires only polarization entanglement. In the remainder of this article we describe the conditions under which correlations are observed, we put bounds on correlations for separable states, we show that the Bell states produce unique NPI signatures, we discuss the NPI version of the CHSH-Bell test, and we present experimental results verifying these predictions using a phase-stable Sagnac version of the NPI.

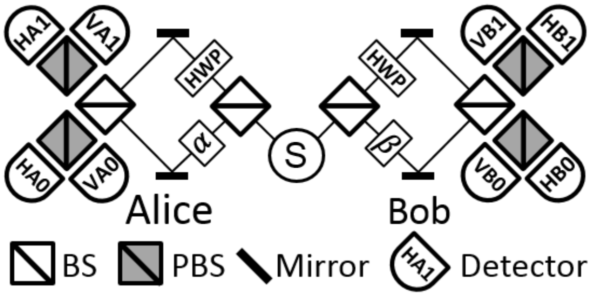

Figure 2.1: The two-photon interferometer is composed of two balanced Mach-Zehnder interferometers sharing a polarization entangled source. Nonlocal interference effects are observed while single-photon interference is suppressed.

2.2 Nonlocal Interference

Nonlocal two-photon interference occurs when Alice and Bob share a polarization entangled source such as the Bell state

$$\left|\Psi^{+}\right\rangle = (1/\sqrt{2})\left(|H_A\rangle \otimes |V_B\rangle + |V_A\rangle \otimes |H_B\rangle\right). \tag{2.1}$$

Given this source, it is straightforward to show that the probability for a single photon to exit any given port of Alice or Bob's Mach-Zehnder interferometer is 1/4, regardless of phase. That is, no single-photon interference is observed. However, nonlocal interference is observed in the coincidences between Alice and Bob's detectors. The probability that the signal and idler exit Alice's port y and Bob's port z is

$$P_{\substack{jAy\\sBz}}(\alpha,\beta)=\begin{cases}\frac{1}{16}\left\{1+(\text{-}1)^{z+y}\cos\left[\alpha+\beta\right]\right\} & j\neq s\\ \frac{1}{16}\left\{1+(\text{-}1)^{z+y}\cos\left[\alpha-\beta\right]\right\} & j=s\end{cases} \tag{2.2}$$

where A and B indicate Alice and Bob detectors, respectively, indices $j, s \in \{H, V\}$ indicate the polarization of the detected photons, $y, z \in \{0, 1\}$ indicate the detection port, and the phases α and β result from the path length mismatch in Alice and Bob's interferometers. In Fig. 2.2 the count rate for coincidence event $HA0$-$HB1$ is given versus the path length in Alice's interferometer. As predicted, a sinusoidal dependence on the phase is observed. This date was taken with a preliminary Mach-Zehnder based experiment. A similar curve using the final experimental design is given in Fig. 2.8.

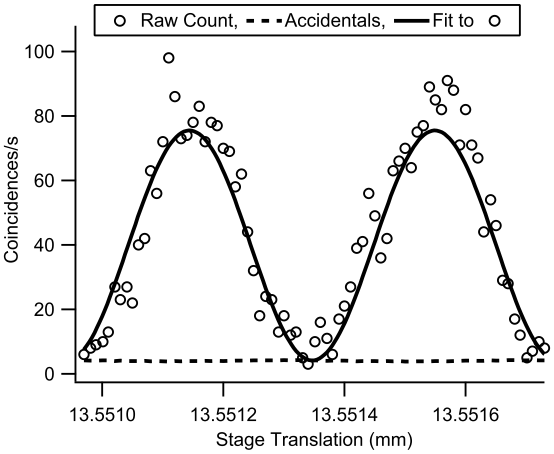

Figure 2.2: Non-Local Franson Interference for detectors HA0 and HB1 with 99.6 ± 2.6% corrected visibility and a 89.5 ± 2.3% raw visibility. This date was collected using a preliminary Mach-Zehnder experiment.

Nonlocal interference in the NPI can be understood with the help of Figs. 2.3 and 2.4, which show four ways that a coincidence can occur. For the input state given in Eq. 2.1, we see in Fig. 2.3 that orthogonally polarized photons are detected

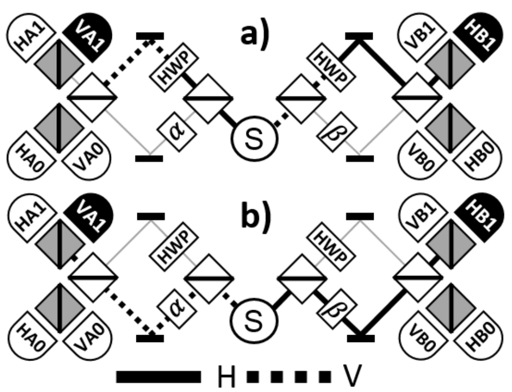

Figure 2.3: Nonlocal interference observed for an orthogonal polarization event VA1HB1 is due to indistinguishable cases a) and b).

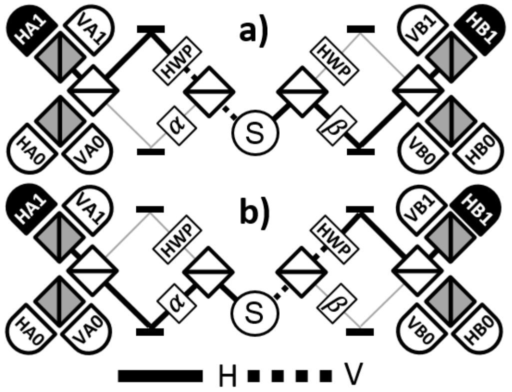

Figure 2.4: Nonlocal interference observed for an identical polarization event HA1HB1 is due to indistinguishable cases a) and b).

only if the polarizations of the photons are both rotated by 90 degrees or if they are both left un-rotated, i.e., if both photons take the upper paths or both take the lower paths. These cases are indistinguishable and equally likely, thereby leading to the orthogonal ($j{\neq}s$) interference pattern of Eq. 2.2. Likewise, in Fig. 2.4 we see that the photons are detected with identical polarizations only if one travels the upper path and one the lower. Interference between these indistinguishable cases leads to the parallel ($j{=}s$) interference pattern in Eq. 2.2.

2.3 A Phase Stable Implementation

The Mach-Zehnder version of the NPI is simple and provides insight into the indistinguishable cases leading to interference. However, the Mach-Zehnder interferometer requires active phase stabilization in order to produce stable nonlocal correlations. To avoid this difficulty, we use a Sagnac-based device that allows observation of the same nonlocal interference effects but in a phase-stable configuration. Typically, a fixed Sagnac or ring interferometer's phase cannot be adjusted due to the common path nature of the device. However, our implementation uses directionally dependent phase modulators (DDPM) as well as directionally dependent polarization rotators.

The DDPM design is reported in [57] as a polarization independent phase modulator. This design is indeed polarization independent, but it is also directionally dependent, i.e. it matters which port the photon is incident. A schematic of our Sagnac NPI design is given in Fig. 2.5.

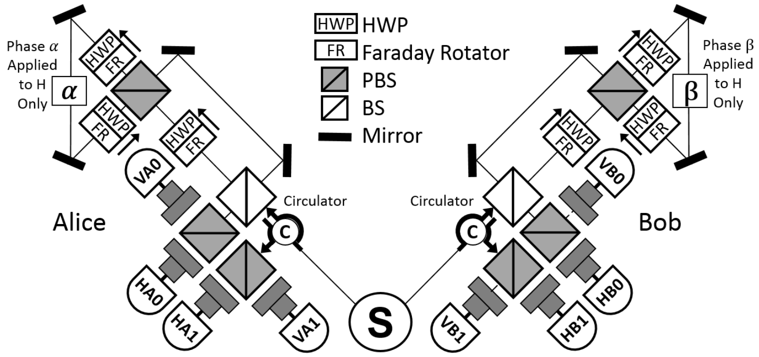

Figure 2.5: Sagnac interferometer setup including directionally dependent phase modulator and dual polarization circulator.

Referencing Bob's interferometer in this figure, photons pass through a circulator to the first BS where they randomly choose the reflected, clockwise (CW), path or they choose the transmitted, counter-clockwise (CCW), path. Photons taking the CW path are then incident on the upper PBS input port of the DDPM. The vertical component of these photons travels CW in the DDPM and the horizontal component travels CCW. In either path, the photons encounter Faraday rotator (FR) and half-wave plate (HWP) combinations that are configured to rotate the polarization 90° in the direction indicated by the arrow aside the FR-HWP. In the direction opposite these arrows the photon polarization is not changed. The phase modulation β is applied only to photons whose polarization is horizontal when they encounter the modulator indicated by β in the figure. It is clear that photons taking the reflected (CW) path in Bob's interferometer gain a phase β, while photons taking the transmitted (CCW) path gain no phase, no matter the polarization. The additional FR-HWP combination in the transmitted path of Bob's interferometer takes on the role of the HWP in the Mach-Zehnder device; It suppresses single-photon interference with a 90° polarization rotation for CCW propagating photons. Given that Alice and

Bob share the Bell state Ψ^+ as in the Mach-Zehnder description, an orthogonal event, Alice and Bob measure different polarizations, in the Sagnac NPI could have resulted from the indistinguishable cases that both Alice and Bob's photons are transmitted through the first BS, or both are reflected. Parallel events, Alice and Bob measure the same polarization, occur from the indistinguishable cases that Alice's photon takes the transmitted path and Bob's the reflected or vice-versa.

2.4 Separable and Entangled States

Assume Alice and Bob share a two-photon state with a density matrix in the polarization basis

$$\rho = \begin{pmatrix} a & b & c & d \\ b^* & e & f & g \\ c^* & f^* & h & j \\ d^* & g^* & j^* & k \end{pmatrix}. \tag{2.3}$$

The NPI includes two input ports per interferometer, with H and V polarization components. The two-photon state is distributed through one input port of each interferometer, while the remaining port is vacuum, see Fig. 2.1 or 2.5. The 16x16 density matrix including all of these components is

$$\rho^{'} = \begin{pmatrix} a & b & 0 & 0 & c & d & 0 & \cdots & 0 \\ b^* & e & 0 & 0 & f & g & 0 & \cdots & 0 \\ 0 & 0 & 0 & 0 & 0 & 0 & 0 & \cdots & 0 \\ 0 & 0 & 0 & 0 & 0 & 0 & 0 & \cdots & 0 \\ c^* & f^* & 0 & 0 & h & k & 0 & \cdots & 0 \\ d^* & g^* & 0 & 0 & k^* & l & 0 & \cdots & 0 \\ 0 & 0 & 0 & 0 & 0 & 0 & 0 & \cdots & 0 \\ \vdots & \vdots & \vdots & \vdots & \vdots & \vdots & \vdots & \ddots & \\ 0 & 0 & 0 & 0 & 0 & 0 & 0 & & 0 \end{pmatrix}.$$

where the zero elements include vacuum components.

The operator representing either Alice or Bob's Sagnac interferometer is

$$M(\phi) = (B \otimes I) \cdot \left(e^{i\phi} Z \oplus X\right) \cdot (B \otimes I)$$

where $\phi \in \{\alpha, \beta\}$,

$$I = \begin{pmatrix} 1 & 0 \\ 0 & 1 \end{pmatrix}, \quad B = \frac{1}{\sqrt{2}} \begin{pmatrix} i & 1 \\ 1 & i \end{pmatrix},$$
$$X = \begin{pmatrix} 0 & 1 \\ 1 & 0 \end{pmatrix}, \quad \text{and} \quad Z = \begin{pmatrix} 1 & 0 \\ 0 & -1 \end{pmatrix}.$$

The operator $\otimes$ indicates the Kronecker product and $\oplus$ indicates the direct sum. The operation $B \otimes I$ expands the BS operation from a single component at each input and output port to include both horizontal and vertical polarization components. The operation $e^{i\phi} Z \oplus X$ represents operations for each path in an interferometer. Photons taking the reflected path in either interferometer have phase modulation ϕ applied. Vertical photons taking the reflected path gain an additional π phase resultant from the subtleties of the FR-HWP polarization rotation. Photons taking the transmitted path have their polarization rotated 90° but gain no phase. The operator for the Mach-Zehnder version of the NPI is found by replacing Z with I. This subtle difference changes the form of many of the equations to come, though the same information is extractable from either device. We will use the Sagnac NPI operator, since our experimental results were taken with this device.

The final density matrix post interferometers is

$$\rho^{''}(\alpha, \beta) = U(\alpha, \beta) \rho^{'} U^{\dagger}(\alpha, \beta)$$

where $U(\alpha,\beta) = M(\alpha)\otimes M(\beta)$. The probability of a coincidence for each combination of Alice and Bob's detectors is given by the diagonal elements of $\rho^{''}(\alpha,\beta)$,

$$\begin{aligned}
P_{\substack{HA0\\HB0}}(\alpha,\beta) &= \rho^{''}_{11}(\alpha,\beta) & P_{\substack{HA0\\VB0}}(\alpha,\beta) &= \rho^{''}_{22}(\alpha,\beta)\\
P_{\substack{HA0\\HB1}}(\alpha,\beta) &= \rho^{''}_{33}(\alpha,\beta) & P_{\substack{HA0\\VB1}}(\alpha,\beta) &= \rho^{''}_{44}(\alpha,\beta)\\
P_{\substack{VA0\\HB0}}(\alpha,\beta) &= \rho^{''}_{55}(\alpha,\beta) & P_{\substack{VA0\\VB0}}(\alpha,\beta) &= \rho^{''}_{66}(\alpha,\beta)\\
P_{\substack{VA0\\HB1}}(\alpha,\beta) &= \rho^{''}_{77}(\alpha,\beta) & P_{\substack{VA0\\VB1}}(\alpha,\beta) &= \rho^{''}_{88}(\alpha,\beta)\\
P_{\substack{HA1\\HB0}}(\alpha,\beta) &= \rho^{''}_{99}(\alpha,\beta) & P_{\substack{HA1\\VB0}}(\alpha,\beta) &= \rho^{''}_{\substack{10\\10}}(\alpha,\beta)\\
P_{\substack{HA1\\HB1}}(\alpha,\beta) &= \rho^{''}_{\substack{11\\11}}(\alpha,\beta) & P_{\substack{HA1\\VB1}}(\alpha,\beta) &= \rho^{''}_{\substack{12\\12}}(\alpha,\beta)\\
P_{\substack{VA1\\HB0}}(\alpha,\beta) &= \rho^{''}_{\substack{13\\13}}(\alpha,\beta) & P_{\substack{VA1\\VB0}}(\alpha,\beta) &= \rho^{''}_{\substack{14\\14}}(\alpha,\beta)\\
P_{\substack{VA1\\HB1}}(\alpha,\beta) &= \rho^{''}_{\substack{15\\15}}(\alpha,\beta) & P_{\substack{VA1\\VB1}}(\alpha,\beta) &= \rho^{''}_{\substack{16\\16}}(\alpha,\beta).
\end{aligned}$$

When the source is a Bell state,

$$\begin{aligned}
\left|\Phi^{\pm}\right\rangle &= (1/\sqrt{2})\left(|H_A\rangle\otimes|H_B\rangle \pm |V_A\rangle\otimes|V_B\rangle\right) \quad \text{or}\\
\left|\Psi^{\pm}\right\rangle &= (1/\sqrt{2})\left(|H_A\rangle\otimes|V_B\rangle \pm |V_A\rangle\otimes|H_B\rangle\right),
\end{aligned}$$

we find the probabilities

$$P_{\substack{jAy\\sBz}}(\alpha,\beta) = \begin{cases} \frac{1}{16}\left\{1+\ell(\text{-}1)^{z+y}\cos\left[\alpha+m\beta\right]\right\} & j\neq s\\[2ex] \frac{1}{16}\left\{1+\ell(\text{-}1)^{z+y}\cos\left[\alpha-m\beta\right]\right\} & j=s \end{cases} \tag{2.4}$$

where ℓ, m values for each Bell state are Ψ^{+}:{1,1},Ψ^{-}:{-1,1},Φ^{+}:{1,-1}, and Φ^{-}:{-1,-1}.

The probability of coincidence for any given port combination depends on the density matrix elements given in Eq. 2.3. This dependence varies with the phases α and β. However, the case α=β= $\pi/4$ is particularly interesting. It is this case that the remainder of this paper will focus on. We refer to the NPI configured with α=β=

$\pi/4$ as NPI$_{\pi/4}$, the standard configuration. With these settings, it is straightforward to show that for the general density matrix ρ given in Eq. 2.3 that

$$P_{\substack{jAy\\sBz}}\Big(\frac{\pi}{4},\frac{\pi}{4}\Big)=\begin{cases}\frac{1}{16}\left[1-(\text{-}1)^{y+z}\left\{d+d^*+i(\delta_{jH}-\delta_{jV})(f-f^*)\right\}+(\text{-}1)^y\sigma_{jA}+(\text{-}1)^z\sigma_{sB}\right] & j\neq s\\ \frac{1}{16}\left[1+(\text{-}1)^{y+z}\left\{i(\delta_{jH}-\delta_{jV})(d-d^*)+f+f^*\right\}+(\text{-}1)^y\sigma_{jA}+(\text{-}1)^z\sigma_{sB}\right] & j=s\end{cases}$$

where

$$\begin{aligned}\sigma_{HA}&=e^{i\pi/4}\{-c-g+i(c^*+g^*)\},\\ \sigma_{VA}&=e^{i\pi/4}\{c^*+g^*-i(c+g)\},\\ \sigma_{HB}&=e^{i\pi/4}\{-b-k+i(b^*+k^*)\},\text{ and}\\ \sigma_{VB}&=e^{i\pi/4}\{b^*+k^*-i(b+k)\}\end{aligned}$$

are proportional to the marginal coherences, i.e. single-photon interference. Defining the polarization dependent correlation coefficient as

$$\mathcal{E}_{js}\equiv\frac{P_{\substack{jA0\\sB0}}(\frac{\pi}{4},\frac{\pi}{4})+P_{\substack{jA1\\sB1}}(\frac{\pi}{4},\frac{\pi}{4})-P_{\substack{jA0\\sB1}}(\frac{\pi}{4},\frac{\pi}{4})-P_{\substack{jA1\\sB0}}(\frac{\pi}{4},\frac{\pi}{4})}{P_{\substack{jA0\\sB0}}(\frac{\pi}{4},\frac{\pi}{4})+P_{\substack{jA1\\sB1}}(\frac{\pi}{4},\frac{\pi}{4})+P_{\substack{jA0\\sB1}}(\frac{\pi}{4},\frac{\pi}{4})+P_{\substack{jA1\\sB0}}(\frac{\pi}{4},\frac{\pi}{4})},\tag{2.5}$$

we find the real-valued coefficients

$$\mathcal{E}_{HH}=f+f^*-i(d-d^*),\tag{2.6}$$

$$\mathcal{E}_{VV}=f+f^*+i(d-d^*),\tag{2.7}$$

$$\mathcal{E}_{HV}=-d-d^*-i(f-f^*),\text{ and}\tag{2.8}$$

$$\mathcal{E}_{VH}=-d-d^*+i(f-f^*)\tag{2.9}$$

where d, d^*, f, and f^* are the anti-diagonal elements of the density matrix ρ given in Eq. 2.3. The correlation coefficients have values $-1\leq\mathcal{E}\leq 1$, with 1(-1) indicating perfect correlation(anti-correlation). Clearly, we have the resulting relations

$$f + f^* = \frac{\mathcal{E}_{HH} + \mathcal{E}_{VV}}{2} \text{ and} \tag{2.10}$$

$$d + d^* = \frac{-\mathcal{E}_{HV} - \mathcal{E}_{VH}}{2}. \tag{2.11}$$

These relations indicate that parallel correlations, HH and VV, are proportional to $f + f^*$. Similarly, orthogonal correlations, HV and VH, are proportional to $d + d^*$. Referencing Table 2.1, Fig. 2.6, and 2.7 we see that each of the Bell states has a unique correlation signature in the NPI. As an example, when measurements are made on the Bell state Ψ^+ we expect no correlation for orthogonal events and perfect correlation for parallel events.

Additionally, it should be clear that the correlation coefficients 2.6, 2.7, 2.8, and 2.9 may also be used to identify the "shifted" Bell states

$$\left|\Phi_s^{\pm}\right\rangle = (1/\sqrt{2})\left(|H_A\rangle \otimes |H_B\rangle \pm i\,|V_A\rangle \otimes |V_B\rangle\right) \tag{2.12}$$

$$\left|\Psi_s^{\pm}\right\rangle = (1/\sqrt{2})\left(|H_A\rangle \otimes |V_B\rangle \pm i\,|V_A\rangle \otimes |H_B\rangle\right). \tag{2.13}$$

Thus, eight maximally entangled states may be uniquely identified, statistically, in the NPI.

Table 2.1: Bell state signatures for $f + f^*$ and $d + d^*$.

	Ψ^+	Ψ^-	Φ^+	Φ^-
$d + d^*$	0	0	1	-1
$f + f^*$	1	-1	0	0

For any state, $|f + f^*| \leq 1$ and $|d + d^*| \leq 1$. However, if we consider the density matrix for a separable pure state

$$\rho_A \otimes \rho_B = |A\rangle\langle A| \otimes |B\rangle\langle B|$$

where

$$|A\rangle = \begin{pmatrix} \sin(a) \\ \cos(a)e^{i\theta_A} \end{pmatrix} \quad \text{and} \quad |B\rangle = \begin{pmatrix} \sin(b) \\ \cos(b)e^{i\theta_B} \end{pmatrix},$$

we find

$$f + f^* = (1/2)\sin(2a)\sin(2b)\cos(\theta_A - \theta_B)$$
$$d + d^* = (1/2)\sin(2a)\sin(2b)\cos(\theta_A + \theta_A)$$

which requires

$$|f + f^*| \leq \frac{1}{2} \quad \text{and} \quad |d + d^*| \leq \frac{1}{2}. \tag{2.14}$$

These inequalities also hold for any separable mixed state of the form

$$\rho_{mix} = \sum_\lambda p_\lambda \rho_A^\lambda \otimes \rho_B^\lambda,$$

since, in this case,

$$f + f^* = \sum_\lambda p_\lambda \left(f_\lambda + f_\lambda^*\right) \quad \text{and}$$
$$d + d^* = \sum_\lambda p_\lambda \left(d_\lambda + d_\lambda^*\right).$$

Thus, the conditions $|f + f^*| > 1/2$ or $|d + d^*| > 1/2$ are required for an entangled state.

Knowledge of $f + f^*$ and $d + d^*$ also determine the minimum Bell state fidelities. The fidelities or overlap of the generic density matrix from Eq. 2.3 with each Bell state are

$$F_{\Phi^\pm} = \left\langle \Phi^\pm \right| \rho \left| \Phi^\pm \right\rangle = \left(a + k \pm [d + d^*]\right)/2 \quad \text{and} \tag{2.15}$$

$$F_{\Psi^\pm} = \left\langle \Psi^\pm \right| \rho \left| \Psi^\pm \right\rangle = \left(e + h \pm [f + f^*]\right)/2. \tag{2.16}$$

Since all density matrices must be positive semi-definite, $\langle\phi|\,\rho\,|\phi\rangle \geq 0$, Eq. 2.15 and 2.16 require

$$a + k \geq |d + d^*| \qquad \text{and} \qquad e + h \geq |f + f^*|\,.$$

These inequalities lead to the minimum fidelity values

$$\begin{aligned}
F_{\psi^+} &\geq (|f + f^*| + f + f^*)/2, \\
F_{\psi^-} &\geq (|f + f^*| - f - f^*)/2, \\
F_{\phi^+} &\geq (|d + d^*| + d + d^*)/2, \text{ and} \\
F_{\phi^-} &\geq (|d + d^*| - d - d^*)/2.
\end{aligned}$$

Only one of these can exceed 1/2 for a given state.

Experimentally, we determine the expectation value of the correlation coefficient given in Eq. 2.5 as

$$\langle \mathcal{E}_{js} \rangle = \frac{\mathcal{C}_{\substack{jA0\\sB0}}(\frac{\pi}{4},\frac{\pi}{4}) + \mathcal{C}_{\substack{jA1\\sB1}}(\frac{\pi}{4},\frac{\pi}{4}) - \mathcal{C}_{\substack{jA0\\sB1}}(\frac{\pi}{4},\frac{\pi}{4}) - \mathcal{C}_{\substack{jA1\\sB0}}(\frac{\pi}{4},\frac{\pi}{4})}{\mathcal{C}_{\substack{jA0\\sB0}}(\frac{\pi}{4},\frac{\pi}{4}) + \mathcal{C}_{\substack{jA1\\sB1}}(\frac{\pi}{4},\frac{\pi}{4}) + \mathcal{C}_{\substack{jA0\\sB1}}(\frac{\pi}{4},\frac{\pi}{4}) + \mathcal{C}_{\substack{jA1\\sB0}}(\frac{\pi}{4},\frac{\pi}{4})},$$

where $\mathcal{C}_{\substack{jAy\\sBz}}(\frac{\pi}{4},\frac{\pi}{4})$ are accidental corrected and normalized coincidence counts for detector combinations jAy and sBz. The experimental measurements of $f + f^*$ and $d + d^*$ made on many copies of an identical state are

$$\begin{aligned}
\langle f + f^* \rangle &= \frac{\langle \mathcal{E}_{HH} \rangle + \langle \mathcal{E}_{VV} \rangle}{2} \text{ and} \\
\langle d + d^* \rangle &= \frac{-\langle \mathcal{E}_{HV} \rangle - \langle \mathcal{E}_{VH} \rangle}{2}.
\end{aligned}$$

Entanglement is detected when sufficient experimental statistics are gathered to indicate that

$$|\,\langle f + f^* \rangle\,| > 1/2 \text{ or} \tag{2.17}$$

$$|\,\langle d + d^* \rangle\,| > 1/2. \tag{2.18}$$

Maximally entangled states will have experimental values $|\langle f + f^* \rangle| \rightarrow 1$ or $|\langle d + d^* \rangle| \rightarrow 1$. For any experiment in which the source is static, unchanging, these simple frequency based statistics will hold, and confirmation of Eq. 2.17 or 2.18 will indicate an entangled state with high confidence. Experimental results for each Bell state are plotted in Fig. 2.6 along with a graphical depiction of the bounds given for separable and entangled states. These results with standard deviations are also given in Table 2.2. We have also given the expected and observed values for the correlation coefficients $\mathcal{E}_{HH}$, $\mathcal{E}_{VV}$, $\mathcal{E}_{HV}$, and $\mathcal{E}_{VH}$ for each Bell state in the standard configuration in Fig. 2.7. Each of these figures graphically depicts each Bell state's unique correlation signature.

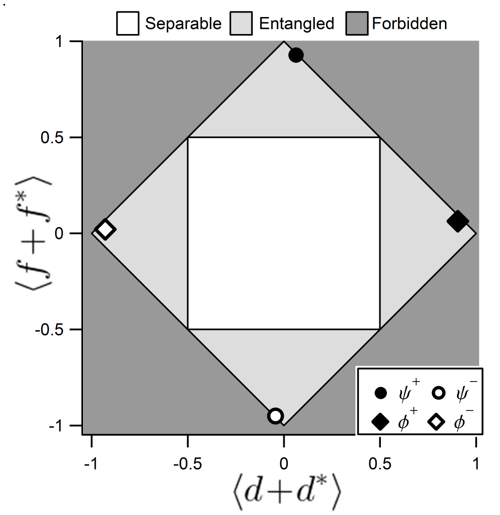

Figure 2.6: Separable and entangled state bounds for parameters $f + f^*$ and $d + d^*$ with corresponding measurement values for the four Bell states indicated by dots and diamonds.

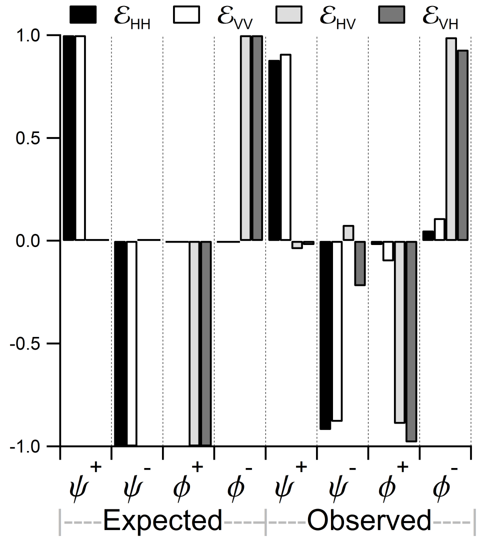

Figure 2.7: Expected and observed values for the correlation coefficients $\mathcal{E}_{HH}$, $\mathcal{E}_{VV}$, $\mathcal{E}_{HV}$, and $\mathcal{E}_{VH}$ in the standard configuration for each Bell state. Standard deviations for these coefficients are ≤ 0.06.

To further illustrate that correlations are directly linked to $f + f^*$ and $d + d^*$, we vary these values using a phase modulator and experimentally determine their value. Results for "ψ"-like states $\psi(\theta) \propto HV + e^{i\theta} VH$ are given in Fig. 2.8 (a), where $\cos\theta = f + f^*$ and θ varies with voltage. Similarly, the results for "ϕ"-like states

$\phi(\gamma) \propto HH + e^{i\gamma}VV$ are given in Fig. 2.8 (b), where $\cos\gamma = d + d^*$ and γ varies with voltage. The voltages $V_{2\pi}$ and V_π are associated with "+" and "-" Bell states, respectively. The phase dependence on voltage is nonlinear but approaches linearity in the region between $V_{2\pi}$=1.15V and V_π=1.75V.

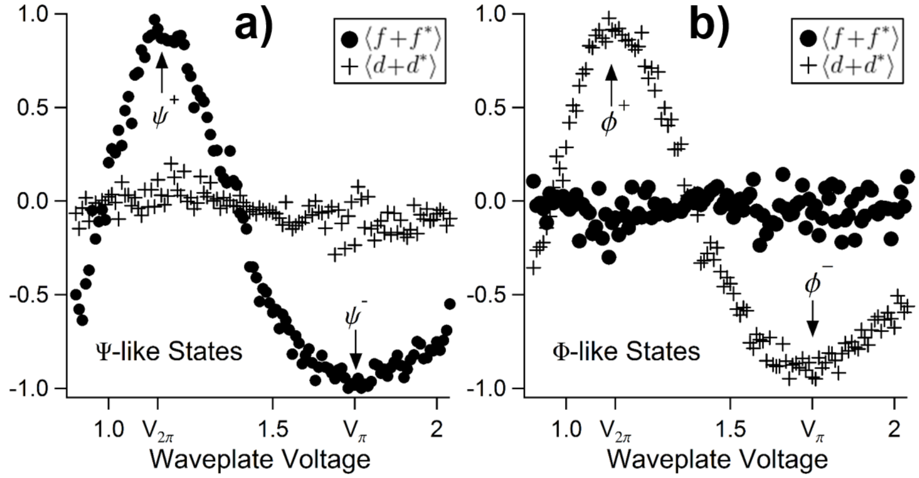

Figure 2.8: a) Variation of phase θ in state $\psi(\theta) \propto HV + e^{i\theta}VH$ using a liquid crystal waveplate. b) Variation of phase γ in state $\phi(\gamma) \propto HH + e^{i\gamma}VV$ using a liquid crystal waveplate.

2.5 A Novel Bell Test

CHSH-Bell tests [45] are commonly carried out using a polarization-based experiment as seen in Fig. 2.9. For states that obey locality constraints, the Bell parameter S obeys the inequality

$$|S| = |E(a_0, b_0) + E(a_0, b_1) + E(a_1, b_0) - E(a_1, b_1)| \leq 2$$

where $a_0, a_1, b_0,$ and b_1 are local realities such as polarization rotation, and the correlation coefficient is

$$E(a, b) = P_{HH}(a, b) + P_{VV}(a, b) - P_{HV}(a, b) - P_{VH}(a, b)$$

where $P_{js}(a,b)$ is the probability of a coincidence between Alice's j polarization detector and Bob's s polarization detector given the local realities a and b for Alice and Bob, respectively. The experimental estimate of the correlation coefficient in the CHSH-Bell test is

$$\langle E(a,b)\rangle = \frac{\mathcal{C}_{HH}(a,b)+\mathcal{C}_{VV}(a,b)-\mathcal{C}_{HV}(a,b)-\mathcal{C}_{VH}(a,b)}{\mathcal{C}_{HH}(a,b)+\mathcal{C}_{VV}(a,b)+\mathcal{C}_{HV}(a,b)+\mathcal{C}_{VH}(a,b)}$$

with coincidence counts $\mathcal{C}_{js}(a,b)$.

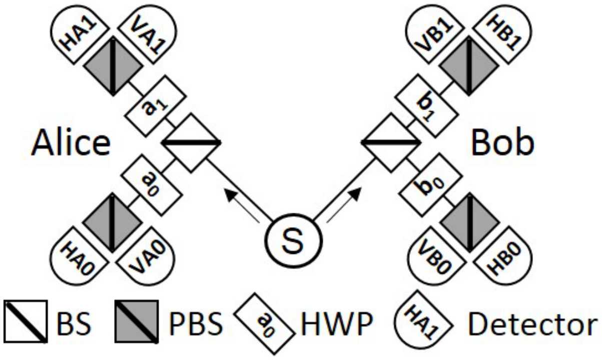

Figure 2.9: A typical Bell test. An entangled photon pair is shared between Alice and Bob whose local measurement settings or local realities a_0, a_1, b_0, and b_1 are randomly chosen by a symmetric beamsplitter.

Since the polarization of any photon exiting the NPI is random, the final photon polarization represents a "local reality". Therefore, a unique CHSH-Bell test may be performed based on the four random photon polarization outcomes HH, VV, HV, or VH. To maximize violation of the inequality, Bob applies a $\pi/4$ phase to his vertical photon prior to its entry into his interferometer. We call this configuration $\mathrm{NPI}^{\mathrm{Bell}}_{\pi/4}$.

In this case, the correlation coefficients are

$$\mathcal{E}^{'}_{HH} = \frac{1}{\sqrt{2}}\left(f+f^{*}-i(f-f^{*})+d+d^{*}+i(d-d^{*})\right) \tag{2.19}$$

$$\mathcal{E}^{'}_{VV} = \frac{1}{\sqrt{2}}\left(f+f^{*}-i(f-f^{*})-d-d^{*}-i(d-d^{*})\right) \tag{2.20}$$

$$\mathcal{E}^{'}_{HV} = \frac{1}{\sqrt{2}}\left(-f-f^{*}-i(f-f^{*})-d-d^{*}+i(d-d^{*})\right) \tag{2.21}$$

$$\mathcal{E}^{'}_{VH} = \frac{1}{\sqrt{2}}\left(f+f^{*}+i(f-f^{*})-d-d^{*}+i(d-d^{*})\right). \tag{2.22}$$

We define the two Bell parameters

$$S_{\psi} \equiv \mathcal{E}^{'}_{HH} + \mathcal{E}^{'}_{VV} - \mathcal{E}^{'}_{HV} + \mathcal{E}^{'}_{VH} = 2\sqrt{2}(f+f^{*}) \text{ and} \tag{2.23}$$

$$S_{\phi} \equiv \mathcal{E}^{'}_{HH} - \mathcal{E}^{'}_{VV} - \mathcal{E}^{'}_{HV} - \mathcal{E}^{'}_{VH} = 2\sqrt{2}(d+d^{*}). \tag{2.24}$$

The Bell parameter S is proportional to the anti-diagonal elements of the density matrix, similar to the results in the last section. As indicated by Eq. 2.14, these Bell parameters have a separable state bound of $|S| \leq \sqrt{2}$ based on quantum mechanics, not on arguments of locality. Clearly, the S parameters' dependence on $f+f^{*}$ and $d+d^{*}$ enable Bell state identification, as was possible in the standard configuration $\mathrm{NPI}_{\pi/4}$. As in the standard configuration, Bell parameters can be defined for each of the shifted Bell states. The experimental measurements

$$\langle S_{\psi}\rangle = \langle \mathcal{E}^{'}_{HH}\rangle + \langle \mathcal{E}^{'}_{VV}\rangle - \langle \mathcal{E}^{'}_{HV}\rangle + \langle \mathcal{E}^{'}_{VH}\rangle = 2\sqrt{2}\langle f+f^{*}\rangle$$
$$\langle S_{\phi}\rangle = \langle \mathcal{E}^{'}_{HH}\rangle - \langle \mathcal{E}^{'}_{VV}\rangle - \langle \mathcal{E}^{'}_{HV}\rangle - \langle \mathcal{E}^{'}_{VH}\rangle = 2\sqrt{2}\langle d+d^{*}\rangle$$

for each Bell state are graphically depicted in Fig. 2.10 and given with standard deviations in Table 2.2. As they should, the Bell parameters $\langle S_{\psi}\rangle$ and $\langle S_{\phi}\rangle$ exceed the $|S| \leq 2$ bound for the appropriate Bell states. We have also given the expected and observed values for the correlation coefficients $\mathcal{E}_{HH}$, $\mathcal{E}_{VV}$, $\mathcal{E}_{HV}$, and $\mathcal{E}_{VH}$ for each

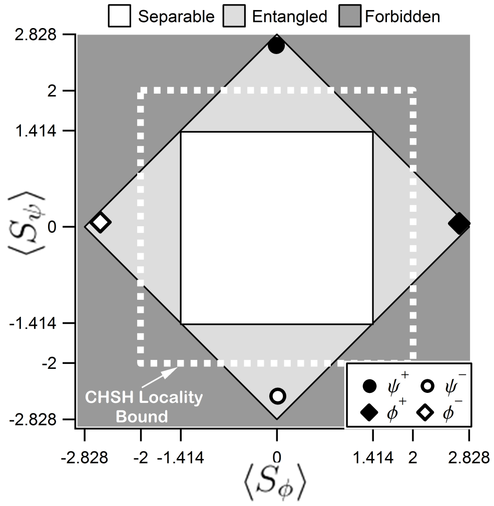

Figure 2.10: Separable and entangled state bounds for parameters $\mathcal{S}_\psi$ and $\mathcal{S}_\phi$ with corresponding measurement values for the four prepared Bell states indicated by dots and diamonds.

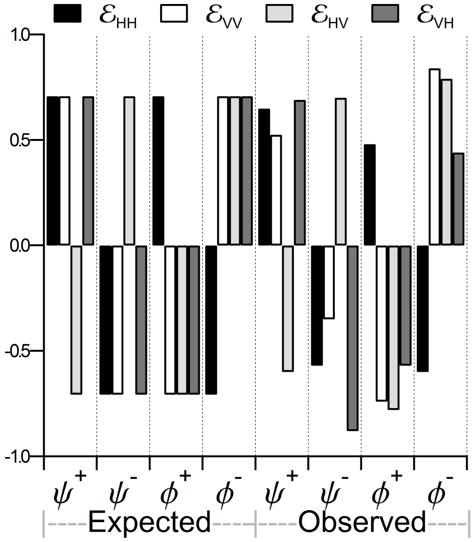

Figure 2.11: Expected and observed values for the correlation coefficients $\mathcal{E}_{HH}$, $\mathcal{E}_{VV}$, $\mathcal{E}_{HV}$, and $\mathcal{E}_{VH}$ in the CHSH configuration for each Bell state. Standard deviations for these coefficients are ≤ 0.06.

Bell state in the CHSH configuration in Fig. 2.11. Each of these figures graphically depicts the unique correlation signatures for each Bell state.

2.6 Experimental Demonstration

Our experimental results were observed using the apparatus shown in Fig. 2.12. In this experiment 0.9 mW of 405 nm continuous-wave (CW) diode laser light pumps a PPKTP crystal generating approximately 1.4×10^6 Type II signal-idler pairs per second at a wavelength of 810 nm from the spontaneous parametric downconversion process. The signal and idler pass through a compensation system which removes the phase resultant from the polarization-dependent walk-off due to the nonlinear crystal and optical fiber. After passing through the fiber, photons are incident on a BS which produces a polarization entangled shared state when the signal and idler are spectrally indistinguishable[*]. This indistinguishability requirement may be removed by using a true polarization entangled source [58, 59]. Beamsplitters are used as lossy circulators. Phase modulation in each interferometer is applied using liquid crystal variable wave plates. At each interferometer output port a PBS routes each polarization to separate single-photon detectors through single-mode fiber. In order to determine coincidence rates we time-stamp the detection signal from each single-photon detector into 5 ns time bins using an FPGA[†]. Eight Perkin-Elmer, now Excelitas, SPCM devices are used to count single-photons. Single photon count rates range from 3-10 kcps and average coincidence rates range from 2-20 cps. Results in Fig. 2.6, 2.7, 2.10, 2.11, and Table 2.2 were generated from 100 sec counts. Results of phase variation, seen in Fig. 2.8, were generated from 5 sec counts at each voltage setting.In order to normalize our coincidence counts, we calibrate the NPI with a known unentangled source[‡] which provides the same flux of photons in each path. This enables determination of the relative efficiency of each detector combination. Due to imperfect optics and experimental shortcomings, single-photon interference is observed with 1% visibility.

---

[*] A non-degenerate signal and idler would destroy the polarization entanglement, since the photon energy would be associated with a specific polarization. This setup also leads to local two-photon interference when the photons both go to Alice or Bob's interferometers. A local effect observed is Hong-Ou-Mandel (HOM) interference which is maximized when the signal and idler are spectrally indistinguishable. The visibility of HOM interference was used to tune the signal and idler indistinguishability.

[†] See www.zedboard.com and www.xillybus.com.

[‡] The signal and idler were made spectrally distinguishable by tuning the temperature of the PPKTP crystal. Distinguishability was verified by vanishing local HOM interference, see * above. This distinguishability destroys the polarization entanglement.

Table 2.2: Experimental results for $\langle f + f^* \rangle$ and $\langle d + d^* \rangle$ and Bell parameters $\langle \mathcal{S}_\psi \rangle$ and $\langle \mathcal{S}_\phi \rangle$ using accidental corrected and normalized 100 second coincidence counts. These results demonstrate unique signatures for each Bell state.

	Ψ^+	Ψ^-	Φ^+	Φ^-
$\langle f + f^* \rangle$	0.96±0.01	-0.94±0.05	-0.07±0.05	0.07±0.04
$\langle d + d^* \rangle$	0.08±0.05	-0.07±0.05	0.90±0.04	-0.90±0.01
$\langle \mathcal{S}_\psi \rangle$	2.46±0.26	-2.51±0.35	0.04±0.36	-0.01±0.23
$\langle \mathcal{S}_\phi \rangle$	0.04±0.26	-0.05±0.35	2.57±0.36	-2.66±0.23

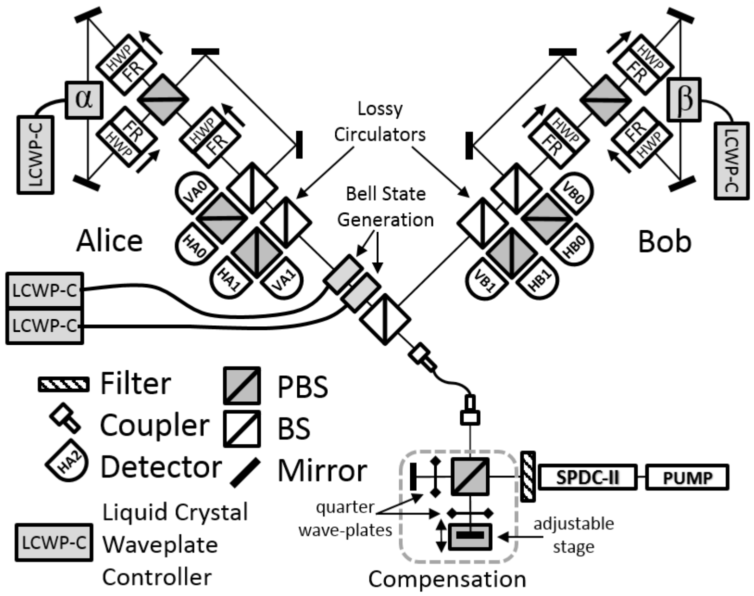

Figure 2.12: The NPI Sagnac experiment includes a polarization entangled source dependent on the spectral indistinguishability of the signal and idler photons. Bell states were generated by polarization rotation and phase modulation in the path to Alice's interferometer.

Our experimental results qualitatively agree with our theoretical predictions. This can be seen for the standard configuration by comparing Eqs. 2.6, 2.7, 2.8, 2.9, 2.10, 2.11, and Table 2.1 with Figs. 2.6, 2.7, and Table 2.2. For the CHSH configuration, compare Eqs. 2.19, 2.20, 2.21, 2.22, 2.23, 2.24 with Figs. 2.10, 2.11 and Table 2.2. Clearly, these experiments verify the unique correlation signatures predicted for each entangled Bell state.

2.7 Local Two-Photon Interference

The experimental source as described in Section 2.6 results in the two-photon pair (both photons) going to only Alice or only Bob half of the time. Consider the Mach-Zehnder configuration in Fig. 2.1. When both photons enter Bob's interferometer, two types of interference effects can be observed. In the first, the two photons reach the detectors with orthogonal polarizations. As illustrated in Fig. 2.13(a), this can happen only if both photons take the same local path, both in the upper path or both in the lower path. The probability for this type of coincidence is

$$P_{\substack{jBz \\ sBy}} \propto \frac{1}{2}\left\{1 + (-1)^{z+y}\cos\left[2\beta\right]\right\} \quad (s \perp j) \tag{2.25}$$

where $2\beta \approx 2\pi c/\lambda_p$ and λ_p is the pump wavelength. Because the probability of coincidence depends on the wavelength of the biphoton, a composite particle made up of the signal and idler with wavelength approximately equal to the pump wavelength λ_p, we refer to this as de Broglie interference [60, 61]. As is seen in Eq. 2.25, de Broglie interference reveals Bob's local phase β. In this configuration, maximum correlations are achieved when the signal and idler are spectrally and temporally indistinguishable.

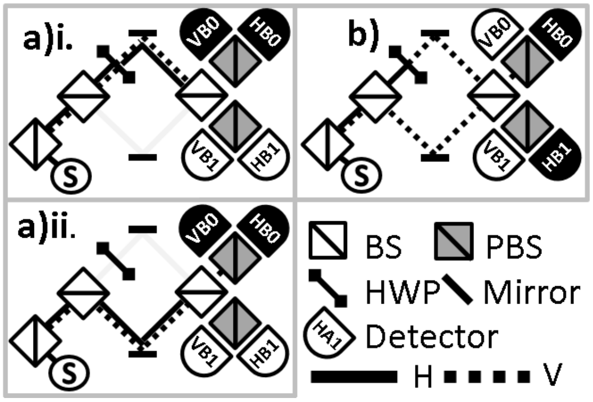

Figure 2.13: a) Indistinguishable cases (i) and (ii) lead to de Broglie Interference observed in Bob's interferometer by detectors VB0 and HB0. b) Indistinguishable photons incident on different ports of a beamsplitter lead to Hong-Ou-Mandel interference observed as a dip in different port coincidences.

The second type of local interference is observed when the two photons emerge from the interferometer with identical polarizations. Because they enter the interferometer with orthogonal polarizations, this can happen only if the two photons take different paths, as depicted in Fig. 2.13(b). In this case, the polarization of one photon is rotated by 90°, and they meet at the second beam splitter (BS) with identical polarizations. This results in HOM [24] interference, and the coincidence rate is predicted to fall to zero when the photons are spectrally and temporally indistinguishable.

A preliminary experiment based on the the Mach-Zehnder interferometer allowed observation of both de Broglie and HOM interference as seen in Fig. 2.14 and 2.15. Additionally, as mentioned in Section 2.6, the visibility of HOM interference was used to establish indistinguishability in the Sagnac NPI experiment.

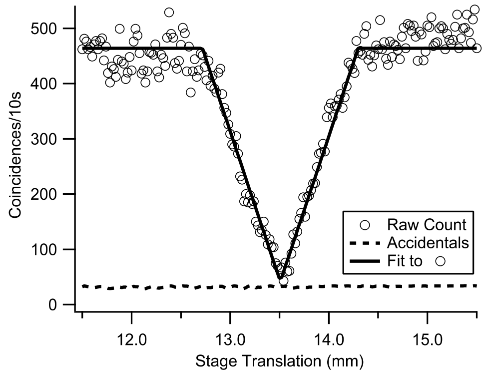

Figure 2.14: Hong-Ou-Mandel Dip in Bob's Interferometer with 97.8 ± 0.5% corrected visibility and a 91 ± 0.5% raw visibility.

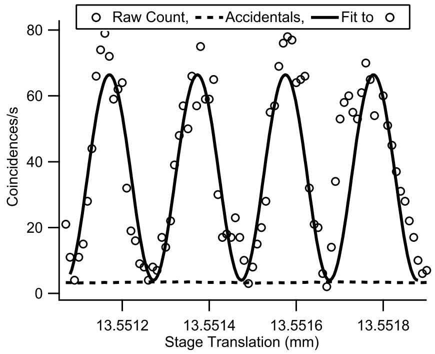

Figure 2.15: Local de Broglie Interference observed in Bob's interferometer by detectors VB0 and HB1 with 98 ± 4% corrected visibility and a 88.8 ± 3.5% raw visibility.

2.8 A Multi-Mode Analysis

In this section a full multi-mode treatment of the NPI is given. One feature made clear from this calculation is that the coherence properties of the pump photon are typically insignificant. This can be compared to the Franson interferometer which only works if the pump photon's coherence time exceeds the interferometer imbalance which in turn exceeds the single photon coherence time. The balanced nature of the NPI and its single-photon interference suppression using polarization rotation allows utilization of a pulsed pump or, perhaps, a more economical pumping option with poor coherence properties. These statements are assuming that the source is not such that the spectral properties of the signal and idler correlate with the polarization. This would be the case in the experimental demonstration, described in Section 2.5, using a short coherence time pump.

As in [23] let us assume an inexhaustible horizontally polarized pump state $|\alpha_h\rangle$, a spectral amplitude $A(\omega)$ representing a stationary random process, and a power spectrum $S(\omega)$ such that

$$\hat{a}_h(\omega)|\alpha_h\rangle = A(\omega)|\alpha_H\rangle, \tag{2.26}$$

$$\langle A^*(\omega') A(\omega)\rangle = 2\pi S(\omega)\,\delta(\omega' - \omega). \tag{2.27}$$

If we assume experimental conditions such that the down-conversion interaction is maximized, the two-photon state is

$$|\psi_0\rangle = \gamma \iint d\omega d\omega' \phi(\omega, \omega')\, A(\omega + \omega')\hat{a}_H^\dagger(\omega)\hat{a}_V^\dagger(\omega')\,|0\rangle \tag{2.28}$$

with γ defined by Eq. A.46. Integrals without limits of integration will be understood here and after to be integrated over $\{-\infty, \infty\}$.

The phase-matching function is

$$\phi(\omega, \omega') = L\ \operatorname{sinc}(\Delta k L/2)\, e^{-i\Delta k L/2} \tag{2.29}$$

with nonlinear crystal length L. The phase mismatch for a Type II process is approximately [25]

$$\Delta k = k_p - k - k' \approx \left(\omega - \frac{\omega_p}{2}\right)\gamma_o + \left(\omega' - \frac{\omega_p}{2}\right)\gamma_e \tag{2.30}$$

with $\gamma_i = \left.\frac{\partial k_i(\omega)}{\partial \omega}\right|_{\omega=\omega_p/2} - \left.\frac{\partial k_p(\omega)}{\partial \omega}\right|_{\omega=\omega_p}$ and $i = \{o, e\}$ indicating ordinary and extraordinary, respectively.

Assume that the optical configuration, for example see [58], allows the state given in Eq. 2.28 to evolve into the polarization entangled state

$$|\Psi_0\rangle = \frac{\gamma}{\sqrt{2}} \iint d\omega d\omega' A(\omega + \omega')\phi(\omega, \omega') \left(\hat{a}^\dagger_{Ha}(\omega)\hat{a}^\dagger_{nb}(\omega') + \ell \hat{a}^\dagger_{Va}(\omega)\hat{a}^\dagger_{n'b}(\omega')\right)|0\rangle \tag{2.31}$$

which represents each of the Bell states given specific values for n, n' and ℓ as seen in Table 2.3.

Table 2.3: Variables for Bell state representation.

	Ψ^+	Ψ^-	Φ^+	Φ^-
n	V	V	H	H
n'	H	H	V	V
ℓ	1	-1	1	-1

The state at the detectors is

$$|\Psi\rangle = \frac{\gamma}{\sqrt{8}} \iint d\omega d\omega' A(\omega + \omega')\phi(\omega, \omega') \sum_{g,h=H}^{V} \sum_{q,p=0}^{1} (\text{-}i)^{q+p} F_{\substack{gq\\hp}}(\omega, \omega')\hat{a}^\dagger_{gaq}(\omega)\hat{a}^\dagger_{hbp}(\omega')|0\rangle \tag{2.32}$$

with

$$
\begin{aligned}
F_{\substack{gq\\hp}}(\omega,\omega') =&\delta_{gH}\delta_{hn}\Big(e^{i(\omega t_{ar}+\omega' t_{br}+t_{aH}+t_{bn})}+\ell(\text{-}1)^{q+p}e^{i(\omega t_{at}+\omega' t_{bt}+t_{aV}+t_{bn'})}\Big)\\
&-\delta_{gH}\delta_{hn'}\Big(e^{i(\omega t_{ar}+\omega' t_{bt}+t_{aH}+t_{bn})}+\ell(\text{-}1)^{q+p}e^{i(\omega t_{at}+\omega' t_{br}+t_{aV}+t_{bn'})}\Big)\\
&-\delta_{gV}\delta_{hn}\Big(e^{i(\omega t_{at}+\omega' t_{br}+t_{aH}+t_{bn})}+\ell(\text{-}1)^{q+p}e^{i(\omega t_{ar}+\omega' t_{bt}+t_{aV}+t_{bn'})}\Big)\\
&+\delta_{gV}\delta_{hn'}\Big(e^{i(\omega t_{at}+\omega' t_{bt}+t_{aH}+t_{bn})}+\ell(\text{-}1)^{q+p}e^{i(\omega t_{ar}+\omega' t_{br}+t_{aV}+t_{bn'})}\Big). \qquad (2.33)
\end{aligned}
$$

where $t_{ar}(t_{br})$ and $t_{at}(t_{bt})$ are the time-of-flight for the path reflected and transmitted from Alice's(Bob's) first beamsplitter, respectively. The times $t_{aH}(t_{bH})$ and $t_{aV}(t_{bV})$ are times-of-flight for horizontally and vertically polarized photons, respectively, from the source to Alice's(Bob's) interferometer. These times in the ideal case are equal for each interferometer, but effects such as polarization mode dispersion in optical fiber can create a differential between them.

Using the second-correlation function

$$
\begin{aligned}
\Gamma^{(2)}_{\substack{jAy\\sBz}}(t,\tau) &= \left|\langle 0|\,\hat{a}_{sBz}(t+\tau)\hat{a}_{jAy}(t)|\psi\rangle\right|^2\\
&=\Bigg|\langle 0|\,\frac{\gamma}{8\pi\sqrt{2}}\iiiint d\omega d\omega' d\Omega d\Omega' A(\omega+\omega')\phi(\omega,\omega')\\
&\qquad\times\sum_{g,h=H}^{V}\sum_{q,p=0}^{1}(-i)^{q+p}F_{\substack{gq\\hp}}(\omega,\omega')e^{i\Omega'(t+\tau)}e^{i\Omega t}\hat{a}_{jay}(\Omega)\hat{a}_{sbz}(\Omega')\hat{a}^{\dagger}_{gaq}(\omega)\hat{a}^{\dagger}_{hbp}(\omega')\,|0\rangle\Bigg|^2\\
&=\left|\frac{\gamma}{8\pi\sqrt{2}}\iint d\omega d\omega' A(\omega+\omega')\phi(\omega,\omega')(-i)^{y+z}F_{\substack{jy\\sz}}(\omega,\omega')e^{i(\omega+\omega')t}e^{i\omega'\tau}\right|^2\\
&=\frac{\gamma^2}{64\pi}\iint d\omega d\omega' S(\omega+\omega')\delta(\omega+\omega'-\Omega-\Omega')\phi^*(\Omega,\Omega')\phi(\omega,\omega')\\
&\qquad\qquad\times F^*_{\substack{jy\\sz}}(\Omega,\Omega')F_{\substack{jy\\sz}}(\omega,\omega')e^{i(\omega+\omega'-\Omega-\Omega')t}e^{i(\omega'-\Omega')\tau}, \quad (2.34)
\end{aligned}
$$

the probability that a signal photon exits interferometer port jxy at time t and an idler photon exits port suz at a relative time between -T_R and T_R is

$$P_{\substack{jxy\\suz}}(t)=\int_{-T_R}^{T_R} d\tau \Gamma^{(2)}_{\substack{jxy\\suz}}(t,\tau). \tag{2.35}$$

In an actual experiment more than a single signal-idler pair will be generated and the experiment occurs over a finite time. We assume there is an average time between down-conversion events T_{DC}, a timing resolution T_R, and a single-photon coherence time T_C. If $T_{DC} >> T_R >> T_C$, we can let $T_R \to \infty$ in the calculation. In other words, we have the opportunity to detect each photon pair well before another pair arrives and the window for a detection is much larger than the single-photon temporal wave packet. Note that these timing assumptions are less stringent than the comparable calculation for the Franson interferometer. The NPI calclulation is simpler because no cases are temporally excluded like they are in Franson's desgin. Using the relation

$$\int_{-\infty}^{\infty} dte^{i(\omega-\Omega)t} = 2\pi\delta(\omega-\Omega) \tag{2.36}$$

we get the time-independent coincidence probability

$$\begin{aligned}
P_{\substack{jAy\\sBz}} &= \frac{\gamma^2}{32}\iint d\omega d\omega' S(\omega+\omega')|\phi(\omega,\omega')|^2 |F_{\substack{jy\\sz}}(\omega,\omega')|^2 \\
&= \frac{\gamma^2}{32}\iint d\omega d\omega' S(\omega+\omega')|\phi(\omega,\omega')|^2 \\
&\qquad \times \delta_{jH}\delta_{sV}\Big(2+\ell(\text{-}1)^{y+z}\Big\{e^{-i\omega(\Delta_a-\delta_a)}e^{-i\omega' m(\Delta_b+\delta_b)}+c.c.\Big\}\Big) \\
&\qquad + \delta_{jH}\delta_{sH}\Big(2+\ell(\text{-}1)^{y+z}\Big\{e^{-i\omega(\Delta_a-\delta_a)}e^{i\omega' m(\Delta_b-\delta_b)}+c.c.\Big\}\Big) \\
&\qquad + \delta_{jV}\delta_{sV}\Big(2+\ell(\text{-}1)^{y+z}\Big\{e^{i\omega(\Delta_a+\delta_a)}e^{-i\omega' m(\Delta_b+\delta_b)}+c.c.\Big\}\Big) \\
&\qquad + \delta_{jV}\delta_{sH}\Big(2+\ell(\text{-}1)^{y+z}\Big\{e^{i\omega(\Delta_a+\delta_a)}e^{i\omega' m(\Delta_b-\delta_b)}+c.c.\Big\}\Big)
\end{aligned} \tag{2.37}$$

where $\Delta_a = t_{ar} - t_{at}$, $\delta_a = t_{aV} - t_{aH}$, $\Delta_b = t_{br} - t_{bt}$, $\delta_b = t_{bV} - t_{bH}$, and ℓ, m values for each Bell state are Ψ^+:{1,1},Ψ^-:{-1,1},Φ^+:{1,-1}, and Φ^-:{-1,-1}. Now we make the change of variables

$$\omega = \frac{\omega_p}{2} + \Omega \quad \text{and} \quad \omega' = \frac{\omega_p}{2} - \Omega \tag{2.38}$$

the probability may be rewritten

$$\begin{aligned} P_{\substack{jAy \\ sBz}} = \frac{\gamma^2}{32} \int d\omega_p \, d\Omega \;\; S(\omega_p) \left| \phi\left(\Omega\right) \right|^2 \times \\ \Big[\delta_{jH}\delta_{sV} \Big(2 + \ell(\text{-}1)^{y+z} \Big\{ e^{-i\frac{\omega_p}{2}(\Delta_a + m\Delta_b - \delta_a + m\delta_b)} e^{-i\Omega(\Delta_a - m\Delta_b - \delta_a - m\delta_b)} + c.c. \Big\} \Big) \\ + \delta_{jH}\delta_{sH} \Big(2 + \ell(\text{-}1)^{y+z} \Big\{ e^{-i\frac{\omega_p}{2}(\Delta_a - m\Delta_b - \delta_a + m\delta_b)} e^{-i\Omega(\Delta_a + m\Delta_b - \delta_a - m\delta_b)} + c.c. \Big\} \Big) \\ + \delta_{jV}\delta_{sV} \Big(2 + \ell(\text{-}1)^{y+z} \Big\{ e^{-i\frac{\omega_p}{2}(\Delta_a - m\Delta_b + \delta_a - m\delta_b)} e^{i\Omega(\Delta_a + m\Delta_b + \delta_a + m\delta_b)} + c.c. \Big\} \Big) \\ + \delta_{jV}\delta_{sH} \Big(2 + \ell(\text{-}1)^{y+z} \Big\{ e^{-i\frac{\omega_p}{2}(\Delta_a + m\Delta_b + \delta_a - m\delta_b)} e^{i\Omega(\Delta_a - m\Delta_b + \delta_a + m\delta_b)} + c.c. \Big\} \Big) \Big] \end{aligned} \tag{2.39}$$

where the phase-matching function square norm is

$$\left| \phi\left(\Omega\right) \right|^2 = L^2 \, \mathrm{Sinc}^2 \left(\frac{\Omega}{2\Omega_-} \right), \tag{2.40}$$

$\Omega_- = (L|\gamma_e - \gamma_o|)^{-1}$, and the power spectrum is assumed to be Gaussian

$$S(\omega_p) = \frac{1}{\sqrt{2\pi\sigma^2}} e^{-\frac{(\omega_p - \omega_{p0})^2}{2\sigma^2}}. \tag{2.41}$$

We use the integral

$$\int_{-\infty}^{\infty} \mathrm{Sinc}^2\left(x\right) e^{iax} = \pi \bigwedge \left(a/2\right) \tag{2.42}$$

where the triangular function is defined as

$$\bigwedge\left(x\right) = \begin{cases} 1 - |x| & \text{if } |x| \leq 1 \\ 0 & \text{otherwise,} \end{cases} \tag{2.43}$$

the integral

$$\frac{1}{\sqrt{2\pi\sigma^2}}\int_{-\infty}^{\infty} e^{-\frac{(\omega_p-\omega_{p0})^2}{2\sigma^2}} e^{ia\omega_p} = e^{-\frac{\sigma^2}{2}a} e^{ia\omega_{p0}}, \tag{2.44}$$

and, calculating from Eq. A.46, that

$$\gamma^2 = \frac{1}{2\Omega_- L^2} \tag{2.45}$$

to obtain the result

$$\begin{aligned}
&P_{\substack{jAy\\sBz}} = \frac{1}{16}\times \\
&\Big\{\ \delta_{jH}\delta_{sV}\Big[1+\ell(\text{-}1)^{y+z} e^{-\frac{\sigma^2}{4}(\Delta_a+m\Delta_b-\delta_a+m\delta_b)} \bigwedge\left(\Omega_-\{\Delta_a-m\Delta_b-\delta_a-m\delta_b\}\right) \\
&\qquad\qquad \times\text{Cos}\left(\frac{\omega_{p0}}{2}\{\Delta_a+m\Delta_b-\delta_a+m\delta_b\}\right)\Big] \\
&+\delta_{jH}\delta_{sH}\Big[1+\ell(\text{-}1)^{y+z}\bigwedge\left(\Omega_-\{\Delta_a+m\Delta_b+\delta_a+m\delta_b\}\right) \\
&\qquad\qquad \times\text{Cos}\left(\frac{\omega_{p0}}{2}\{\Delta_a-m\Delta_b+\delta_a-m\delta_b\}\right)\Big] \\
&+\delta_{jV}\delta_{sV}\Big[1+\ell(\text{-}1)^{y+z}\bigwedge\left(\Omega_-\{\Delta_a+m\Delta_b-\delta_a-m\delta_b\}\right) \\
&\qquad\qquad \times\text{Cos}\left(\frac{\omega_{p0}}{2}\{\Delta_a-m\Delta_b-\delta_a+m\delta_b\}\right)\Big] \\
&+\delta_{jV}\delta_{sH}\Big(1+\ell(\text{-}1)^{y+z}\bigwedge\left(\Omega_-\{\Delta_a-m\Delta_b+\delta_a+m\delta_b\}\right) \\
&\qquad\qquad \times\text{Cos}\left(\frac{\omega_{p0}}{2}\{\Delta_a+m\Delta_b+\delta_a-m\delta_b\}\right)\Big]\Big\}
\end{aligned} \tag{2.46}$$

where ℓ, m values for each Bell state are Ψ^+:{1,1},Ψ^-:{-1,1},Φ^+:{1,-1}, and Φ^-:{-1,-1}. Under typical conditions $\delta_a = \delta_b = 0$, reducing the probability to

$$\begin{aligned} P_{\substack{jAy\\sBz}} &= \frac{1}{16}\times \\ &\Big[\ (\delta_{jH}\delta_{sV}+\delta_{jV}\delta_{sH})\left(1+\ell(\text{-}1)^{y+z}e^{-\frac{\sigma^2}{4}(\Delta_a+m\Delta_b)^2}\bigwedge\left(\Omega_-\left[\Delta_a-m\Delta_b\right]\right)\mathrm{Cos}\left(\frac{\omega_{p0}}{2}\left[\Delta_a+m\Delta_b\right]\right)\right) \\ &+(\delta_{jH}\delta_{sH}+\delta_{jV}\delta_{sV})\left(1+\ell(\text{-}1)^{y+z}e^{-\frac{\sigma^2}{4}(\Delta_a-m\Delta_b)^2}\bigwedge\left(\Omega_-\left[\Delta_a+m\Delta_b\right]\right)\mathrm{Cos}\left(\frac{\omega_{p0}}{2}\left[\Delta_a-m\Delta_b\right]\right)\right)\Big]. \end{aligned} \tag{2.47}$$

The NPI is "balanced" such that the path length mismatches approach 0, $\Delta_a \to 0$ and $\Delta_b \to 0$. Assuming that the spectral properties of the photon pair do not correlate with their polarization, the visibility of nonlocal interference has little dependence on the bandwidth of the pump, proportional to σ. Certainly for any continuous wave sources, linewidths 1 kHz - 1GHz, the pump bandwidth is insignificant. The pump bandwidth becomes significant only when the pump pulse length becomes comparable to the central wavelength of the pump, in the greater than 1 THz regime. Thus, pulsed sources of pulse duration greater than 1 ps, or spectral widths less than 1 nm, should be suitable to produce high visibility nonlocal interference in the NPI.

Equation 2.47 can also be rewritten to resemble previous expressions as

$$\begin{aligned} P_{\substack{jAy\\sBz}} &= (1/16)\times \\ &\left[\ (\delta_{jH}\delta_{sV}+\delta_{jV}\delta_{sH})\left(1+\ell(\text{-}1)^{y+z}e^{-\frac{\sigma^2}{\omega_{p0}^2}(\alpha+m\beta)^2}\bigwedge\left(2\Omega_-\left[\alpha-m\beta\right]/\omega_{p0}\right)\mathrm{Cos}(\alpha+m\beta)\right)\right. \\ &\left.+(\delta_{jH}\delta_{sH}+\delta_{jV}\delta_{sV})\left(1+\ell(\text{-}1)^{y+z}e^{-\frac{\sigma^2}{\omega_{p0}^2}(\alpha-m\beta)^2}\bigwedge\left(2\Omega_-\left[\alpha+m\beta\right]/\omega_{p0}\right)\mathrm{Cos}(\alpha-m\beta)\right)\right] \end{aligned} \tag{2.48}$$

where the variables $\alpha = (\omega_{p0}/2)\Delta_a$ and $\beta = (\omega_{p0}/2)\Delta_b$. This prediction then agrees qualitatively with the continuous-wave cases given by Eq. 2.4 with the additional triangle and exponential functions representing the temporal and spectral properties of the two photon state. Eq. 2.4 is recovered exactly as $\Delta_a, \Delta_b \rightarrow 0$.

Chapter 3

Time-To-Polarization Mapper

A phase-stable nonlocal interferometer based on optical birefringence and temporal discrimination is proposed which maps robust time entangled states to polarization entangled states allowing implementation of the BB84 or 6-state quantum key distribution protocols. The interferometer is common path and copropagating which simplifies alignment and encourages entanglement retention.

3.1 Overview

Distributing entanglement in time is robust to decoherence relative to polarization entanglement. However, polarization is easy to manipulate and measure experimentally. Additionally, quantum key distribution (QKD) security proofs for BB84 [5] and 6-state [62] protocols are given in the polarization basis [63, 64]. We propose a phase-stable interferometer that maps time-entangled photons to polarization entangled states, capitalizing on the strengths of both the temporal and polarization degrees of freedom.

Alice and Bob share a time entangled source which is robust to decoherence over long distances [36], this state is mapped to polarization using a phase-stable nonlocal interferometer based on the two modes of 0.25 km spools of telecom polarization maintaining fiber (PMF) as seen in Fig. 3.1. Phase stability is achieved due to the copropagating common path configuration in which the birefringence of the PMF provides a stable temporal delay between the horizontal (H) and vertical (V) photon paths. These paths can be compared to the long and short paths of the Franson interferometer [30]. To maintain the desired phase in the Franson's original design, active stabilization or highly stable interferometers such as planar light wave circuits (PLC) [36] must be used. Our phase-stable design does not require active stabilization and also maps the time-entanglement to polarization which simplifies the execution of QKD protocols compared to common interferometric designs, including those utilizing PLC interferometers.

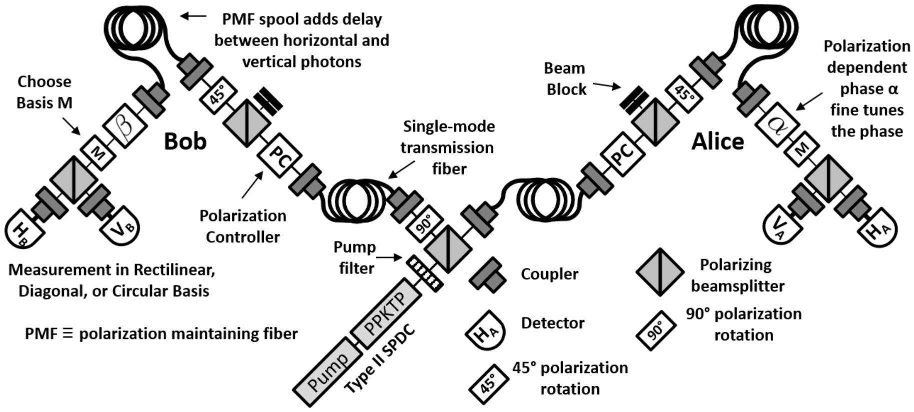

Figure 3.1: Alice and Bob share a time-entangled two-photon source. The two modes of two polarization maintaining fibers, one held by Alice and one by Bob, realize a phase-stable nonlocal interferometer. This interferometer maps the time-entangled state to a polarization entangled state within the coincidence window. Alice and Bob make standard polarization measurements to carry out the BB84 or 6-state protocol.

3.2 Mapping

A source shared by Alice and Bob produces Type II photon pairs from a spontaneous parametric downconersion (SPDC) process which is pumped by a laser with a coherence time exceeding the birefringence delay in the PMF. After propagating through the single-mode transmission fiber, photons are incident on a polarizing beam splitter (PBS) which transmits only a single polarization mode. This polarizer ensures the correct probability amplitudes in the interferometer. Polarization correction of the photons received by Alice and Bob only affects the overall bit rate, but not the error rate or degree of entanglement [*]. Photons transmitted through the PBS are rotated 45° and then pass into the PMF which randomizes their path selection, H or V, long or short. A 0.25 km spool of telecom PMF adds a 1 ns propagation delay between the H and V photons due to the birefringence in the PMF. After exiting the PMF, the photons pass through a polarization dependent phase modulator (PDPM), which could be implemented using a static Babinet-Soleil compensator or an active liquid crystal waveplate. The PDPM allows fine phase tuning. The state shared by Alice and Bob after this propagation is

$$|\psi\rangle = \frac{1}{2}\left(|H_A H_B\rangle + e^{i(\phi_A+\phi_B)}|V_A V_B\rangle + e^{i\phi_B}|H_A V_B\rangle + e^{i\phi_A}|V_A H_B\rangle\right). \tag{3.1}$$

The phases are

$$\phi_A = \frac{\omega \Delta n L_A}{c} - \alpha \quad \text{and} \quad \phi_B = \frac{\omega \Delta n L_B}{c} - \beta$$

where L_A and L_B are the lengths of the PMF spools, $L_A \approx L_B$ [†], Δn is the optical fiber birefringence, ω is the single-photon angular frequency, and α and β phases are from the PDPM. When the coincidence time resolution and single photon temporal packet are smaller than the birefringence delay $\Delta t \approx \frac{\Delta n L_A}{c}$, the $|HV\rangle$ and $|VH\rangle$ components in Eq. 3.1 are excluded, leaving

$$|\psi'\rangle = \frac{1}{\sqrt{2}}\left(|H_A H_B\rangle + e^{i(\phi_A+\phi_B)}|V_A V_B\rangle\right). \tag{3.2}$$

---

[*] Polarization correction may be carried out by maximizing the single detector count rates. This is due to phase flips being irrelevant during transmission of the single polarization mode from source to user. Additionally, polarization correction can be slow and ongoing since it only affects the raw key rate and not the entanglement quality or error rate.

[†] The fibers held by Alice and Bob should have lengths approximately the same $L_A \approx L_B$. The tolerance for mismatched fibers is higher for our interferometer than a Mach-Zehnder style fiber interferometer since it is common path and the birefringence is small, $\Delta n \approx 1E-3$. A tolerance in the cm range should be sufficient. This can be compared with a fiber interferometer requiring tolerances in the micron range. The free space path lengths are irrelevant due the common path nature of the interferometer.

For time entangled photon pairs with a biphoton coherence length much greater than the birefringence delay and a suitable choice of the phases α and β, Alice and Bob share the Bell state

$$\left|\Phi^{+}\right\rangle = \frac{1}{\sqrt{2}}\left(\left|H_A H_B\right\rangle + \left|V_A V_B\right\rangle\right), \tag{3.3}$$

as is more rigorously shown in the last section of this Chapter. This will be a stable phase selection and will not need frequent adjustment. Thus, the time-entanglement shared between Alice and Bob is mapped to a polarization entangled state. Ideally, this is the only state leading to coincidences. However, due to decoherence, accidental coincidences, and imperfections other states will also be measured.

3.3 BB84 with Time-to-Polarization Mapping

In Fig. 3.2, a practical BB84 implementation using a pulsed pump and time-multiplexed measurement configuration is shown. Measurement in the rectilinear or diagonal basis is random. Alice's rectilinearly measured photons take the long measurement path and the diagonally measured photons take the short path. Bob's measurement paths are the opposite. Therefore, coincidences separated by ΔT, the delay between short and long measurement paths, are those from the state given in Eq. 3.3. Whether Alice or Bob's photon is early or late identifies which basis was chosen. Photons arriving at other times are excluded. The figure illustrates that much of the configuration can utilize inline optics and splices to reduce transmission losses. After initial coupling at the source, the photons remain in optical fiber until the measurement process, only making low loss splice transitions between elements. All fiber photon pair sources have been demonstrated [65] which would remove these coupling losses, but these sources are still complex and require cryogenics.

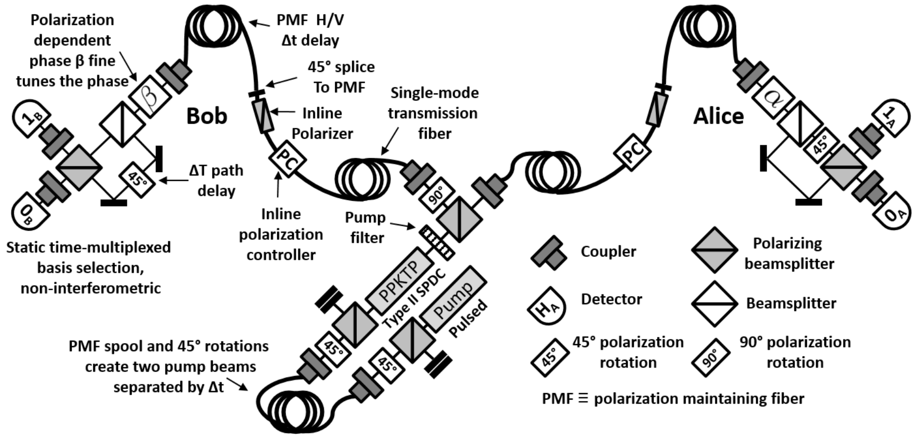

Figure 3.2: A practical BB84 implementation using a pulsed source and time-multiplexed measurement in the rectilinear and diagonal bases.

3.4 Loss and Bit Flips

Franson interferometry produces a 50% bit loss by design due to the excluded paths. However, in return for this loss, we predict a reduction in the bit flip dependent error rate in the BB84 and 6-state protocols. It is sufficient for QKD security to assume that Alice and Bob share a state diagonal in the Bell basis [64]. With this assumption, bounds on the security of a shared raw key can be made by estimating the contribution from each Bell state. This is done by measuring in the diagonal and rectilinear basis for BB84, or these bases as well as the circular basis for the 6-state protocol. Assume post-interferometer and pre-measurement Alice, Bob, and an adversary Eve share the purification

$$|\psi_{ABE}\rangle = \sqrt{\lambda_1}|\Phi^+\rangle|e_1\rangle + \sqrt{\lambda_2}|\Phi^-\rangle|e_2\rangle + \sqrt{\lambda_3}|\Psi^+\rangle|e_3\rangle + \sqrt{\lambda_4}|\Psi^-\rangle|e_4\rangle \tag{3.4}$$

where the Bell states are held by Alice and Bob while Eve holds the orthogonal states $|e_i\rangle$. Alice and Bob hold the density matrix

$$\rho_{AB} = \lambda_1|\Phi^+\rangle\langle\Phi^+| + \lambda_2|\Phi^-\rangle\langle\Phi^-| + \lambda_3|\Psi^+\rangle\langle\Psi^+| + \lambda_4|\Psi^-\rangle\langle\Psi^-|, \tag{3.5}$$

while Eve holds the density matrix

$$\rho_E = \lambda_1 |e_1\rangle\langle e_1| + \lambda_2 |e_2\rangle\langle e_2| + \lambda_3 |e_3\rangle\langle e_3| + \lambda_4 |e_4\rangle\langle e_4|. \tag{3.6}$$

Applying Holevo's bound to the Bell diagonal purification given in Eq. 3.4, a lower bound on the secret key rate in the limits of perfect error correction for the BB84 and 6-state protocols is found to be dependent on Eve's Shannon information [63, 64],

$$\mathrm{R}_{\text{secret}} \geq 1 - H\left(\rho_E\right) = 1 + \sum_{i=1}^{4} \lambda_i \log\left(\lambda_i\right). \tag{3.7}$$

Estimation of the parameters λ_i is done by measuring the error rates in the rectilinear basis ϵ_z, diagonal basis ϵ_x, and circular basis ϵ_y. These error rates are

$$\epsilon_z = \lambda_3 + \lambda_4, \quad \epsilon_x = \lambda_2 + \lambda_4, \text{ and } \quad \epsilon_y = \lambda_2 + \lambda_3. \tag{3.8}$$

For the 6-state protocol it is usually assumed that the state is acted on by a depolarizing channel which assigns the same probability to bit flips, phase flips, and bit-phase flips. In the BB84 protocol one parameter is undetermined, in which case, the parameter λ_4 is optimized for Eve. Unlike a direct measurement on distributed polarization entangled states, with our device, bit flipped states are suppressed in the coincidence window. Thus, the error rate due to bit flips will be reduced to accidental coincidences. When the probability of an accidental is less than the probability of a phase flip the usual error estimates are inappropriate for our interferometer. Instead, we assume a bit flip suppressed channel. In Table 3.1 we have assigned expected values for the depolarizing channel and the bit flip suppressed channel to the state in Eq. 3.4 and matrices given in Eq. 3.5 and 3.6 in terms of the bit or phase flip probability p and the accidental coincidence probability ϵ.

Table 3.1: Predicted eigenvalues for the depolarizing and bit flip suppressed channels for the 6-state and BB84 protocols.

	Depolarizing Channel 6-state	Depolarizing Channel BB84	Bit Flip Suppressed 6-state	Bit Flip Suppressed BB84
λ_1	1-3(p+ϵ)	(1-2(p+ϵ))^2	1-p-3ϵ	(1-2ϵ)(1-p-2ϵ)
λ_2	p+ϵ	2(p+ϵ)(1-2(p+ϵ))	$p+\epsilon$	(1-2ϵ)(p+2ϵ)
λ_3	p+ϵ	2(p+ϵ)(1-2(p +ϵ))	ϵ	2ϵ(1-p-2ϵ)
λ_4	p+ϵ	(p+ϵ)^2	ϵ	2ϵ(p+2ϵ)

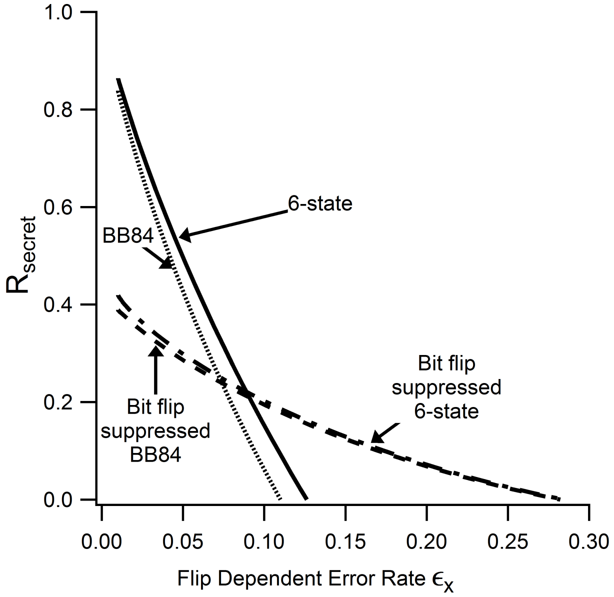

Figure 3.3: Secret key rates in the limit of perfect error correction versus the flip dependent error rate ϵ_x for the 6-state and BB84 protocols given the depolarizing channel or with bit flip suppression. A fixed accidental error rate $\epsilon = 0.01$ has been assumed.

In Fig. 3.3, the secret key rate from Eq. 3.7 is plotted versus the flip dependent error rate in the diagonal basis for the depolarizing channel and the bit flip suppressed channel. In this plot the accidental coincidence rate is fixed to $\epsilon = 0.01$. As can be seen from the plot, our interferometer trades half the key for a reduction in the flip dependent error rate. All this is to say, that the 50% photon pair loss due to the excluded interferometer paths is partially compensated by a reduction in the predicted error rate. In the limit of long distance QKD the accidental rate ϵ dominates, $\epsilon > p$, due to a decreasing signal to noise ratio. In this case, the advantage of bit flip suppression disappears. However, as the distribution distance grows, the time entangled photons will outperform polarization entangled photons in entanglement retention. In this case, equating their phase flip probability, p, is overly generous.

3.5 Discussion

The longest demonstration of time-entanglement distribution over optical fiber to date, over 300 km, [37] has used planar light wave circuit (PLC) Mach-Zehnder interferometers which exhibit excellent phase stability. The phase in these devices is changed by temperature adjustment. Thus, in order to carry out the BB84 protocol each user must have two PLC interferometers each set for a basis, or they must modulate the PLC interferometers by tuning the temperature. Our implementation avoids the complication of multiple interferometers and modulation of the phase by mapping the time-entanglement to polarization, for which, the two basis measurements may easily be time-multiplexed as seen in Fig. 3.2. Furthermore, the insertion and transmission losses for the spliced fibers and optics given in Fig. 3.2 should be competitive with the 2-2.64 dB loss reported using PLC interferometers [38, 39].

In summary, a phase-stable interferometer has been proposed that maps time-entangled photons to polarization entangled states, capitalizing on the strengths of both the temporal and polarization degrees of freedom. The phase-stable configuration, fiber based design, and polarization based measurement scheme offers a ruggedized solution to long distance QKD. In case the “hand waving” argument given prior is unconvincing, we give a multi-mode analysis of the time-to-polarization mapper in the next section.

3.6 Multi-Mode Analysis for the Z, X, and Y Bases

In this calculation we show that the distributed time-entangled state is mapped to the Bell state

$$\left|\Phi^{+}\right\rangle = \frac{1}{\sqrt{2}} \left(|H_A H_B\rangle + |V_A V_B\rangle\right), \tag{3.9}$$

assuming suitable time discrimination and choices of the phases α and β. This is shown by evolving the time-entangled state through Alice and Bob's optics and deriving measurement probabilities in the rectilinear, diagonal, and circular basis.

Assume Alice and Bob share a two-photon source with near perfect spectral entanglement. For instance, this could be a spontaneous parametric downconversion (SPDC) source with a narrowband pump. The SPDC could be a Type I process in which the signal and idler have the same polarization, or Type II SPDC where the signal and idler have different polarizations. What is important is that the photon pair may efficiently be split amongst Alice and Bob using either polarization or frequency. We will assume Type II SPDC as it simplifies the derivation. We also assume that the pump is narrowband with an approximate spectral amplitude

$$A(\omega + \omega') = \delta(\omega + \omega' - \omega_p). \tag{3.10}$$

This approximation makes the representative state unnormalizable. This will not affect the predictions qualitatively and will greatly reduce the complexity of the derivation, see Ou [23]. After generation, the photon pair is split amongst Alice and Bob by polarization. Photons then pass through single-mode fiber, polarization correction, and a polarizer. The state at this point may be written

$$|\Psi_0\rangle \propto \int d\omega d\omega' \delta(\omega + \omega' - \omega_p) \phi(\omega, \omega') \hat{a}^{\dagger}_{HA}(\omega) \hat{a}^{\dagger}_{HB}(\omega') \tag{3.11}$$

where $\hat{a}^\dagger_{jx}(\omega)$ is a photon creation operator for polarization $j \in \{H, V\}$ and user $x \in \{A, B\} \equiv \{\text{Alice}, \text{Bob}\}$.The phase-matching function is

$$\phi\left(\omega, \omega'\right) = L\ \operatorname{sinc}\left(\Delta k L/2\right) e^{-i\Delta k L/2} \tag{3.12}$$

with nonlinear crystal length L. The phase mismatch for a Type II process is approximately [25]

$$\Delta k = k_p - k - k' \approx \left(\omega - \frac{\omega_p}{2}\right)\gamma_o + \left(\omega' - \frac{\omega_p}{2}\right)\gamma_e \tag{3.13}$$

with $\gamma_i = \left.\frac{\partial k_i(\omega)}{\partial \omega}\right|_{\omega=\omega_p/2} - \left.\frac{\partial k_p(\omega)}{\partial \omega}\right|_{\omega=\omega_p}$ and $i = \{o, e\}$ indicating ordinary and extraordinary, respectively.

After propagation through the polarization maintaining optical fiber and application of the polarization dependent phases α and β the state is given in the rectilinear basis as

$$\begin{aligned}|\Psi_r\rangle \propto \int d\omega d\omega' \delta(\omega + \omega' - \omega_p)\phi(\omega, \omega') \Big(&\hat{a}^\dagger_{HA}(\omega)\hat{a}^\dagger_{HB}(\omega') + e^{i(\omega T_A + \omega' T_B)}\hat{a}^\dagger_{VA}(\omega)\hat{a}^\dagger_{VB}(\omega') \\ &+ e^{i\omega T_A}\hat{a}^\dagger_{VA}(\omega)\hat{a}^\dagger_{HB}(\omega') + e^{i\omega' T_B}\hat{a}^\dagger_{HA}(\omega)\hat{a}^\dagger_{VB}(\omega')\Big).\end{aligned} \tag{3.14}$$

The temporal delays are

$$T_A = \frac{\Delta n L_A}{c} - \alpha \quad \text{and} \quad T_B = \frac{\Delta n L_B}{c} - \beta \tag{3.15}$$

with $L_A \approx L_B$ and polarization dependent phase modulations α and β. At this point Alice and Bob choose their basis, rectilinear, diagonal, or circular. In the rectilinear basis nothing changes and we may write the second order correlation function

$$\begin{aligned}\Gamma^{(2)}_{js}(t,\tau) &= \left|\langle 0|\,\hat{a}_{jA}(t+\tau)\hat{a}_{sB}(t)|\Psi_r\rangle\right|^2 \\ &\propto \left|\int d\omega d\omega' \delta(\omega+\omega'-\omega_p)\phi(\omega,\omega')e^{i\omega(t+\tau)}e^{i\omega' t}\right. \\ &\qquad \left.\times\left(\delta_{HA}\delta_{HB}+e^{i(\omega T_A+\omega' T_B)}\delta_{VA}\delta_{VB}+e^{i\omega T_A}\delta_{VA}\delta_{HB}+e^{i\omega T_B}\delta_{HA}\delta_{VB}\right)\right|^2\end{aligned} \tag{3.16}$$

with the annihilation operator

$$\hat{a}_j\left(t\right) = \left(2\pi\right)^{-1/2}\int d\omega \hat{a}_j\left(\omega\right)e^{i\omega t}. \tag{3.17}$$

Making a change of variables $\omega = \frac{\omega_p}{2}+\Omega$ and $\omega' = \frac{\omega_p}{2}-\Omega$ we may rewrite this

$$\begin{aligned}\Gamma^{(2)}_{js}(t,\tau) &= \left|\langle 0|\,\hat{a}_{jA}(t+\tau)\hat{a}_{sB}(t)|\Psi_r\rangle\right|^2 \\ &\propto \left|L\int_{-\infty}^{\infty} d\Omega\ \ \mathrm{Sinc}\left(\frac{\Omega}{2\sigma}\right)e^{i\frac{\Omega}{2\sigma}}e^{i\Omega\tau}\left(\delta_{HA}\delta_{HB}+e^{i\frac{\omega_p}{2}(T_A+T_B)}e^{i\Omega(T_A-T_B)}\delta_{VA}\delta_{VB}\right.\right. \\ &\qquad \left.\left.+e^{i\frac{\omega_p}{2}T_A}e^{i\Omega T_A}\delta_{VA}\delta_{HB}+e^{i\frac{\omega_p}{2}T_B}e^{-i\Omega T_B}\delta_{HA}\delta_{VB}\right)\right|^2\end{aligned} \tag{3.18}$$

where $\sigma = (L|\gamma_e-\gamma_o|)^{-1}$. Carrying out the integral

$$\int_{-\infty}^{\infty} d\Omega\ \ \mathrm{Sinc}\left(\frac{\Omega}{2\sigma}\right)e^{i\frac{\Omega}{2\sigma}x} = 2\pi\sigma\Pi\left(x/2\right) \tag{3.19}$$

with rectangle function

$$\Pi\left(x\right) = \begin{cases}1 & \text{if } |x| \leq 1/2 \\ 0 & \text{otherwise,}\end{cases} \tag{3.20}$$

we simplify the second-order correlation to

$$\begin{aligned}\Gamma^{(2)}_{js}(t,\tau) &= \left|\langle 0|\,\hat{a}_{jA}(t+\tau)\hat{a}_{sB}(t)|\Psi_r\rangle\right|^2 \\ &\propto \Big| 2\pi L\sigma \Big(\delta_{HA}\delta_{HB}\Pi\left(1/2+\sigma\tau\right) + e^{i\frac{\omega_p}{2}(T_A+T_B)}\delta_{VA}\delta_{VB}\Pi\left(1/2+\sigma(\tau+T_A-T_B)\right) \\ &\quad + e^{i\frac{\omega_p}{2}T_A}\delta_{VA}\delta_{HB}\Pi\left(1/2+\sigma(\tau+T_A)\right) + e^{i\frac{\omega_p}{2}T_B}\delta_{HA}\delta_{VB}\Pi\left(1/2+\sigma(\tau-T_B)\right)\Big)\Big|^2 .\end{aligned} \tag{3.21}$$

The probability of detecting a coincidence between Alice's photon with polarization j and Bob's photon with polarization s is

$$P^r_{js} = N(2\pi L\sigma)^2 \int_{-T_r/2}^{T_r/2} \Gamma^{(2)}_{js}(t,\tau) \tag{3.22}$$

where N is a normalization to ensure $\sum_{js} P_{js} = 1$. If the path length difference $T_A \approx T_B >> 1/\sigma = 2\pi/\Delta\omega_s$ where $\Delta\omega_s$ is the single-photon coherence time and the timing resolution is $T_R << T_A$, the rectangle functions for the VH and HV cases in Eq. 3.21 are zero over the interval of integration. With these terms removed

$$P^r_{js} = N(2\pi L\sigma)^2 \int_{-T_r/2}^{T_r/2} \left(\delta_{HA}\delta_{HB}\Pi^2\left(1/2+\sigma(\tau)\right) + \delta_{VA}\delta_{VB}\Pi^2\left(1/2+\sigma(\tau+T_A-T_B)\right)\right). \tag{3.23}$$

The time integral is the convolution of two rectangle functions

$$\int d\tau \Pi\left(1/2+\sigma\tau\right)\Pi\left(1/2+\sigma\left[\tau+X\right]\right) = \frac{1}{\sigma}\wedge(\sigma X) \tag{3.24}$$

with

$$\wedge(x) = \begin{cases} 1-|x| & \text{if } |x| \leq 1 \\ 0 & \text{otherwise.} \end{cases} \tag{3.25}$$

In this case, the rectangle functions completely overlap leaving the normalized probability

$$P^r_{js} = \frac{1}{2}\left(\delta_{HA}\delta_{HB} + \delta_{VA}\delta_{VB}\right). \tag{3.26}$$

As expected, in the rectilinear basis Alice and Bob will both receive H photons or both will receive V photons no matter what phases α or β are chosen. This of course does not demonstrate that the state is polarization entangled. This is easily seen by measuring in the diagonal basis in which case we expect the same outcome, both receive H or both V. Returning to Eq. 3.14, measurement in the diagonal basis is performed by rotating each of the photons 45°. In this case the state is

$$\begin{aligned}|\Psi_d\rangle \propto \int d\omega d\omega' \delta(\omega+\omega'-\omega_p)\phi(\omega,\omega')\\ \times\Big\{\Big(\hat{a}^\dagger_{HA}(\omega)+\hat{a}^\dagger_{VA}(\omega)\Big)\Big(\hat{a}^\dagger_{HB}(\omega')+\hat{a}^\dagger_{VB}(\omega')\Big)\\ +\Big(\hat{a}^\dagger_{HA}(\omega)-\hat{a}^\dagger_{VA}(\omega)\Big)\Big(\hat{a}^\dagger_{HB}(\omega')-\hat{a}^\dagger_{VB}(\omega')\Big)e^{i(\omega T_A+\omega' T_B)}\\ +\Big(\hat{a}^\dagger_{HA}(\omega)-\hat{a}^\dagger_{VA}(\omega)\Big)\Big(\hat{a}^\dagger_{HB}(\omega')+\hat{a}^\dagger_{VB}(\omega')\Big)e^{i\omega T_A}\\ +\Big(\hat{a}^\dagger_{HA}(\omega)+\hat{a}^\dagger_{VA}(\omega)\Big)\Big(\hat{a}^\dagger_{HB}(\omega')-\hat{a}^\dagger_{VB}(\omega')\Big)e^{i\omega' T_B}\Big\}.\end{aligned} \tag{3.27}$$

With the same temporal and bandwidth arguments given above this generates the probability

$$\begin{aligned}P^d_{js} = N(2\pi L\sigma)^2\times\\ \int_{-T_r}^{T_r} d\tau\,\Big\{(\delta_{HA}\delta_{HB}+\delta_{VA}\delta_{VB})\Big(\Pi^2\left({}^1\!/_2+\sigma\tau\right)+\Pi^2\left({}^1\!/_2+\sigma(\tau+T_A-T_B)\right)\\ +2\mathrm{Cos}\left(\frac{\omega_p}{2}\left[T_A+T_B\right]\right)\Pi\left({}^1\!/_2+\sigma\tau\right)\Pi\left({}^1\!/_2+\sigma\left[\tau+T_A-T_B\right]\right)\Big)\\ +(\delta_{VA}\delta_{HB}+\delta_{HA}\delta_{VB})\Big(\Pi^2\left({}^1\!/_2+\sigma\tau\right)+\Pi^2\left({}^1\!/_2+\sigma(\tau+T_A-T_B)\right)\\ -2\mathrm{Cos}\left(\frac{\omega_p}{2}\left[T_A+T_B\right]\right)\Pi\left({}^1\!/_2+\sigma\tau\right)\Pi\left({}^1\!/_2+\sigma\left[\tau+T_A-T_B\right]\right)\Big)\Big\}.\end{aligned} \tag{3.28}$$

Unlike before, we now have cross terms due to the coherence between the two paths. The integral of integration again covers the range of the rectangle functions in the first two terms. However, the coherence terms are unity only when $T_A = T_B$. This is related to the distinguishability of the two path cases, HH or VV in the PMF. This makes the triangle function nonzero for $T_A \neq T_B$. This is, in effect, the "visibility" term. After temporal integration, the probability is

$$P^d_{js} = \frac{1}{4}\left\{1 + (\delta_{HA}\delta_{HB} + \delta_{VA}\delta_{VB} - \delta_{VA}\delta_{HB} - \delta_{HA}\delta_{VB}) \wedge (\sigma\Delta)\,\mathrm{Cos}\left(\frac{\omega_p}{2}\left[T_A{+}T_B\right]\right)\right\} \tag{3.29}$$

where $\Delta = T_A$-T_B. With $\frac{\omega_p}{2}(T_A + T_B) = 2n\pi$, which is the case for the Bell state Φ^+, and mismatch $\Delta \approx 0$,

$$P^d_{js} = \frac{1}{2}\left(\delta_{HA}\delta_{HB} + \delta_{VA}\delta_{VB}\right), \tag{3.30}$$

which agrees with the probability in the rectilinear basis, Eq. 3.26.

Measurement in the circular basis is carried out by applying a $-\pi/2$ phase to the vertical component of the state held by Alice and Bob and then rotating both components 45°. The resulting state starting with Eq. 3.14 is

$$\begin{aligned}
|\Psi_c\rangle \propto \int & d\omega d\omega' \delta(\omega + \omega' - \omega_p)\phi(\omega, \omega') \\
& \times \Big\{ \left(\hat{a}^\dagger_{HA}(\omega) + \hat{a}^\dagger_{VA}(\omega)\right)\left(\hat{a}^\dagger_{HB}(\omega') + \hat{a}^\dagger_{VB}(\omega')\right) \\
& \quad - \left(\hat{a}^\dagger_{HA}(\omega) - \hat{a}^\dagger_{VA}(\omega)\right)\left(\hat{a}^\dagger_{HB}(\omega') - \hat{a}^\dagger_{VB}(\omega')\right) e^{i(\omega T_A + \omega' T_B)} \\
& \quad - i\left(\hat{a}^\dagger_{HA}(\omega) - \hat{a}^\dagger_{VA}(\omega)\right)\left(\hat{a}^\dagger_{HB}(\omega') + \hat{a}^\dagger_{VB}(\omega')\right) e^{i\omega T_A} \\
& \quad - i\left(\hat{a}^\dagger_{HA}(\omega) + \hat{a}^\dagger_{VA}(\omega)\right)\left(\hat{a}^\dagger_{HB}(\omega') - \hat{a}^\dagger_{VB}(\omega')\right) e^{i\omega' T_B} \Big\}.
\end{aligned} \tag{3.31}$$

With the same temporal and bandwidth arguments given above this generates the probability

$$\begin{aligned}
P^c_{js} = N(2\pi L\sigma)^2 \times \\
\int_{-\infty}^{\infty} d\tau \, \Big\{ & (\delta_{HA}\delta_{HB} + \delta_{VA}\delta_{VB}) \left(\Pi^2\left({}^1\!/\!{}_2{+}\sigma\tau\right) + \Pi^2\left({}^1\!/\!{}_2{+}\sigma(\tau + T_A - T_B)\right)\right. \\
& \left. -2\mathrm{Cos}\left(\frac{\omega_p}{2}\left[T_A{+}T_B\right]\right)\Pi\left({}^1\!/\!{}_2{+}\sigma\tau\right)\Pi\left({}^1\!/\!{}_2{+}\sigma\left[\tau{+}T_A{-}T_B\right]\right)\right) \\
& + (\delta_{VA}\delta_{HB} + \delta_{HA}\delta_{VB}) \left(\Pi^2\left({}^1\!/\!{}_2{+}\sigma\tau\right) + \Pi^2\left({}^1\!/\!{}_2{+}\sigma(\tau + T_A - T_B)\right)\right. \\
& \left. +2\mathrm{Cos}\left(\frac{\omega_p}{2}\left[T_A{+}T_B\right]\right)\Pi\left({}^1\!/\!{}_2{+}\sigma\tau\right)\Pi\left({}^1\!/\!{}_2{+}\sigma\left[\tau{+}T_A{-}T_B\right]\right)\right)\Big\} .
\end{aligned} \tag{3.32}$$

We again have cross terms due to the coherence between the two paths. With the same integration as before this reduces to

$$P^c_{js} = \frac{1}{4}\left\{1 - (\delta_{HA}\delta_{HB} + \delta_{VA}\delta_{VB} - \delta_{VA}\delta_{HB} - \delta_{HA}\delta_{VB}) \wedge (\sigma\Delta)\,\mathrm{Cos}\left(\frac{\omega_p}{2}\left[T_A{+}T_B\right]\right)\right\} \tag{3.33}$$

where $\Delta = T_A$-T_B. With $\frac{\omega_p}{2}(T_A + T_B) = 2n\pi$, which is the case for the Bell state Φ^+, and mismatch $\Delta \approx 0$, the probability is

$$P^c_{js} = \frac{1}{2}\left(\delta_{HA}\delta_{VB} + \delta_{VA}\delta_{HB}\right), \tag{3.34}$$

which agrees with the expected bit flip when measuring in the circular basis, $\Phi^+_Z \rightarrow \Psi^+_Y$. These probabilities demonstrate that Alice and Bob's shared time-entangled state is mapped to a polarization entangled state in a suitable window of coincidence. This Φ^+_Z Bell state behaves as it should, retaining its form in the diagonal basis, and transforming to the state Ψ^+_Y in the circular basis. In each measurement basis, Alice and Bob can reliably predict the other's outcome due to the mapping of their time entangled state to a polarization entangled state.

Chapter 4

Estimating Correlations with Bayes' Rule

In this Chapter, a method of estimating correlations with Bayes' rule is proposed. We present theory that through logical steps results in a method of estimation using distributions that outperforms the traditional "ratio" method. Surprisingly, we even find different, better, estimations of the most likely probability of correlation. This approach also allows comparison of relative likelihoods between probabilities. For instance, experimental data may suggest an entangled state as the most likely explanation. If there is a known maximum probability for separable states, the relative likelihood of these probabilities may be determined. With this approach all quantities of interest are calculated from the distribution including the standard deviation. This avoids needing a separate theoretical approach to estimating uncertainties. Additionally, this approach avoids pitfalls found when using the Gaussian distribution to represent the probability estimation and uncertainty. These pitfalls include exceeding the probability bounds, $0 < p < 1$, having "soft tails"[66], no logical basis for determining the aforementioned entangled-separable likelihood ratio, and poor most likelihood estimation when experiments include asymmetries. The basis for this Chapter's comparisons is numerical simulation of two-channel photon experiments in which determining the probability of correlation is challenged by transmission losses, asymmetric detector efficiencies, and low count rates.

4.1 Overview

Correlation coefficients, security parameter estimation, and probabilities are at the statistical heart of quantum information. The term "correlation coefficient" was coined at least by 1978 [67] where it was used by Clauser, Shimony, and Abner in their review and discussion of work related to Bell's theorem prior to that time. In 1982, it was used by Aspect [16] in reference to the quantity

$$E(a,b) = P_{HH}(a,b)+P_{VV}(a,b)-P_{HV}(a,b)-P_{VH}(a,b) \tag{4.1}$$

which is an expectation value describing the nature of spatially separated quantum correlations given local independent parameters a and b, as defined by Bell. In the experiment shown in Fig. 4.1, $P_{HH}(a,b)$ is the probability that there is a horizontal-horizontal (HH) coincidence.

If $P_{HH}(a,b)=P_{VV}(a,b) \approx 1/2$, the correlation coefficient $E(a,b) \approx 1$, the events are correlated. Likewise, it could be that $P_{HV}(a,b)=P_{VH}(a,b) \approx 1/2$, $E(a,b) \approx -1$, and the events are anti-correlated. The correlation coefficient is a well known quantity as it is fundamental to expressing the Bell parameter

$$|S| = |E(a_0,b_0) + E(a_0,b_1) + E(a_1,b_0) - E(a_1,b_1)| \leq 2$$

in the case of two-channel Bell tests [15, 16].

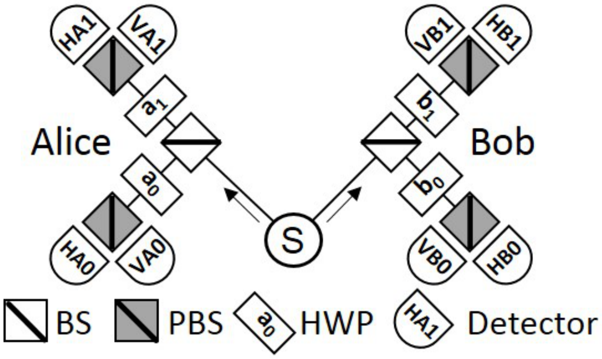

Figure 4.1: A typical Bell test. An entangled photon pair is shared between Alice and Bob whose local measurement settings or local realities a_0, a_1, b_0, and b_1 are randomly chosen by a symmetric beamsplitter (BS). HWP ≡ half-wave plate, PBS ≡ polarizing beamsplitter

Aspect measured the correlation coefficient using the ratio of coincidence counts

$$\langle E(a,b)\rangle = \frac{\mathcal{C}_{HH}(a,b)+\mathcal{C}_{VV}(a,b)-\mathcal{C}_{HV}(a,b)-\mathcal{C}_{VH}(a,b)}{\mathcal{C}_{HH}(a,b)+\mathcal{C}_{VV}(a,b)+\mathcal{C}_{HV}(a,b)+\mathcal{C}_{VH}(a,b)}. \tag{4.2}$$

It is not clear if Aspect used a normalization procedure on this quantity, but it is common to do so for proof of principle experiments demonstrating entanglement distribution or quantifying experimental quality. If unnormalized, Eq. 4.2 is a poor measure of correlation when the detector and transmission efficiencies vary between detector pairs. Conveniently, the singles counts S_{ij}, $i \in \{A, B\}$ and $j \in \{H, V\}$, can typically be used to normalize the coincidence count rate since

$$S_{AH} \approx \frac{\eta_{AH} F}{2} \quad \text{and} \quad \mathcal{C}_{HH} \approx \frac{\eta_{AH}\eta_{BH}\; p\; F}{2} \tag{4.3}$$

where p is the probability of correlation, eta_{ij} are the combined transmission and detection efficiencies, and F is the flux of photon pairs. These proportionalities make the normalized coincidence count

$$\mathcal{N}_{HH} = \frac{\mathcal{C}_{HH}}{S_{AH} S_{BH}} \tag{4.4}$$

a convenient choice in expressing the correlation coefficient,

$$\langle E(a,b)\rangle = \frac{\mathcal{N}_{HH}(a,b)+\mathcal{N}_{VV}(a,b)-\mathcal{N}_{HV}(a,b)-\mathcal{N}_{VH}(a,b)}{\mathcal{N}_{HH}(a,b)+\mathcal{N}_{VV}(a,b)+\mathcal{N}_{HV}(a,b)+\mathcal{N}_{VH}(a,b)}. \tag{4.5}$$

In quantum information applications, this type of “correlated/anti-correlated”, “either/or”, or “+/-” quantity shows up any many variations. In Chapter 2, the nonlocal polarization interferometer’s ability to detect entanglement and statistically identify Bell states relies completely on the estimation of correlations coefficients. The form of Eq. 4.5 is a lot like another common quantity in quantum information, the visibility

$$V = \frac{max - min}{max + min}. \tag{4.6}$$

The *max* and *min* quantities are typically the maximum and minimum values in an interference pattern. When that pattern is from two photon correlations it is representing the same quantity as the correlation coefficient, albeit at the maximal points whereas Bell tests are done at submaximal points. In quantum key distribution, measurement of the error rate q is necessary to quantify the security of the system and determine the amount of privacy amplification [68, 69] needed. The error rate is simply the percentage of uncorrelated events measured out of the total. For instance a two-channel polarization setup that is intended to produce the correlated measurements HH and VV would have a count dependent error rate

$$q = \frac{\mathcal{C}_{HV} + C_{VH}}{C_{HH} + C_{VV} + C_{HV} + C_{VH}}. \tag{4.7}$$

As is, this represents what component of the measured bits are useful to the end users. However, to estimate the true security, this error rate must be represented as a probability for which the unnormalized ratio given in Eq. 4.7 may be a poor estimator. After normalization, the conservative approach would be to take the higher of the two error rates as the estimation.

Is there a better way to make these estimates, or is the “ratio” method the best we can do? In this Chapter we suggest an alternative approach using Bayes’ rule which has found applications in quantum state [70] and entanglement [71] estimation. Additionally, Asher Peres proposed Bayesian methods in evaluations of Bell inequalities [72]. In this Chapter, we apply Bayes’ rule to derive a probability distribution from which all quantities of interest may be calculated. We show that this approach leads to better correlation predictions on average. Surprisingly we also find different maximum likelihood predictions than the ratio method. These predictions are, on average, closer to the true value. In addition to outperforming the ratio method in simulations, our approach avoids logical pitfalls found when translating the ratio method results into a distribution, specifically the Gaussian distribution.

Instead of concerning ourselves with the correlation coefficient $\mathcal{E} \in \{-1, 1\}$. We may equivalently consider the probability of correlation $p \in \{0, 1\}$. Knowledge of either is equivalent to knowing both. Necessarily, the probability of anti-correlation is $1 - p$. These quantities have the simple relations

$$\mathcal{E} = 2p - 1, \quad p = \frac{1+\mathcal{E}}{2}, \text{ and } \quad 1 - p = \frac{1-\mathcal{E}}{2}. \tag{4.8}$$

Unfortunately, this Chapter deals with probability distributions for the probability of correlation, i.e. probabilities of probabilities! The probability distribution as a whole will be referred to as capital P with lower case p as the variant. The maximum point of the distribution P is the most likely estimate for the probability of correlation p_{ml}.

The goal is to determine p_{ml}, the most likely probability, and the uncertainty or standard deviation of that estimate. Let us consider a traditional approach to this estimation. An experiment similar to Fig. 4.1 is performed, and a physicist would like to measure p_{ml}. With local settings appropriate for maximal correlation, he counts for some time to ensure sufficient statistics and plugs the singles counts and coincidence counts into Eq. 4.1. From this he gets a most likely estimate $p_{ml}=\frac{1+\mathcal{E}_{ml}}{2}$. The common approach [73] in determining the uncertainty is to determine the variation of the quantity of interest, p_{ml}, with respect to the variables used in its calculation, and multiply these variations by the uncertainty of those variables. These are then summed in quadrature. The uncertainty for all counts, assuming a Poisson distribution, is simply their square root. The resultant standard deviation estimate is

$$\sigma_p = \sqrt{\left(\sum_{i=A}^{B}\sum_{j=H}^{V}\frac{\partial p}{\partial S_{ij}}\right)^2 S_{ij} + \sum_{\ell,k=H}^{V}\left(\frac{\partial p}{\partial \mathcal{C}_{\ell k}}\right)^2 C_{\ell k}}. \tag{4.9}$$

The derivatives will not be carried out, but, as one can see, there are many terms in the full estimate. The physicist finds a value $p_{ml} = 0.995$ with $\sigma_p = \pm 0.005$ and pats himself on the back. He decides a nice Gaussian probability distribution plot would look great in his paper, and he plugs his data into his plotting software, disaster! As can be seen in Fig. 4.2 a significant portion of his distribution lies above $p = 1$. In other words, according to his distribution there is a 15.8% chance that the true value of p is more than 1. This is of course nonsensical.

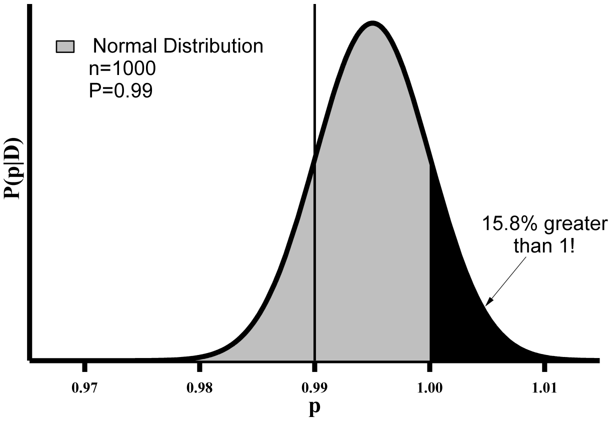

Figure 4.2: The Normal distribution does not conform to the probability upper bound of 1. This distribution suggests that there is a 15.8% chance the probability is greater than 1! This behavior is undesirable.

Our physicist decides the plot isn't such a great idea, after all. He then remembers that in his theoretical prediction unentangled states have a definite upper bound for the correlation probability $p_s = 0.75$. He decides to instead use his probability distribution to compare the likelihood of his measured p_{ml} and the best case scenario for a separable state p_s. At first, he plans to use a probability ratio with values from his Gaussian distribution, but is confounded when he remembers that a large portion of that distribution is over p=1. How should this be accounted for? Additionally, there seems to be no logical reason to use a Gaussian distribution other than conformity to tradition. After some consideration, he decides that these correlations are really a lot like coin flipping. For example, the probability that a coin with unknown fairness has a probability of heads p_h is flipped n times gives heads k times is given by the binomial distribution

$$\binom{n}{k} p_h^k (1-p)^{n-k}. \tag{4.10}$$

He figures that he can compare the likelihood of his p_{ml} and p_s using the ratio

$$\frac{p_{ml}^k (1-p_{ml})^{n-k}}{p_s^k (1-p_s)^{n-k}} \tag{4.11}$$

where k is the number of correlations and $n-k$ is the number of anti-correlations. Liking the logic behind this process, he decides to use a normalized binomial distribution for his probability plot, voila!

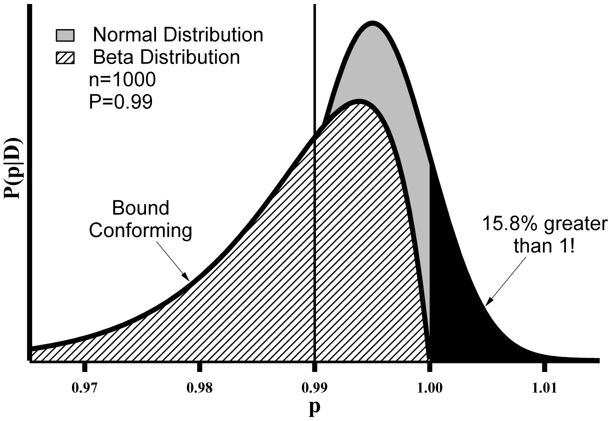

Figure 4.3: Unlike the Normal distribution, the Beta distribution naturally conforms to the probability bounds.

He has plotted the Beta distribution

$$P(p|n,k) = \frac{p_h^k(1-p)^{n-k}}{\text{Beta}\left[1+k, 1+n-k\right]} \tag{4.12}$$

and, as can be seen in Fig. 4.3 it is well behaved at the probability boundary. In fact, the Beta distribution is a common approach when representing probability distributions [74, 75, 66]. The key leap our physicist has made is that embedded in all the counts, coincidences, efficiencies, ports, and detectors, it is ultimately a single quantity he seeks to know, the probability of correlation. Our physicist has approached the problem logically, and lucky for him his experiment had perfectly symmetric detection efficiencies. In general, just using the Beta distribution doesn't outperform the ratio method. If his experiment had included asymmetries, he would have predicted the wrong answer. This is because his raw counts would not have been proportional to just the probability of correlation, but also the probability the photon is lost. Clearly, a more systematic approach is needed.

4.2 Bayes' Rule

Bayes' rule is

$$P\left(A|B\right) = \frac{P\left(B|A\right)P\left(A\right)}{P\left(B\right)} \tag{4.13}$$

the probability of A given B, $P\left(A|B\right)$, is given by the probability of B given A, $P\left(B|A\right)$, weighted by the prior probability of A, $P\left(A\right)$, divided by the total probability of B over all A, $P\left(B\right) = \sum_i P\left(B|A_i\right)P\left(A_i\right)$. The denominator on the right hand side (RHS) of the rule is just the numerator summed or integrated over all values of A. Thus the RHS is a distribution.

The utility of the rule is made clear with the following familiar example. Consider that we want to know the fairness of a coin. We flip the coin n times getting heads k times and we want to know the probability p that the coin lands on heads. Using Bayes' rule and our knowledge that such probabilities obey the binomial distribution we find the distribution

$$P(p|n,k) = \frac{\binom{n}{k} p^k (1-p)^{n-k} P(p)}{\binom{n}{k} \int_0^1 \, dp p^k (1-p)^{n-k} P(p)} \tag{4.14}$$

where $P(p)$ is probability of heads prior to flipping the coin. If we expect a fair coin, we would choose $P(p) = p(1-p)$. If we have no prior information, we could just pick a uniform prior $P(p) = 1$. Assuming a uniform prior, Eq. 4.14 reduces to

$$P(p|n,k) = \frac{p^k (1-p)^{n-k}}{\text{Beta}\left[1+k, 1+n-k\right]} \tag{4.15}$$

which is the Beta distribution. The most likely value for p coincides with what we expect

$$p_{ml} = \frac{k}{n}. \tag{4.16}$$

If we want to know the standard deviation of p,

$$\sigma = \sqrt{\langle p^2 \rangle - \langle p \rangle^2}, \tag{4.17}$$

we calculate it from the distribution, using

$$\left\langle p^2 \right\rangle = \int_0^1 P(p|n,k) p^2 dp \tag{4.18}$$

and

$$\langle p \rangle = \int_0^1 P(p|n,k) p \; dp. \tag{4.19}$$

This results in the simple expression

$$\sigma = \sqrt{\frac{k(n-k)}{n^2(n+1)}}. \tag{4.20}$$

This is a very nice example that results in simple answers. Perhaps Bayes' rule was not even needed to validate this approach. However, the answers we find in our approach to correlation estimation, while nice looking, do not permit such simple algebraic execution. In addition to having a more complex model for the probability distribution, estimating most likelihoods and uncertainties requires numerical computation. However, compared to the traditional approach, we get better answers.

4.3 Estimating Correlations

As a model for our derivation, consider a two channel experiment as seen in Fig. 4.4. A source generating photon pair flux F is shared between Alice and Bob. Alice and Bob each have a measurement apparatus consisting of a half-wave plate, a polarizing beamsplitter, and a pair of detectors. Here we have equated the horizontal port to 0 and the vertical to 1. For example, with this configuration they could carry out the QKD Ekert protocol [6]. For a series of measurements, let the individual detector counts be A_0, A_1, B_0, and B_1 for Alice and Bob, respectively. Let the coincidence count for two detectors A_i and B_j be c_{ij}, or c_{00}, c_{11}, c_{01}, and c_{10}. The last parameters we will need are the efficiencies of detection, transmission and detector dependent, η_{a0}, η_{a1}, η_{b0}, and η_{b1}.

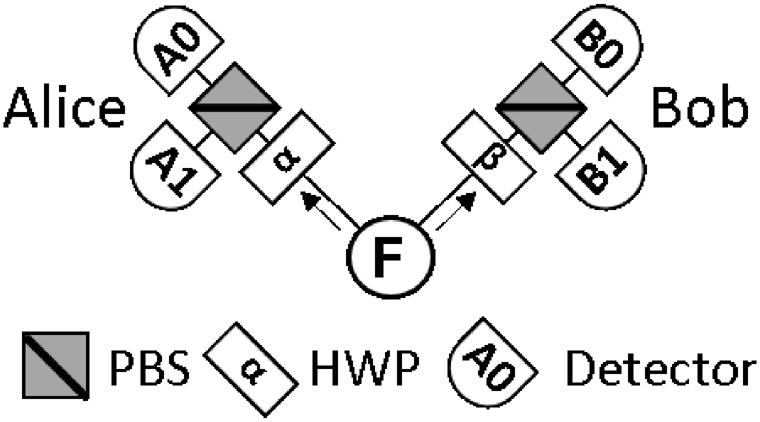

Figure 4.4: A two-channel experiment using polarization. Alice and Bob each have two possible detection outcomes, $H \equiv 0$ or $V \equiv 1$.

In preparation for the full treatment we first consider the treatment of detection probabilities. If n photons are incident through an experimental pathway "destined" to arrive at detection port 0, but subject to the probability of loss $1-\eta_0$, the probability we detect k_0 of these events is

$$P(k_0) = \binom{n}{k_0}\eta_0^{k_0}(1-\eta_0)^{n-k_0}, \tag{4.21}$$

the binomial distribution, again. Next, consider that in addition to the efficiency of detection, the photon is no longer destined to this specific detector, but has a probability p of going to detector 0 and a probability $1-p$ of going to detector 1 with its own path efficiency. What is the probability of k_0 counts in detector 0 and k_1 counts in detector 1? The probability is

$$\begin{aligned} &P(k_0, k_1|p) \\ &\quad= \sum_{m=k_0}^{n-k_1}\binom{n}{m}\binom{n-m}{k_1}\binom{m}{k_0}(p\eta_0)^{k_0}(p(1-\eta_0))^{m-k_0}((1-p)\eta_1)_1^k((1-p)(1-\eta_1))^{n-m-k_1} \\ &\quad= \sum_{m=k_0}^{n-k_1}\binom{n}{m}\binom{n-m}{k_1}\binom{m}{k_0}p^m(1-p)^{n-m}\eta_0^{k_0}(1-\eta_0)^{n-k_0}\eta_1^{k_1}(1-\eta_1)^{n-m-k_1}. \end{aligned} \tag{4.22}$$

This is considerably more complex, since now we have to account for all the ways that things can happen. We now ask, given that we count k_0 and k_1 what is the probability p of the photon choosing the detector 0 pathway? We use Bayes' rule,

$$P(p|k_0, k_1) = \frac{P(k_0, k_1|p)}{\int_0^1 dp P(k_0, k_1|p)} \tag{4.23}$$

where we have assumed a uniform prior probability $P(p) = 1$ and $P(k_0, k_1|p)$ is given by Eq. 4.22. We now have a distribution from which we can predict the most likely probability p_{ml} the photon goes to detector 0 and any other quantities we want to calculate such as the standard deviation. This is the basic procedure we will use albeit with more possibilities.

We pose the problem in the following manner. Consider that Alice has made a detection, she has heralded a photon pair. What is the probability that the photon Bob measures is correlated? Posing the problem in this manner removes the unknown parameter F, the true photon flux, from the problem. We could, of course, equally consider the problem from Bob's perspective, but A's come before B's. The distribution we seek represents the probability that Bob's photon is correlated or anti-correlated given that Alice has detected at either her 0 or 1 port. Let the probabilities of a 00 coincidence be p_0, 11 is p_1, 01 is p_2, and 10 is p_3. Considering all the possibilities simultaneously gives the distribution

$$P(p|\mathcal{A},\mathcal{C}) = \frac{\iiiint dp_0 dp_1 dp_2 dp_3 \delta(p-p_0-p_1)\delta(1-p-p_2-p_3)P(\mathcal{P}|\mathcal{A},\mathcal{C})}{\int_0^1 \iiiint dp dp_0 dp_1 dp_2 dp_3 \delta(p-p_0-p_1)\delta(1-p-p_2-p_3)P(\mathcal{P}|\mathcal{A},\mathcal{C})} \tag{4.24}$$

where a uniform prior $P(p) = 1$ is assumed, $\mathcal{P} = \{p_0, p_2, p_2, p_3\}$, $\mathcal{A} = \{A_0, A_1\}$, and $\mathcal{C} = \{c_{00}, c_{11}, c_{01}, c_{10}\}$. The delta functions ensure that the probability of correlation is the sum $p = p_0 + p_1$, the sum of the probability of measuring 00 and 11, and the probability of anti-correlation is $1 - p = p_2 + p_3$, the sum of the probability of measuring 01 and 10. Let us consider the numerator alone, remembering that in order to normalize the distribution we will ultimately have to divide through by the denominator. Again, the denominator is simply the numerator integrated over the range of $p \in \{0, 1\}$.

The integrand in the numerator is

$$\begin{aligned} P(\mathcal{P}|\mathcal{A},\mathcal{C}) = &\sum_{n=c_{00}}^{A_0-c_{01}} \binom{A_0}{n}\binom{A_0-n}{c_{01}}\binom{n}{c_{00}} p_0^n p_2^{A_0-n} \eta_{b0}^{c00}(1-\eta_{b0})^{n-c_{00}} \eta_{b1}^{c_{01}}(1-\eta_{b1})^{A_0-n-c_{01}} \\ &\times \sum_{m=c_{11}}^{A_1-c_{10}} \binom{A_1}{m}\binom{A_1-m}{c_{10}}\binom{m}{c_{11}} p_1^m p_3^{A_1-m} \eta_{b1}^{c11}(1-\eta_{b1})^{m-c_{11}} \eta_{b0}^{c_{10}}(1-\eta_{b0})^{A_1-m-c_{10}} \end{aligned} \tag{4.25}$$

with the first sum corresponding to photon pairs heralded by Alice detecting at her 0 port and the second sum corresponding to Alice detecting at her 1 port. Given that Alice has made a detection, the probability Bob detects a photon at either of his ports is related to both the probability of correlation, but also the efficiency of that port. Each of the two sums includes components of the correlation probability, $p = p_0 + p_1$, and anti-correlation probability, $1 - p = p_2 + p_3$. Thus, they cannot be treated independently, the integrations must include the product of these sums.

Using the binomial theorem

$$\sum_{k=0}^{n} \binom{n}{k} x^k y^{n-k} = (x+y)^n, \tag{4.26}$$

Eq. 4.25 can be reduced to

$$\begin{aligned} P(\mathcal{P}|\mathcal{A},\mathcal{C}) = & \frac{\eta_{b0}^{c_{00}+c_{10}} \eta_{b1}^{c_{11}+c_{01}} A_{0(c_{00}+c_{01})} A_{1(c_{11}+c_{10})}}{c_{00}!c_{11}!c_{01}!c_{10}!} p_0^{c_{00}} p_1^{c_{11}} p_2^{c_{01}} p_3^{c_{10}} \\ & \times \left(p_0(1-\eta_{b0})+p_2(1-\eta_{b1})\right)^{A_0-c_{00}-c_{01}} \left(p_1(1-\eta_{b1})+p_3(1-\eta_{b0})\right)^{A_1-c_{11}-c_{10}} \end{aligned} \tag{4.27}$$

where $x_{(y)} = \frac{\Gamma(x+y)}{\Gamma(x)}$ is the Pochammer symbol and $\Gamma(x)$ the Gamma function. The ratio in the first line of Eq. 4.27 is a constant and in principle can be disregarded, it would be removed anyway when the normalization procedure is carried out. However, it turns out that keeping it is best for the numerical computation which works with very small or very large numbers. Retaining this constant keeps the magnitude of the numbers in check. Integrating p_1 and p_3 over delta functions simplifies Eq. 4.24 to

$$P(p|\mathcal{A},\mathcal{C}) = \frac{\int_0^p dp_0 \int_0^{1-p} dp_2 P(p_0, p_2|\mathcal{A},\mathcal{C})}{\int_0^1 dp \int_0^p dp_0 \int_0^{1-p} dp_2 P(p_0, p_2|\mathcal{A},\mathcal{C})} \tag{4.28}$$

where

$$\begin{aligned} &P(p_0, p_2|\mathcal{A}, \mathcal{C}) \\ &\quad = \frac{\eta_{b0}^{c_{00}+c_{10}} \eta_{b1}^{c_{11}+c_{01}} A_{0(c_{00}+c_{01})} A_{1(c_{11}+c_{10})}}{c_{00}!c_{11}!c_{01}!c_{10}!} p_0^{c_{00}} (p-p_0)^{c_{11}} p_2^{c_{01}} (1-p-p_2)^{c_{10}} \\ &\quad \times (p_0(1-\eta_{b0})+p_2(1-\eta_{b1}))^{A_0-c_{00}-c_{01}} ((p-p_0)(1-\eta_{b1})+(1-p-p_2)(1-\eta_{b0}))^{A_1-c_{11}-c_{10}} . \end{aligned} \tag{4.29}$$

Unfortunately, no further simplification appears possible. Though, this doesn't mean a simpler form cannot be found. Integrating over p_0 and p_2 leads to hypergeometric series representations that only slow the numerical calculation. It may be worth considering that choosing Bob as the herald instead should lead to the same distribution. The distribution from Bob's perspective is similar to Eq. 4.28 with dependence on Bob's detections and Alice's efficiencies. Some computational simplification may result from this seeming equality, but this has not yet occured. Thus, the probability distribution given in Eq. 4.28 is the main result of this Chapter. This result takes as its inputs the singles counts A_0, A_1, and coincidence counts c_{00}, c_{11}, c_{01}, and c_{10}. Additionally, the efficiencies η_{b0} and η_{b1} are required. This was not a requirement in the ratio method, since in that normalization procedure the efficiencies factor out. Thus, these efficiencies can either be experimentally determined, or they can be determined through the following minimization procedure.

The efficiencies of detections obey the proportionality relations

$$\frac{c_{00}}{\eta_{b0}} + \frac{c_{01}}{\eta_{b1}} \approx \frac{\eta_{a0}\eta_{b0}p(F/2)}{\eta_{b0}} + \frac{\eta_{a0}\eta_{b1}(1-p)(F/2)}{\eta_{b1}} = \eta_{a0}(F/2) = A_0. \tag{4.30}$$

The other relations are

$$A_1 \approx \frac{c_{11}}{\eta_{b1}} + \frac{c_{10}}{\eta_{b0}}, \quad B_0 \approx \frac{c_{00}}{\eta_{a0}} + \frac{c_{10}}{\eta_{a1}}, \quad B_1 \approx \frac{c_{01}}{\eta_{a0}} + \frac{c_{11}}{\eta_{a1}}. \tag{4.31}$$

The approximate efficiencies are

$$\begin{aligned}\eta_{a0}(\mathcal{C},\mathcal{B}) &= \frac{c_{01}c_{10}-c_{00}c_{11}}{c_{10}B_1-c_{11}B_0}, \quad \eta_{a1}(\mathcal{C},\mathcal{B}) = \frac{c_{01}c_{10}-c_{00}c_{11}}{c_{01}B_0-c_{00}B_1},\\ \eta_{b0}(\mathcal{C},\mathcal{A}) &= \frac{c_{01}c_{10}-c_{00}c_{11}}{c_{01}A_1-c_{11}A_0}, \quad \eta_{b1}(\mathcal{C},\mathcal{A}) = \frac{c_{01}c_{10}-c_{00}c_{11}}{c_{10}A_0-c_{00}A_1},\end{aligned} \tag{4.32}$$

where $\mathcal{A}=\{A_0,A_1\}$, $\mathcal{B}=\{B_0,B_1\}$, and $\mathcal{C}=\{c_{00},c_{11},c_{01},c_{10}\}$. In addition to these relations, we use the approximate efficiency ratios

$$\frac{\eta_{ij}}{\eta_{m\ell}} \approx \frac{i_j}{m_\ell}, \tag{4.33}$$

for example, $\eta_{a0}/\eta_{b0} \approx A0/B0$.

Combining all these relations, we minimize the function

$$\begin{aligned} M &= \sum_{i,j\in A_0,A_1,B_0,B_1} \left[\left(\frac{i}{j} x_j - \eta_i\left(\mathcal{C},\mathcal{J}\right) \right)^2 \right] \\ &= \Bigg[\left(x_{a0} - \eta_{a0}\left(\mathcal{C},\mathcal{B}\right)\right)^2 + \left(\frac{A_0}{A_1} x_{a1} - \eta_{a0}\left(\mathcal{C},\mathcal{B}\right) \right)^2 + \\ &\qquad \cdots + \left(\frac{B_1}{B_0} x_{b0} - \eta_{b1}\left(\mathcal{C},\mathcal{A}\right) \right)^2 + \left(x_{b1} - \eta_{b1}\left(\mathcal{C},\mathcal{A}\right)\right)^2 \Bigg] \end{aligned} \tag{4.34}$$

where $\mathcal{J}=\mathcal{B}$ for $j=a0,a1$ and $\mathcal{J}=\mathcal{A}$ for $j=b0,b1$. Note that $\eta_{a0} \approx \frac{A_0}{A_1}\eta_{a1}$, thus, the first two terms above are both constraints on η_{a0}. The value of the variables x_{a0}, x_{a1}, x_{b0}, and x_{b1} at the function minimum are taken as the efficiencies. The M function is proportional to the difference amongst all the relationships given prior. This is an effective procedure, as the final numerical results suggest. In the next section, we use Eq. 4.28 and 4.33 in numerical simulations. We compare the estimations to the traditional ratio method and a complimentary traditional distribution, the Gaussian distribution.

4.4 Numerical Simulation Results

We simulate a two-channel experiment as seen in Fig. 4.4. The simulation uses random numbers to initialize a "true" probability of correlation $p_{true} \in \{0.05, 0.95\}$ and the efficiencies $\eta_i \in \{0.1, 0.9\}$. In a computational loop of length F, the photon pair flux, more random numbers decide the final detection and coincidence results. In each iteration, four random numbers r_0, r_1, r_2 and r_3 are generated. If $r_0 < p_{true}$ the pair adopts a correlation pathway, else an anti-correlation pathway. The number r_1 decides with a 50:50 probability between the two possible cases of correlation, 00 or 11, or anti-correlation, 01 or 10. If the number r_2 or r_3 is less than the efficiency of the selected ports, a detection is registered. If both detections are registered, a coincidence is counted.

The following mathematical forms are used in the calculations. The Gaussian distribution

$$G(p) = \frac{1}{\sqrt{2\pi}\sigma_r} e^{-\frac{(p-p^r_{ml})^2}{2\sigma_r^2}} \tag{4.35}$$

is given using the most likely estimate from the ratio method

$$p^r_{ml} = \frac{n_{00} + n_{11}}{n_{00} + n_{11} + n_{01} + n_{10}} \quad \text{with} \quad n_{ij} = \frac{c_{ij}}{A_i B_j} \tag{4.36}$$

and the standard deviation

$$\sigma_r = \sqrt{\left(\sum_{i=A}^{B} \sum_{j=0}^{1} \frac{\partial p_{ml}}{\partial i_j}\right)^2 i_j + \sum_{\ell,k=0}^{1} \left(\frac{\partial p}{\partial c_{\ell k}}\right)^2 c_{\ell k}}. \tag{4.37}$$

The probability contained in the interval from a to b has the closed form

$$\mathrm{G}_{a,b} = \int_a^b dp G(p) = \frac{1}{2}\left(\mathrm{Erf}\left[\frac{p^r_{ml} - a}{\sqrt{2}\sigma_r}\right] - \mathrm{Erf}\left[\frac{p^r_{ml} - b}{\sqrt{2}\sigma_r}\right]\right). \tag{4.38}$$

The proposed distribution $P(p|\mathcal{A},\mathcal{C})$ is given by Eq. 4.28. The most likely value is that which maximizes the distribution

$$p^{p}_{ml} = \underset{p\in\{0,1\}}{\text{argmax}}\left[P(p|\mathcal{A},\mathcal{C})\right]. \tag{4.39}$$

The probability contained in the interval a to b must be numerically integrated,

$$\text{P}_{a,b} = \frac{\int_a^b dpP(p|\mathcal{A},\mathcal{C})}{\int_0^1 dpP(p|\mathcal{A},\mathcal{C})}. \tag{4.40}$$

The proposed standard deviation is also found numerically,

$$\sigma_p = \sqrt{\frac{\int_0^1 dpP(p|\mathcal{A},\mathcal{C})\; p^2}{\int_0^1 dpP(p|\mathcal{A},\mathcal{C})} - \left(\frac{\int_0^1 dpP(p|\mathcal{A},\mathcal{C})\; p}{\int_0^1 dpP(p|\mathcal{A},\mathcal{C})}\right)^2}. \tag{4.41}$$

This simulation is carried out in *Mathematica 9.0* [76] with and without determination of the efficiencies using minimization in the proposed method. The figures of merit we will be using for comparison are the following. First, we compare the probability given for p_{true} by the Gaussian distribution with ratio method parameters p^{r}_{ml} and σ_r and that given using the proposed distribution. Next, the distance of the most likely probability from the true $d=$Abs$(p_{ml}-p_{true})$ is compared for the ratio and proposed methods. This simply represents which most likely estimation is closer to the true value. Last, the probability for p_{true} is compared with increasingly asymmetric efficiency choices as represented by the standard deviation of these choices σ_η. This comparison is focused on the hypothesis that the ratio method is a poor estimator when detection efficiencies are asymmetric.

The first set of data resulted from 2837 simulations of particle flux $F = 1000$, with detection efficiencies determined by minimizing the function M given in Eq. 4.34. Regarding the probability of p_{true} given by the distributions, the proposed distribution (PD) beats the ratio-Gaussian distribution (RGD) 68.6% of the time. On average, PD gives a 14.3% higher probability to p_{true} than RG. The proposed most likely value p^p_{ml} is closest to p_{true} 56% of the time. On average p^p_{ml} is 5% closer to p_{true} than p^r_{ml}. To compare the estimation performance versus the asymmetries in the efficiencies, we plot the ratios $P_p/(P_p + P_{rg})$ and $P_{rg}/(P_p + P_{rg})$ where P_p and P_{rg} are the probabilities given p_{true} by PD and RGD, respectively. PD gives a better performance trend as the efficiency asymmetry, as measured by the efficiency standard deviation σ_η, increases as seen in Fig. 4.5.

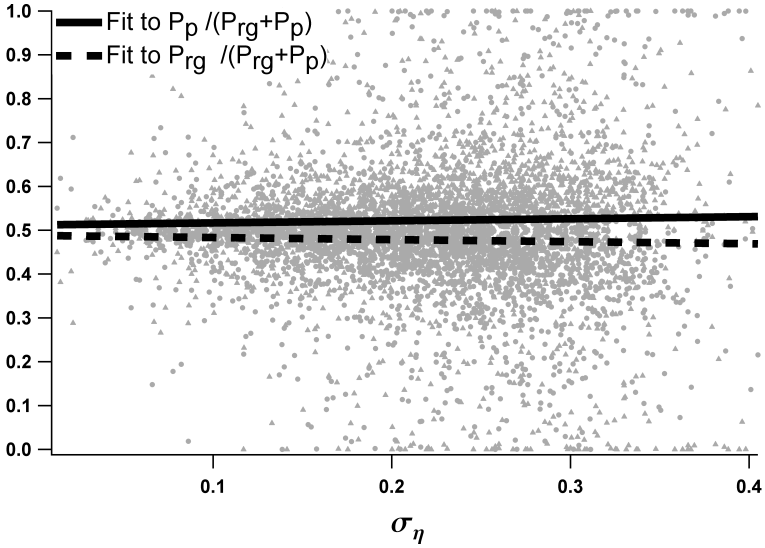

Figure 4.5: Estimating the efficiency, the proposed distribution outperforms the ratio-Gaussian distribution, on average, as asymmetries in the efficiencies increase, as measured by the efficiency standard deviation σ_η.

The second set of data resulted from 2000 simulations of particle flux $F = 1000$, with detection efficiencies given. Regarding the probability of p_{true} given by the distributions, the proposed distribution (PD) beats the ratio-Gaussian distribution (RGD) 71.9% of the time. On average, PD gives a 20% higher probability to p_{true} than RG. The proposed most likely value p^p_{ml} is closest to p_{true} 59% of the time. On average p^p_{ml} is 20% closer to p_{true} than p^r_{ml}. To compare the estimation performance versus the asymmetries in the efficiencies, we plot the ratios $P_p/(P_p + P_{rg})$ and $P_{rg}/(P_p + P_{rg})$ where P_p and P_{rg} are the probabilities given p_{true} by PD and RGD, respectively. PD gives a better performance trend as the efficiency asymmetry, as measured by the efficiency standard deviation σ_η, increases as seen in Fig. 4.6. A summary of the most relevant data is given in Fig. 4.7.

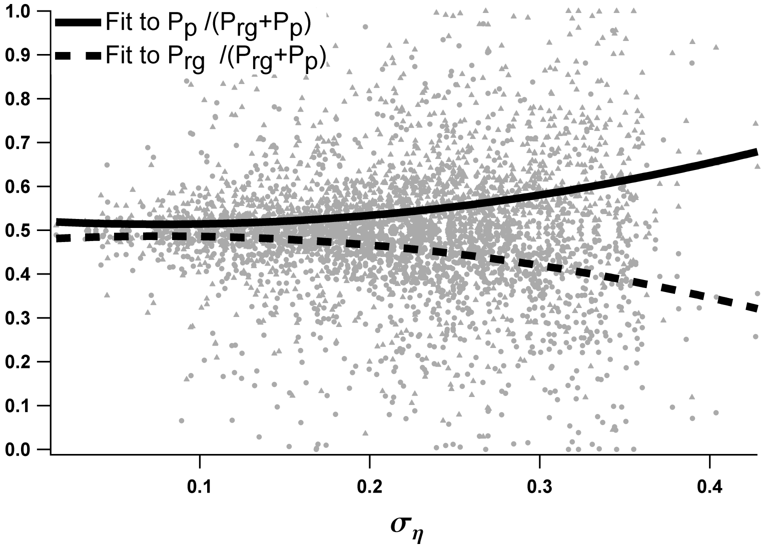

Figure 4.6: Given the efficiencies, the proposed distribution outperforms the ratio-Gaussian distribution, on average, as asymmetries in the efficiencies increase, as measured by the efficiency standard deviation σ_η.

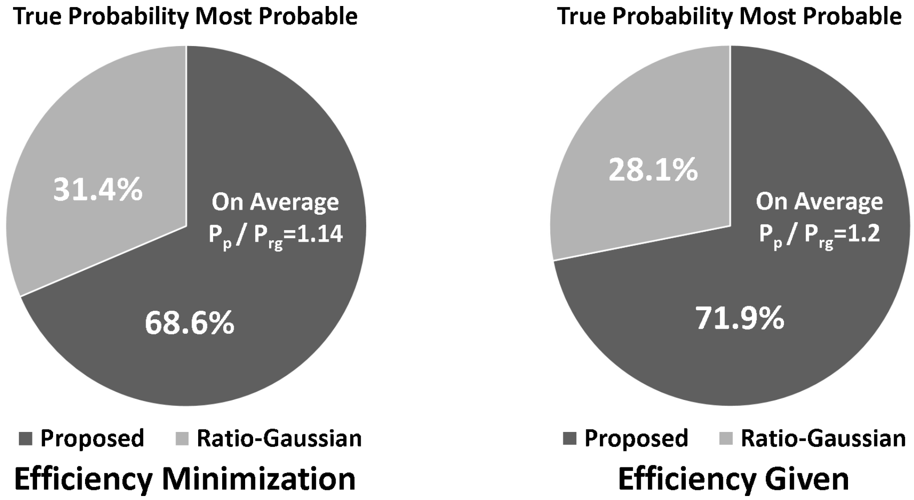

Figure 4.7: For the efficiency minimization method, the proposed distribution has the probability of correlation p_{true} as more probable 68.6% of the time, with a 14% higher probability on average. In the case that the efficiencies are known, the proposed distribution has p_{true} as more probable 71.9% of the time, with a 20% higher probability on average.

4.5 Discussion

The results in the preceding section confirm our hypotheses regarding correlation estimation using the traditional approach. As a first pass, this research suggests further consideration of Bayes' rule in estimating the probabilities associated with quantum information tasks. In addition, the model presented simplifies comparison with known theoretical results. For example, the nonlocal polarization interferometer from Chapter 2, predicts that separable states cannot have a probability of correlation exceeding 75%. Thus, upon experimentally determining the probability of correlation and using this model to produce a distribution $P(p|\mathcal{A},\mathcal{C})$, the relative likelihood of the most likely probability p_{ml} can be compared to the best case for a separable state $p_s = 0.75$,

$$\text{relative likelihood} = \frac{P(p_{ml}|\mathcal{A},\mathcal{C})}{P(p_s|\mathcal{A},\mathcal{C})}. \tag{4.42}$$

With this comparison, physicists may weigh the likelihood of their entanglement prediction. While a large number is more indicative of an entangled state, the appropriate "lines in the sand" are debatable. This idea is discussed further by Blume-Kohout [77]. Use of a Gaussian distribution for this ratio would not be appropriate, since it does not model the physics.

Future research into estimating correlations with Bayes' rule will focus on simplifying or approximating the results to overcome computational cost and interpreting model predictions in a appropriate, sensible, and useful way.

Bibliography

[1] Asher Peres. *Quantum theory: concepts and methods*, volume 57. Springer, 1995. 2

[2] Michael A Nielsen and Isaac L Chuang. *Quantum computation and quantum information*. Cambridge university press, 2010. 2

[3] Niels Bohr. *The quantum postulate and the recent development of atomic theory*. Printed in Great Britain by R. & R. Clarke, Limited, 1928. 3

[4] Frank Miller. *Telegraphic code to insure privacy and secrecy in the transmission of telegrams*. CM Cornwell, 1882. 3

[5] Charles H Bennett, Gilles Brassard, et al. Quantum cryptography: Public key distribution and coin tossing. In *Proceedings of IEEE International Conference on Computers, Systems and Signal Processing*, volume 175. New York, 1984. 3, 49

[6] Artur K. Ekert. Quantum cryptography based on bells theorem. *Phys. Rev. Lett.*, 67:661–663, Aug 1991. 3, 8, 20, 73

[7] Paul Adrien Maurice Dirac. The principles of quantum mechanics. 1930. 3

[8] E. Merzbacher. *Quantum Mechanics*. Wiley, 1998. 3

[9] A. Einstein, B. Podolsky, and N. Rosen. Can quantum-mechanical description of physical reality be considered complete? *Phys. Rev.*, 47:777–780, May 1935. 4

[10] E. Schrdinger. Die gegenwrtige situation in der quantenmechanik. *Naturwissenschaften*, 23(48):807–812, 1935. 4

[11] John D. Trimmer. The present situation in quantum mechanics: A translation of schrdinger's "cat paradox" paper. *Proceedings of the American Philosophical Society*, 124(5):pp. 323–338, 1980. 4

[12] E. Schrdinger. Discussion of probability relations between separated systems. *Mathematical Proceedings of the Cambridge Philosophical Society*, 31:555–563, 10 1935. 4

[13] John S Bell et al. On the einstein-podolsky-rosen paradox. *Physics*, 1(3):195–200, 1964. 4

[14] John F Clauser and Michael A Horne. Experimental consequences of objective local theories. *Physical review D*, 10(2):526, 1974. 4

[15] Alain Aspect, Philippe Grangier, and Gérard Roger. Experimental tests of realistic local theories via bell's theorem. *Physical review letters*, 47(7):460, 1981. 4, 65

[16] Alain Aspect, Philippe Grangier, and Gérard Roger. Experimental realization of einstein-podolsky-rosen-bohm gedankenexperiment: a new violation of bell's inequalities. *Physical review letters*, 49(2):91, 1982. 4, 65

[17] Alain Aspect, Jean Dalibard, and Gérard Roger. Experimental test of bell's inequalities using time-varying analyzers. *Physical review letters*, 49(25):1804, 1982. 4

[18] Marissa Giustina, Alexandra Mech, Sven Ramelow, Bernhard Wittmann, Johannes Kofler, Jörn Beyer, Adriana Lita, Brice Calkins, Thomas Gerrits, Sae Woo Nam, et al. Bell violation using entangled photons without the fair-sampling assumption. *Nature*, 497(7448):227–230, 2013. 4

[19] BG Christensen, KT McCusker, JB Altepeter, B Calkins, T Gerrits, AE Lita, A Miller, LK Shalm, Y Zhang, SW Nam, et al. Detection-loophole-free test of quantum nonlocality, and applications. *Physical review letters*, 111(13):130406, 2013. 4

[20] Y. Aharonov and D. Bohm. Significance of electromagnetic potentials in the quantum theory. *Phys. Rev.*, 115:485–491, Aug 1959. 4

[21] Stuart J Freedman and John F Clauser. Experimental test of local hidden-variable theories. *Physical Review Letters*, 28(14):938, 1972. 5

[22] P. R. Tapster, J. G. Rarity, and P. C. M. Owens. Violation of bell's inequality over 4 km of optical fiber. *Phys. Rev. Lett.*, 73:1923–1926, Oct 1994. 5

[23] Z.Y. Jeff Ou. *Multi-Photon Quantum Interference*. Springer, New York, NY, 2007. 5, 10, 12, 41, 57, 95, 103

[24] C. K. Hong, Z. Y. Ou, and L. Mandel. Measurement of subpicosecond time intervals between two photons by interference. *Phys. Rev. Lett.*, 59:2044–2046, Nov 1987. 6, 40

[25] W. P. Grice and I. A. Walmsley. Spectral information and distinguishability in type-ii down-conversion with a broadband pump. *Phys. Rev. A*, 56:1627–1634, Aug 1997. 6, 10, 12, 42, 58, 95

[26] Carsten Schuck, Gerhard Huber, Christian Kurtsiefer, and Harald Weinfurter. Complete deterministic linear optics bell state analysis. *Physical review letters*, 96(19):190501, 2006. 6

[27] Barry C. Sanders. Quantum dynamics of the nonlinear rotator and the effects of continual spin measurement. *Phys. Rev. A*, 40:2417–2427, Sep 1989. 6

[28] Agedi N. Boto, Pieter Kok, Daniel S. Abrams, Samuel L. Braunstein, Colin P. Williams, and Jonathan P. Dowling. Quantum interferometric optical lithography: Exploiting entanglement to beat the diffraction limit. *Phys. Rev. Lett.*, 85:2733–2736, Sep 2000. 6

[29] J. G. Rarity, P. R. Tapster, E. Jakeman, T. Larchuk, R. A. Campos, M. C. Teich, and B. E. A. Saleh. Two-photon interference in a mach-zehnder interferometer. *Phys. Rev. Lett.*, 65:1348–1351, Sep 1990. 6

[30] J. D. Franson. Bell inequality for position and time. *Phys. Rev. Lett.*, 62:2205–2208, May 1989. 7, 21, 50

[31] JG Rarity and PR Tapster. Experimental violation of bells inequality based on phase and momentum. *Physical Review Letters*, 64(21):2495, 1990. 7

[32] Z. Y. Ou, X. Y. Zou, L. J. Wang, and L. Mandel. Observation of nonlocal interference in separated photon channels. *Phys. Rev. Lett.*, 65:321–324, Jul 1990. 7

[33] P. G. Kwiat, W. A. Vareka, C. K. Hong, H. Nathel, and R. Y. Chiao. Correlated two-photon interference in a dual-beam michelson interferometer. *Phys. Rev. A*, 41:2910–2913, Mar 1990. 7

[34] Hannes Hübel, Michael R. Vanner, Thomas Lederer, Bibiane Blauensteiner, Thomas Lorünser, Andreas Poppe, and Anton Zeilinger. High-fidelity transmission of polarization encoded qubits from an entangled source over 100 km of fiber. *Opt. Express*, 15(12):7853–7862, Jun 2007. 7

[35] D. V. Strekalov, T. B. Pittman, A. V. Sergienko, Y. H. Shih, and P. G. Kwiat. Postselection-free energy-time entanglement. *Phys. Rev. A*, 54:R1–R4, Jul 1996. 7

[36] J. F. Dynes, H. Takesue, Z. L. Yuan, A. W. Sharpe, K. Harada, T. Honjo, H. Kamada, O. Tadanaga, Y. Nishida, M. Asobe, and A. J. Shields. Efficient entanglement distribution over 200 kilometers. *Opt. Express*, 17(14):11440–11449, Jul 2009. 8, 49, 50

[37] Takahiro Inagaki, Nobuyuki Matsuda, Osamu Tadanaga, Masaki Asobe, and Hiroki Takesue. Entanglement distribution over 300 km of fiber. *Optics express*, 21(20):23241–23249, 2013. 8, 56

[38] Hiroki Takesue and Kyo Inoue. Generation of 1.5-μ m band time-bin entanglement using spontaneous fiber four-wave mixing and planar light-wave circuit interferometers. *Physical Review A*, 72(4):041804, 2005. 8, 56

[39] T Honjo, K Inoue, and H Takahashi. Differential-phase-shift quantum key distribution experiment with a planar light-wave circuit mach-zehnder interferometer. *Optics letters*, 29(23):2797–2799, 2004. 8, 56

[40] Charles H. Bennett and Stephen J. Wiesner. Communication via one- and two-particle operators on einstein-podolsky-rosen states. *Phys. Rev. Lett.*, 69:2881–2884, Nov 1992. 8, 20

[41] Charles H. Bennett, Gilles Brassard, Claude Crépeau, Richard Jozsa, Asher Peres, and William K. Wootters. Teleporting an unknown quantum state via dual classical and einstein-podolsky-rosen channels. *Phys. Rev. Lett.*, 70:1895–1899, Mar 1993. 8, 20

[42] Ryszard Horodecki, Paweł Horodecki, Michał Horodecki, and Karol Horodecki. Quantum entanglement. *Rev. Mod. Phys.*, 81:865–942, Jun 2009. 8, 9, 20

[43] Jian-Wei Pan, Zeng-Bing Chen, Chao-Yang Lu, Harald Weinfurter, Anton Zeilinger, and Marek Żukowski. Multiphoton entanglement and interferometry. *Rev. Mod. Phys.*, 84:777–838, May 2012. 8, 20

[44] Otfried Ghne and Gza Tth. Entanglement detection. *Physics Reports*, 474(16):1 – 75, 2009. 9, 20

[45] John F. Clauser, Michael A. Horne, Abner Shimony, and Richard A. Holt. Proposed experiment to test local hidden-variable theories. *Phys. Rev. Lett.*, 23:880–884, Oct 1969. 9, 20, 33

[46] G. Vidal and R. F. Werner. Computable measure of entanglement. *Phys. Rev. A*, 65:032314, Feb 2002. 9, 20

[47] Asher Peres. Separability criterion for density matrices. *Physical Review Letters*, 77(8):1413, 1996. 9

[48] Michal Horodecki, Pawel Horodecki, and Ryszard Horodecki. Separability of mixed states: necessary and sufficient conditions. *Physics Letters A*, 223(12):1 – 8, 1996. 9, 20

[49] Barbara M. Terhal. Bell inequalities and the separability criterion. *Physics Letters A*, 271(56):319 – 326, 2000. 9, 20

[50] M. Barbieri, F. De Martini, G. Di Nepi, P. Mataloni, G. M. D'Ariano, and C. Macchiavello. Detection of entanglement with polarized photons: Experimental realization of an entanglement witness. *Phys. Rev. Lett.*, 91:227901, Nov 2003. 9

[51] David C Burnham and Donald L Weinberg. Observation of simultaneity in parametric production of optical photon pairs. *Physical Review Letters*, 25(2):84, 1970. 10

[52] Oliver Benson, Charles Santori, Matthew Pelton, and Yoshihisa Yamamoto. Regulated and entangled photons from a single quantum dot. *Physical Review Letters*, 84(11):2513, 2000. 10

[53] R Mark Stevenson, Robert J Young, Paola Atkinson, Ken Cooper, David A Ritchie, and Andrew J Shields. A semiconductor source of triggered entangled photon pairs. *Nature*, 439(7073):179–182, 2006. 10

[54] Brian P. Williams, Travis S. Humble, and Warren P. Grice. Nonlocal polarization interferometer for entanglement detection. *Phys. Rev. A*, 90:042121, Oct 2014. 19

[55] I. Marcikic, H. de Riedmatten, W. Tittel, H. Zbinden, M. Legré, and N. Gisin. Distribution of time-bin entangled qubits over 50 km of optical fiber. *Phys. Rev. Lett.*, 93:180502, Oct 2004. 20

[56] Jeremy L O'Brien. Optical quantum computing. *Science*, 318(5856):1567–1570, 2007. 20

[57] Tien Tjuen Ng, Darwin Gosal, Anta Lamas-Linares, and Christian Kurtsiefer. Sagnac-loop phase shifter with polarization-independent operation. *Review of Scientific Instruments*, 82(1):–, 2011. 24

[58] Taehyun Kim, Marco Fiorentino, and Franco N. C. Wong. Phase-stable source of polarization-entangled photons using a polarization sagnac interferometer. *Phys. Rev. A*, 73:012316, Jan 2006. 37, 42

[59] P. G. Evans, R. S. Bennink, W. P. Grice, T. S. Humble, and J. Schaake. Bright source of spectrally uncorrelated polarization-entangled photons with nearly single-mode emission. *Phys. Rev. Lett.*, 105:253601, Dec 2010. 37

[60] Z. Y. Ou, X. Y. Zou, L. J. Wang, and L. Mandel. Experiment on nonclassical fourth-order interference. *Phys. Rev. A*, 42:2957–2965, Sep 1990. 39

[61] E. J. S. Fonseca, C. H. Monken, and S. Pádua. Measurement of the de broglie wavelength of a multiphoton wave packet. *Phys. Rev. Lett.*, 82:2868–2871, Apr 1999. 39

[62] Dagmar Bruß. Optimal eavesdropping in quantum cryptography with six states. *Physical Review Letters*, 81(14):3018, 1998. 49

[63] Valerio Scarani, Helle Bechmann-Pasquinucci, Nicolas J. Cerf, Miloslav Dušek, Norbert Lütkenhaus, and Momtchil Peev. The security of practical quantum key distribution. *Rev. Mod. Phys.*, 81:1301–1350, Sep 2009. 49, 54

[64] Renato Renner, Nicolas Gisin, and Barbara Kraus. Information-theoretic security proof for quantum-key-distribution protocols. *Phys. Rev. A*, 72:012332, Jul 2005. 49, 53, 54

[65] Shellee D Dyer, Martin J Stevens, Burm Baek, and Sae Woo Nam. High-efficiency, ultra low-noise all-fiber photon-pair source. *Optics express*, 16(13):9966–9977, 2008. 52

[66] David JC MacKay. *Information theory, inference, and learning algorithms*, volume 7. Citeseer, 2003. 64, 71

[67] John F Clauser and Abner Shimony. Bell's theorem. experimental tests and implications. *Reports on Progress in Physics*, 41(12):1881, 1978. 65

[68] Charles H Bennett, Gilles Brassard, Claude Crépeau, and Ueli M Maurer. Generalized privacy amplification. *Information Theory, IEEE Transactions on*, 41(6):1915–1923, 1995. 67

[69] David Deutsch, Artur Ekert, Richard Jozsa, Chiara Macchiavello, Sandu Popescu, and Anna Sanpera. Quantum privacy amplification and the security of quantum cryptography over noisy channels. *Physical Review Letters*, 77(13):2818, 1996. 67

[70] Robin Blume-Kohout. Optimal, reliable estimation of quantum states. *New Journal of Physics*, 12(4):043034, 2010. 68

[71] Pavel Lougovski and S. J. van Enk. Characterizing entanglement sources. *Phys. Rev. A*, 80:052324, Nov 2009. 68

[72] Asher Peres. Bayesian analysis of bell inequalities. *arXiv preprint quant-ph/9905084*, 1999. 68

[73] John Taylor. *Introduction to error analysis, the study of uncertainties in physical measurements*, volume 1. 1997. 68

[74] George Casella and Roger L Berger. *Statistical inference*, volume 2. Duxbury Pacific Grove, CA, 2002. 71

[75] Thomas M Cover and Joy A Thomas. *Elements of information theory.* John Wiley & Sons, 2012. 71

[76] 80

[77] Robin Blume-Kohout, Jun OS Yin, and SJ van Enk. Entanglement verification with finite data. *Physical review letters*, 105(17):170501, 2010. 83

[78] Nicolaas Bloembergen. *Nonlinear optics.* World Scientific, 1996. 95

[79] R. Loudon. *The Quantum Theory of Light.* Oxford University Press, 2000. 95, 97, 99

[80] Kevin A ODonnell and Alfred B URen. Time-resolved up-conversion of entangled photon pairs. *Physical review letters*, 103(12):123602, 2009. 95

[81] Kevin A ODonnell. Observations of dispersion cancellation of entangled photon pairs. *Physical review letters*, 106(6):063601, 2011. 95

[82] Nicolas Sangouard, Bruno Sanguinetti, Noé Curtz, Nicolas Gisin, Rob Thew, and Hugo Zbinden. Faithful entanglement swapping based on sum-frequency generation. *Physical review letters*, 106(12):120403, 2011. 95

[83] Thiago Guerreiro, Enrico Pomarico, Bruno Sanguinetti, Nicolas Sangouard, JS Pelc, C Langrock, MM Fejer, Hugo Zbinden, Robert T Thew, and Nicolas Gisin. Interaction of independent single photons based on integrated nonlinear optics. *Nature communications*, 4, 2013. 95

[84] Robert W Boyd. *Nonlinear optics.* Academic press, 2003. 96

[85] Leonard Mandel and Emil Wolf. *Optical coherence and quantum optics.* Cambridge university press, 1995. 101

Appendix

Appendix A

The Two-Photon State from Downconversion

In this appendix, we derive unitary operators for downconversion and upconversion as approximations of the true nonlinear processes, spontaneous parametric downconversion (SPDC) and frequency upconversion, SPDC's conjugate process. This derivation is a conglomeration of methods and results from [78, 25, 23, 79]. As implied by the citations, this is not a new result. However, it combines a sufficient description of the origin of the two photon state from SPDC sufficient to describe the states in the presented and similar research. The similarities between downconversion and upconversion also allow adoption of an operational approach that should ease theoretical descriptions involving both downconversion and upconversion. The most simple case being upconversion of a previously downconverted pair in an identical crystal [80, 81]. Theoretical treatments upconverting previously unentangled photons, such as entanglement swapping [82, 83], may also benefit from this description. Once the downconversion and upconversion operators have been approximated, the downconversion operator is used to generate a two-photon state whose variants are applied in Chapter 1 and 2.

A.1 Downconversion and Upconversion Operators

The Hamiltonian for the electric and magnetic fields in a medium is given by

$$H = \frac{1}{2}\int_V d^3r \left[\mathbf{D}\left(\mathbf{r},t\right)\cdot\mathbf{E}\left(\mathbf{r},t\right) + \frac{1}{\mu_0}\mathbf{B}^2\left(\mathbf{r},t\right)\right] \tag{A.1}$$

with the displacement field

$$\mathbf{D}\left(\mathbf{r},t\right) = \epsilon_0\mathbf{E}(\mathbf{r},t) + \mathbf{P}(\mathbf{r},t) \tag{A.2}$$

and polarization $\mathbf{P}(\mathbf{r},t)$. Combining (A.1) and (A.2)

$$H = \frac{1}{2}\int_V d^3r \left[\epsilon_0\mathbf{E}^2\left(\mathbf{r},t\right) + \frac{1}{\mu_0}\mathbf{B}^2\left(\mathbf{r},t\right)\right] + \frac{1}{2}\int_V d^3r \left[\mathbf{E}\left(\mathbf{r},t\right)\cdot\mathbf{P}\left(\mathbf{r},t\right)\right] \tag{A.3}$$

Let us write the free electric field as a sum of discrete mode plane waves, see [84] , as

$$\mathbf{E}\left(\mathbf{r},t\right) = \sum_{n=-\infty}^{\infty}\mathbf{E}\left(\omega_n\right)e^{-i\omega_n t} \tag{A.4}$$

$$\mathbf{E}\left(\omega_n\right) = \mathbf{A}_n e^{i\mathbf{k}_n\cdot\mathbf{r}} \tag{A.5}$$

The polarization must be expanded into linear relationships with individual modes and components of the applied field. This results in the proportionality factor χ, the susceptibility, being a tensor. The polarization is then

$$P_i(\omega_n) = \lim_{N\to\infty}\epsilon_0\sum_{n=1}^{N}\sum_{m_1\cdot\cdot m_N}\sum_{j_1\cdot\cdot j_N}\delta_{\omega_n(\sum_n\omega_{m_n})}\chi_{ij_1\cdot\cdot j_N}(\omega_n,\omega_{m_1},\cdot\cdot,\omega_{m_N})\,E_{j_1}(\omega_{m_1})\cdot\cdot E_{j_N}(\omega_{m_N}) \tag{A.6}$$

from which we are concerned only with the second-order contribution

$$P_i^{(2)}(\omega_n) = \epsilon_0 \sum_{m,u=-\infty}^{\infty} \sum_{j,\ell=1}^{3} \delta_{\omega_n(\omega_m+\omega_u)} \chi_{ij\ell}(\omega_n, \omega_m, \omega_u)\, E_j(\omega_m)\, E_\ell(\omega_u)\,. \tag{A.7}$$

In the experiment of interest χ does not change appreciably over the frequency range. With this key approximation Eq. A.7 reduces to

$$\mathbf{P}\left(\mathbf{r},t\right) = \epsilon_0 \chi_{ij\ell} E_j\left(\mathbf{r},t\right) E_\ell\left(\mathbf{r},t\right) \mathbf{e}_i \tag{A.8}$$

We can now rewrite (A.3)

$$\begin{aligned} H =& \frac{1}{2}\int_V d^3r \left[\epsilon_0 \mathbf{E}^2\left(\vec{r},t\right) + \frac{1}{\mu_0}\mathbf{B}^2\left(\vec{r},t\right)\right] \\ &+ \frac{\epsilon_0}{2}\int_V d^3r \chi_{ij\ell} E_i\left(\mathbf{r},t\right) E_j\left(\mathbf{r},t\right) E_\ell\left(\mathbf{r},t\right) \end{aligned} \tag{A.9}$$

This Hamiltonian represents the energy stored in electromagnetic field and it's interaction with the medium. Next we will quantize the electric field, see [79], in order to evolve our downconversion and upconversion system/state.

$$\mathbf{E}\left(\mathbf{r},t\right) \to \hat{\mathbf{E}}\left(\mathbf{r},t\right) = \hat{\mathbf{E}}^+\left(\mathbf{r},t\right) + \hat{\mathbf{E}}^-\left(\mathbf{r},t\right) \tag{A.10}$$

$$\mathbf{B}\left(\mathbf{r},t\right) \to \hat{\mathbf{B}}\left(\mathbf{r},t\right) = \hat{\mathbf{B}}^+\left(\mathbf{r},t\right) + \hat{\mathbf{B}}^-\left(\mathbf{r},t\right) \tag{A.11}$$

$$\hat{\mathbf{E}}^+\left(\mathbf{r},t\right) = i\sum_{\mathbf{k}}\sum_{\lambda=1,2} \mathbf{e}_{\mathbf{k}\lambda}\sqrt{\frac{\hbar\omega}{2\epsilon_0 V n\left(\omega\right)}}\hat{a}_{\mathbf{k}\lambda} e^{i(\mathbf{k}\cdot\mathbf{r}-\omega_k t)} \tag{A.12}$$

$$\hat{\mathbf{B}}^+\left(\mathbf{r},t\right) = i\sum_{\mathbf{k}}\sum_{\lambda=1,2} \left(\kappa \times \mathbf{e}_{\mathbf{k}\lambda}\right)\sqrt{\frac{\hbar\omega n\left(\omega\right)}{2\epsilon_0 V c^2}}\hat{a}_{\mathbf{k}\lambda} e^{i(\mathbf{k}\cdot\mathbf{r}-\omega_k t)} \tag{A.13}$$

where $\kappa = \mathbf{k}/k$.

$$\hat{H}\left(t\right) = \hat{H}_0 + \hat{H}_I\left(t\right) \tag{A.14}$$

$$\hat{H}_0 = \sum_{\mathbf{k}} \sum_{\nu} \hbar\omega_k \left[\hat{a}^{\dagger}_{\mathbf{k}\lambda} \hat{a}_{\mathbf{k}\lambda} + \frac{1}{2} \right] \tag{A.15}$$

$$\hat{H}_I (t) = \frac{\epsilon_0}{2} \int_V d^3r \chi_{ij\ell} \hat{E}_i (\mathbf{r}, t) \hat{E}_j (\mathbf{r}, t) \hat{E}_\ell (\mathbf{r}, t) \tag{A.16}$$

At each crystal interaction we can assume only downconversion or upconversion are occurring, since the unwanted processes either have negligible contribution or can be filtered out post-interaction. We will assume the fields interacting are all linearly polarized and have real polarization vectors.

$$\hat{H}_I (t) = \hat{H}_\downarrow (t) + \hat{H}_\uparrow (t) \tag{A.17}$$

$$\hat{H}_\uparrow (t) = \hat{H}^{\dagger}_\downarrow (t) \tag{A.18}$$

$$\hat{H}_\downarrow (t) = \frac{\epsilon_0}{2} \int_V d^3r \chi_{ij\ell} \hat{E}^-_j (\mathbf{r}, t) \hat{E}^-_\ell (\mathbf{r}, t) \hat{E}^+_i (\mathbf{r}, t) \tag{A.19}$$

$$\hat{H}_\uparrow (t) = \frac{\epsilon_0}{2} \int_V d^3r \chi_{ij\ell} \hat{E}^-_i (\mathbf{r}, t) \hat{E}^+_\ell (\mathbf{r}, t) \hat{E}^+_j (\mathbf{r}, t) \tag{A.20}$$

where $\hat{H}_\downarrow$ represents the downconversion process and $\hat{H}_\uparrow$ represents the upconversion process. For these second order processes the nonlinear susceptibility $\chi_{ij\ell}$ is in units of $m \cdot volt^{-1}$.

We also will make the approximation that our experiment involves collinear propagation for the pump, signal, and idler. Note that the conjugate process, upconversion, would have signal and idler collinear and coincident with an upconverted photon resulting. The coincident and collinear requirements make the upconversion process orders of magnitude less efficient than downconversion. We will discuss the downconversion case since it is easier, but the upconversion case is the same as long as the temporal properties of the signal and idler are emphasized. In this case, we assume a paraxial path for the nonlinear interaction. This paraxial region will include a cross-section $A = V/L$ as seen in Fig. A.1. This will reduce our theoretical discussion to one-dimension for the propagation and two polarization directions $\lambda = \{h, v\}$. Our positive electric field operator is then given by

$$\hat{E}^{+}_{\lambda}(z,t) = i\sum_{k}\sqrt{\frac{\hbar\omega}{2\epsilon_0 LAn(\omega)}}\hat{a}_{k\lambda}e^{-i(\omega t-kz)} \tag{A.21}$$

with $k \equiv k_z$. We will now move to the continuous representation, $L \to \infty$. In this case $\sum_k \to \frac{1}{\Delta}\int d\omega$ and $\hat{a}_k \to \Delta^{1/2}\hat{a}(\omega)$ with $\Delta = \frac{2\pi c}{L}$, see [79].

$$\hat{E}^{+}_{\lambda}(z,t) = i\int d\omega \frac{\mathcal{E}_\omega}{\sqrt{n(\omega)}}\hat{a}_{\lambda}(\omega)e^{-i\omega t}e^{ikz} \tag{A.22}$$

where $\mathcal{E}_\omega = \sqrt{\frac{\hbar\omega}{4\pi\epsilon_0 Ac}}$.

We can now rewrite (A.14) and (A.15) as:

$$\begin{aligned}\hat{H}_{\downarrow}(t) &= \frac{\epsilon_0\chi_{ij\ell}}{2}\int dA\int_{-L/2}^{L/2}dz\left[\hat{E}^{-}_{j}(z,t)\hat{E}^{-}_{\ell}(z,t)\hat{E}^{+}_{i}(z,t)\right]\\ &= -\frac{iA\epsilon_0\chi_{ij\ell}}{2}\int d\omega d\omega' d\omega'' \frac{\mathcal{E}_\omega\mathcal{E}_{\omega'}\mathcal{E}_{\omega''}}{\sqrt{n(\omega)n(\omega')n(\omega'')}}\hat{a}^{\dagger}_{j}(\omega)\hat{a}^{\dagger}_{\ell}(\omega')\hat{a}_{i}(\omega'')e^{i\Delta\omega t}\int_{-L/2}^{L/2}dze^{-i\Delta kz}\\ &= -\frac{iA\epsilon_0\chi_{ij\ell}}{2}\int d\omega d\omega' d\omega'' \frac{\mathcal{E}_\omega\mathcal{E}_{\omega'}\mathcal{E}_{\omega''}}{\sqrt{n(\omega)n(\omega')n(\omega'')}}\hat{a}^{\dagger}_{j}(\omega)\hat{a}^{\dagger}_{\ell}(\omega')\hat{a}_{i}(\omega'')\phi(\Delta k)e^{i\Delta\omega t}\end{aligned} \tag{A.23}$$

$$\hat{H}_{\uparrow}(t) = \frac{iA\epsilon_0\chi_{ij\ell}}{2}\int d\omega d\omega' d\omega'' \frac{\mathcal{E}_\omega\mathcal{E}_{\omega'}\mathcal{E}_{\omega''}}{\sqrt{n(\omega)n(\omega')n(\omega'')}}\hat{a}^{\dagger}_{i}(\omega'')\hat{a}_{\ell}(\omega')\hat{a}_{j}(\omega)\phi(\Delta k)e^{i\Delta\omega t} \tag{A.24}$$

$$\phi(\Delta k) = L\ \operatorname{sinc}(\Delta kL/2)e^{-i\Delta kL/2} \tag{A.25}$$

where $\Delta k = k + k' - k''$ and $\Delta\omega = \omega'' - (\omega + \omega')$. The spatial integral is taken over the length L of the interaction region.The phase matching of the interaction is represented by $\phi(\Delta k)$.

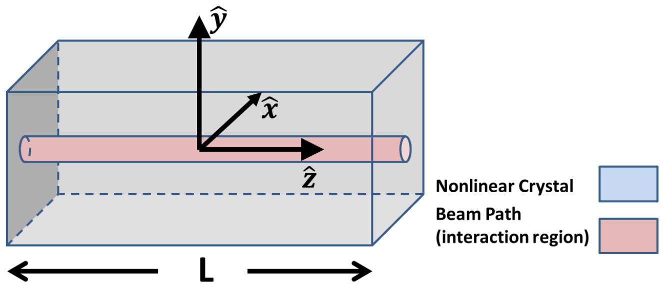

Figure A.1: The spatial integration is over the interaction region. In the paraxial case we simply integrate along the z-axis.

The evolution operator for our Hamiltonian (A.10) in the interaction picture is given by:

$$\begin{aligned}\hat{U}_{\chi}\left(t,t'\right) &= \exp\left(\frac{1}{i\hbar}\int_{t'}^{t} d\tau \hat{H}_{I}\left(\tau\right)\right)\\ &= \exp\left[\frac{1}{i\hbar}\int_{t'}^{t} d\tau \left(\hat{H}_{\downarrow}\left(\tau\right)+\hat{H}_{\uparrow}\left(\tau\right)\right)\right]\end{aligned} \tag{A.26}$$

In an approximately lossless energy conserving process $\Delta\omega \rightarrow 0$. In this case the interaction time $t - t' >> \Delta\omega$ and the limits of integration may be taken to infinity.

$$\int_{-\infty}^{\infty} d\tau \hat{H}_{\downarrow}\left(\tau\right) = -\frac{i\hbar\gamma_{ij\ell}}{2\pi}\int_{-\infty}^{\infty} d\tau \int d\omega d\omega' d\omega'' h\left(\Delta k\right)\hat{a}_{j}^{\dagger}\left(\omega\right)\hat{a}_{\ell}^{\dagger}\left(\omega'\right)\hat{a}_{i}\left(\omega''\right)e^{-i\Delta\omega\tau} \tag{A.27}$$

$$\gamma_{ij\ell} = \frac{A\pi\epsilon_{0}\chi_{ij\ell}\mathcal{E}^{2}_{\frac{\omega_{p0}}{2}}\mathcal{E}_{\omega_{p0}}}{\hbar n(\omega_{p0})n^{2}(\omega_{p0}/2)} \tag{A.28}$$

$$\int_{-\infty}^{\infty} d\tau e^{-i\Delta\omega\tau} = 2\pi\delta\left(\Delta\omega\right) \tag{A.29}$$

$$\int_{-\infty}^{\infty} d\tau \hat{H}_{\downarrow}\left(\tau\right) = -i\hbar\gamma_{ij\ell}\int d\omega d\omega' d\omega'' h\left(\Delta k\right)\hat{a}_{j}^{\dagger}\left(\omega\right)\hat{a}_{\ell}^{\dagger}\left(\omega'\right)\hat{a}_{i}\left(\omega''\right)\left(s\right)\delta\left(\Delta\omega\right) \tag{A.30}$$

$$\int_{-\infty}^{\infty} d\tau \hat{H}_{\downarrow}(\tau) = -i\hbar\gamma_{ij\ell} \int d\omega d\omega' h(\Delta k)\, \hat{a}_j^{\dagger}(\omega)\, \hat{a}_{\ell}^{\dagger}(\omega')\, \hat{a}_i(\omega+\omega') \tag{A.31}$$

$$\int_{-\infty}^{\infty} d\tau \hat{H}_{\uparrow}(\tau) = i\hbar\gamma_{ij\ell} \int d\omega d\omega' h(\Delta k)\, \hat{a}_i^{\dagger}(\omega+\omega')\, \hat{a}_{\ell}(\omega)\, \hat{a}_j(\omega') \tag{A.32}$$

Using the *Campbell-Baker-Hausdorff theorem*, see [85], the unitary evolution operator for downconversion and upconversion is

$$\hat{U}_{\chi} = e^{\frac{1}{i\hbar}\int_{t'}^{t} d\tau\left(\hat{H}_{\downarrow}(\tau)+\hat{H}_{\uparrow}(\tau)\right)} = e^{\frac{1}{i\hbar}\int_{t'}^{t} d\tau\hat{H}_{\downarrow}(\tau)} e^{\frac{1}{i\hbar}\int_{t'}^{t} d\tau\hat{H}_{\uparrow}(\tau)} e^{\left[\frac{1}{i\hbar}\int_{t'}^{t} d\tau\hat{H}_{\downarrow}(\tau), \frac{1}{i\hbar}\int_{t'}^{t} d\tau\hat{H}_{\uparrow}(\tau)\right]}. \tag{A.33}$$

Since, $\chi_{ij\ell}^2 \to 0$ in the exponential containing the commutator

$$\hat{U}_{\chi} \approx e^{\frac{1}{i\hbar}\int_{t'}^{t} d\tau\hat{H}_{\downarrow}(\tau)} e^{\frac{1}{i\hbar}\int_{t'}^{t} d\tau\hat{H}_{\uparrow}(\tau)} = \hat{U}_{\downarrow}\hat{U}_{\uparrow} \tag{A.34}$$

To the first order the unitary upconversion and downconversion operators are

$$\hat{U}_{\downarrow} \approx N\left[\hat{I} - i\gamma_{ij\ell}\int d\omega d\omega' \phi(\omega,\omega')\, \hat{a}_j^{\dagger}(\omega)\, \hat{a}_{\ell}^{\dagger}(\omega')\, \hat{a}_i(\omega+\omega')\right] \tag{A.35}$$

and

$$\hat{U}_{\uparrow} \approx N\left[\hat{I} + i\gamma_{ij\ell}\int d\omega d\omega' \phi(\omega,\omega')\, \hat{a}_i^{\dagger}(\omega+\omega')\, \hat{a}(\omega')_{\ell}\, \hat{a}(\omega)_j\right]. \tag{A.36}$$

We need to normalize $\hat{U}_{\downarrow}$ such that

$$\langle\alpha_{\nu}|\, \hat{U}_{\downarrow}^{\dagger}\hat{U}_{\downarrow}\, |\alpha_{\nu}\rangle = 1. \tag{A.37}$$

We will leave $\chi_{ij\ell}$ general where $i, j, \ell \in \{H, V\}$ are the polarizations for the signal, idler, and pump photon, respectively.

$$\begin{aligned}\hat{U}_{\downarrow}\left|\alpha_{\nu}\right\rangle &= N\left[\hat{I} - i\gamma_{ij\ell}\int d\omega d\omega'\phi\left(\omega,\omega'\right)\hat{a}_{j}^{\dagger}\left(\omega\right)\hat{a}_{\ell}^{\dagger}\left(\omega'\right)\hat{a}_{i}\left(\omega+\omega'\right)\right]\left|\alpha_{\nu}\right\rangle \\ &= N\left[\hat{I} - i\delta_{i\nu}\gamma_{ij\ell}\int d\omega d\omega'\phi\left(\omega,\omega'\right)A\left(\omega+\omega'\right)\hat{a}_{j}^{\dagger}\left(\omega\right)\hat{a}_{\ell}^{\dagger}\left(\omega'\right)\right]\left|\alpha_{\nu},0_{si}\right\rangle \quad \text{(A.38)}\end{aligned}$$

where $\left|\alpha_{\nu},0_{si}\right\rangle$ is the pump state α_{ν} and the vacuum state around the signal and idler frequencies 0_{si}.

$$\left\langle\alpha_{\nu}\right|\hat{U}_{\downarrow}^{\dagger}\hat{U}_{\downarrow}\left|\alpha_{\nu}\right\rangle = N^{2}\left[1+\delta_{i\nu}\gamma_{ij\ell}^{2}\int d\omega d\omega'\left|\phi\left(\omega,\omega'\right)\right|^{2}S\left(\omega+\omega'\right)\right] = 1 \qquad \text{(A.39)}$$

$$N = \left[1+\delta_{i\nu}\gamma_{ij\ell}^{2}\int d\omega d\omega'\left|\phi\left(\omega,\omega'\right)\right|^{2}S\left(\omega+\omega'\right)\right]^{-1/2} \qquad \text{(A.40)}$$

The efficiency of downconversion is

$$\begin{aligned}\eta_{\downarrow} &= \frac{\delta_{i\nu}\gamma_{ij\ell}^{2}\int d\omega d\omega'\left|\phi\left(\omega,\omega'\right)\right|^{2}S\left(\omega+\omega'\right)}{\left[1+\delta_{i\nu}\gamma_{ij\ell}^{2}\int d\omega d\omega'\left|\phi\left(\omega,\omega'\right)\right|^{2}S\left(\omega+\omega'\right)\right]^{1/2}} \\ &\approx \delta_{i\nu}\gamma_{ij\ell}^{2}\int d\omega d\omega'\left|\phi\left(\omega,\omega'\right)\right|^{2}S\left(\omega+\omega'\right) \qquad \text{(A.41)}\end{aligned}$$

Normalization of the upconversion operator is similar. The normalization constant N ensures that $\hat{U}_{\downarrow}$ and $\hat{U}_{\uparrow}$ are unitary. In instances where the conditions are appropriate for downconversion and not upconversion $\hat{U}_{\uparrow} \rightarrow \hat{I}$ and when conditions are appropriate for upconversion and not downconversion $\hat{U}_{\downarrow} \rightarrow \hat{I}$.

A.2 The Two-Photon State

We will assume an inexhaustible macroscopic pump with a power spectrum $S(\omega)$ and linear polarization ν. The pump state $|\alpha_\nu\rangle$ is such that

$$\hat{a}_\lambda(\omega)|\alpha_\nu\rangle = A(\omega)\,\delta_{\lambda\nu}|\alpha_\nu\rangle \tag{A.42}$$

with the spectral amplitude $A(\omega)$ being related to the power spectrum $S(\omega)$ by [23]

$$\langle A^*(\omega')A(\omega)\rangle = 2\pi S(\omega)\,\delta(\omega'-\omega)\,. \tag{A.43}$$

We now apply the downconversion operator from Eq. A.35 to the pump photon which we assume has horizontal polarization, $\nu = H$. We also apply a filter operation $\hat{F}$ which removes the remaining pump components.

$$\begin{aligned}\hat{F}\hat{U}_\downarrow|\alpha_\nu\rangle &= \frac{1}{\sqrt{\eta_\downarrow}}\left[\hat{I} - i\delta_{i\nu}\gamma_{ij\ell}\int d\omega d\omega'\phi(\omega,\omega')A(\omega+\omega')\hat{a}_j^\dagger(\omega)\hat{a}_\ell^\dagger(\omega')\right]|\alpha_H,0_{si}\rangle\\ &= \frac{\gamma_{Hj\ell}}{\sqrt{\eta_\downarrow}}\int d\omega d\omega'\phi(\omega,\omega')A(\omega+\omega')\hat{a}_j^\dagger(\omega)\hat{a}_\ell^\dagger(\omega')|0_{si}\rangle\end{aligned} \tag{A.44}$$

We assume Type II SPDC in this dissertation, since its phase matching function is easier to handle mathematically. As a starting point in Chapter 2 and 3, we assume variations on the state

$$|\psi\rangle = \gamma\int d\omega d\omega'\phi(\omega,\omega')A(\omega+\omega')\hat{a}_H^\dagger(\omega)\hat{a}_V^\dagger(\omega')|0\rangle \tag{A.45}$$

with the constant

$$\gamma = \frac{\gamma_{HHV}}{\sqrt{\eta_\downarrow}} \tag{A.46}$$

typically irrelevant to the derivations.

Vita

Brian lived in Trenton, Tennessee from birth until his Trenton Peabody High School graduation in 1999. He attended the University of Memphis with an academic scholarship until 2005 where he gained a B.S. in Physics and Mathematics. Brian worked for the State of Tennessee Department of Environment and Conservation Division of Radiological Health for four years while gaining a Masters degree in Physics from the University of Tennessee. From 2009 to present he has worked towards completion of his PhD in Physics at the University of Tennessee. In 2012, he married his wife Lydia, who anxiously awaits him attaining a real job. Also in 2012, they got their best friend Julep. Time Brian makes for himself is primarily spent running in the mountains with friends.